

**Final Research Report**  
Research Project T2695, Task 28

**SEISMIC ANALYSIS AND RETROFIT STUDY  
OF THE SR 99–SPOKANE STREET OVER-CROSSING**

by

Blake Inouye  
Graduate Research Assistant

Dawn Lehman  
Assistant Professor

John Stanton  
Professor

Steven Kramer  
Professor

Department of Civil and Environmental Engineering  
University of Washington, Box 352700  
Seattle, Washington 98195

**Washington State Transportation Center (TRAC)**

University of Washington, Box 354802  
1107 NE 45th Street, Suite 535  
Seattle, Washington 98105-4631

Washington State Department of Transportation Technical Monitor  
Ed Henley  
Bridge Management Engineer  
WSDOT Bridge and Structures Office

Prepared for  
**Washington State Transportation Commission**  
Department of Transportation  
and in cooperation with  
**U.S. Department of Transportation**  
Federal Highway Administration

September 2005

## TECHNICAL REPORT STANDARD TITLE PAGE

1. REPORT NO. <b>WA-RD 596.1</b>	2. GOVERNMENT ACCESSION NO.	3. RECIPIENT'S CATALOG NO.	
4. TITLE AND SUBTITLE <b>SEISMIC ANALYSIS AND RETROFIT STUDY OF THE SR 99-SPOKANE STREET OVER-CROSSING</b>		5. REPORT DATE <b>September 2005</b>	
		6. PERFORMING ORGANIZATION CODE	
7. AUTHOR(S) <b>Inouye, Blake; Lehman, Dawn; Stanton, John; Kramer, Steven</b>		8. PERFORMING ORGANIZATION REPORT NO.	
9. PERFORMING ORGANIZATION NAME AND ADDRESS <b>Washington State Transportation Center (TRAC) University of Washington, Box 354802 University District Building; 1107 NE 45th Street, Suite 535 Seattle, Washington 98105-4631</b>		10. WORK UNIT NO.	
		11. CONTRACT OR GRANT NO. <b>Agreement T2695, Task 28</b>	
12. SPONSORING AGENCY NAME AND ADDRESS <b>Research Office Washington State Department of Transportation Transportation Building, MS 47372 Olympia, Washington 98504-7372 Keith Anderson, Project Manager, 360-709-5405</b>		13. TYPE OF REPORT AND PERIOD COVERED <b>Final Research Report</b>	
		14. SPONSORING AGENCY CODE	
15. SUPPLEMENTARY NOTES <b>This study was conducted in cooperation with the U.S. Department of Transportation, Federal Highway Administration.</b>			
16. ABSTRACT <p>The SR 99-Spokane Street over-crossing is located in Seattle, Washington, and was built in the late 1950s. Its construction is mostly of reinforced concrete; the reinforcement detailing is poor by modern seismic standards, particularly with respect to confinement, and the underlying soils are also weak. Furthermore, the structure contains many "outrigger bents," in which columns are displaced from their ideal locations to accommodate passage of railroad tracks beneath the structure. These outrigger bents cause significant asymmetry in the structure that could lead to unusual and undesirable seismic response.</p> <p>In this study, the seismic response of the structure was evaluated analytically, and seismic retrofit strategies were developed and evaluated. In a companion experimental study by Washington State University, the as-existing structure was investigated by testing scale models of representative bents, and one retrofit strategy was also tested.</p> <p>In this report, modeling approaches are discussed in detail, and the results of evaluations of the as-existing structure as well as the retrofit strategies are presented. Some components of the structure (e.g., the deck, the already jacketed columns, and the soil-foundation-structure system) were found to be critical to an accurate determination of response and were therefore modeled in some detail. Site-specific ground motions at three different hazard levels were used.</p> <p>The structure was found to be vulnerable, especially to 72- and 475-year ground motions. The knee-joints that connect the outrigger beams and columns were found to be the most critical components, and their vulnerability was shown to be influenced by the type of retrofit performed on the outrigger column. Retrofit strategies included some designed to increase the strength and ductility of the components, and some intended to reduce the demands on them.</p>			
17. KEY WORDS <b>Knee-joints, Outriggers, Reinforced Concrete, Retrofit, Seismic, Soil-structure Interaction</b>		18. DISTRIBUTION STATEMENT <b>No restrictions. This document is available to the public through the National Technical Information Service, Springfield, VA 22616</b>	
19. SECURITY CLASSIF. (of this report) <b>None</b>	20. SECURITY CLASSIF. (of this page) <b>None</b>	21. NO. OF PAGES	22. PRICE

## **DISCLAIMER**

The contents of this report reflect the views of the authors, who are responsible for the facts and the accuracy of the data presented herein. The contents do not necessarily reflect the official views or policies of the Washington State Department of Transportation. This report does not constitute a standard, specification, or regulation.



# CONTENTS

<b>List of Symbols.....</b>	<b>xi</b>
<b>Executive Summary .....</b>	<b>xvii</b>
<b>1. Introduction .....</b>	<b>1-1</b>
1.1 Background .....	1-1
1.2 Objectives and Scope .....	1-3
1.3 Outline of the Report.....	1-4
<b>2. Previous Work.....</b>	<b>2-1</b>
2.1 Experimental Evaluation of Outrigger Bents .....	2-2
2.2 Experimental Evaluation of the SR 99 Outrigger Bents.....	2-7
2.3 WSDOT Seismic Evaluation of the SR 99–Spokane Street Over-Crossing Structure	2-14
2.4 Field Observation of the SR 99–Spokane Street Over-Crossing.....	2-16
2.5 Summary .....	2-17
<b>3. Modeling of the As-Existing Structure.....</b>	<b>3-1</b>
3.1 Introduction .....	3-1
3.2 Overview of the As-Existing Structure .....	3-3
3.2.1 Bridge Configuration.....	3-3
3.2.2 Phase 1 Retrofit Measures.....	3-6
3.3 Numerical Model of the North Concrete Structure .....	3-7
3.3.1 Overview .....	3-7
3.3.2 Material Properties .....	3-8
3.3.3 Numerical Representation of the Concrete Deck .....	3-9
3.3.4 Transverse Beams .....	3-18
3.3.5 Columns .....	3-18
3.3.6 Expansion Joints.....	3-20
3.3.7 Structural Damping .....	3-21
3.3.8 Outrigger Joint Flexibility .....	3-21
3.4 Modeling of Adjoining Structures.....	3-22
3.4.1 West Off-Ramp .....	3-22
3.4.2 North End Abutment .....	3-24
3.4.3 South End Steel Structure.....	3-25
3.4.4 South End Concrete Structure .....	3-26
3.5 Geotechnical Characteristics of the Site.....	3-26
3.5.1 Site Conditions .....	3-27
3.5.2 Soil Properties .....	3-28
3.6 Modeling of the Soil-Foundation-Structure Interaction .....	3-30
3.6.1 Foundations .....	3-30
3.6.2 Foundation Impedances.....	3-30
3.6.3 Numerical Representation of the Soil-Foundation-Structure Interaction.....	3-33
3.7 Ground Motions .....	3-36
3.8 Model Verification Evaluation.....	3-39
3.8.1 Period Verification .....	3-39
3.8.2 Spectral Verification.....	3-39
3.8.3 Field Verification .....	3-40
3.8.4 Summary of Verification.....	3-41

<b>4. Analysis Results and Evaluation of As-Existing Structure .....</b>	<b>4-1</b>
4.1 Introduction .....	4-1
4.2 Capacity Assessment of Outrigger Bents .....	4-2
4.2.1 Beam and Column Flexural Response .....	4-4
4.2.2 Joint Shear Under Transverse Loading .....	4-10
4.2.3 Radial Tension.....	4-14
4.2.4 Bar Anchorage.....	4-17
4.2.5 Beam Shear .....	4-22
4.2.6 Beam Torsion and Out-of-Plane Shear .....	4-25
4.3 Global Demands on Outrigger Bents .....	4-29
4.3.1 Displacement and Drift Demands .....	4-30
4.3.2 Displacement Ductility Demands.....	4-33
4.4 Demand/Capacity Evaluation of Outrigger Bent Components .....	4-36
4.4.1 Beam and Column Flexural Response .....	4-37
4.4.2 Joint Shear Under Transverse Loading .....	4-41
4.4.3 Radial Tension.....	4-42
4.4.4 Bar Anchorage.....	4-43
4.4.5 Beam Shear .....	4-46
4.4.6 Beam Torsion and Out-of-Plane Shear .....	4-49
4.5 Summary of Results .....	4-56
<b>5 Retrofit Options .....</b>	<b>5-1</b>
5.1 Introduction .....	5-1
5.2 Outrigger Component Retrofit Options.....	5-2
5.2.1 Column Retrofit.....	5-2
5.2.2 Joint .....	5-5
5.3.2 Beam.....	5-9
5.3 System Retrofit Schemes.....	5-12
5.3.1 Introduction .....	5-12
5.3.2 Column Modification Retrofit (Option C) .....	5-13
5.3.3 Joint Retrofit with Optional Column Modification (Options J and J+C).....	5-16
5.3.4 Join and Beam Retrofit (Option J+B).....	5-17
5.3.5 Isolation of Column (Option I).....	5-18
<b>6 Summary and Conclusions.....</b>	<b>6-1</b>
6.1 Summary .....	6-1
6.2 Conclusions .....	6-3
6.2.1 Required Components of the Analytical Model.....	6-3
6.2.2 Response Prediction .....	6-4
6.2.3 Retrofit Options and Design Implications.....	6-6
6.3 Recommendations for Implementation .....	6-7
6.3.1 Recommendations for This Structure.....	6-7
6.3.2 Modeling Recommendations for Other Structures.....	6-7
6.4 Recommendations for Further Research .....	6-8
<b>References.....</b>	<b>7-1</b>
<b>Appendix A. ....</b>	<b>A-1</b>
<b>Appendix B. Moment and Bar Stress Demand Calculation Procedure for As-Existing Outriggers.....</b>	<b>B-1</b>

# FIGURES

<u>Figure</u>	<u>Page</u>
1.1. Site Map of SR 99–Spokane Street Over-Crossing.....	1-1
2.1. Details of the As-Built Test Specimen .....	2-3
2.2. Details of the As-Built Test Specimen .....	2-4
2.3. Details of the Retrofitted Test Specimen.....	2-5
2.4. Details of the As-Built Test Specimen .....	2-6
2.5. Washington State University Test Set-Up for the “Short” Specimen .....	2-8
2.6. Washington State University “Short” Specimen Details.....	2-9
2.7. Washington State University “Long” Specimen Details.....	2-10
2.8. Damage to the “Short” Specimen Under In-Plane Loading.....	2-12
2.9. Damage to the “Long” Specimen Under In-Plane Loading .....	2-12
2.10. Damage to the “Short” Specimen Under Out-of-Plane Loading.....	2-13
2.11. Outrigger at Bent 11 .....	2-16
2.12. Pounding Damage Observed at the Expansion Joint at Bent 13 .....	2-16
3.1. Layout of the North Concrete Structure .....	3-4
3.2. Split Column Details .....	3-5
3.3. Elliptical and Semi-Elliptical Steel Column Jackets .....	3-6
3.4. Functional Representation of North Concrete Model and Peripheral Structures .....	3-7
3.5. Computer Model of North Concrete and Peripheral Structures .....	3-8
3.6. Model 1—Single Spine Beam.....	3-11
3.7. Model 2—Multiple Girders.....	3-12
3.8. Model 3—Horizontal Flat Plates.....	3-13
3.9. Model 4—Box Girder.....	3-14
3.10. Application of Beam (Rotational) Constraints to Connections between Plate and Beam Elements .....	3-14
3.11. Example of Beam Constraint Locations.....	3-15
3.12. Sources of Deformation in the Column.....	3-19
3.13. Underside of the West Off-Ramp.....	3-23
3.14. West Off-Ramp Model.....	3-23
3.15. Modeling of the Drop-In Span .....	3-24
3.16. Modeling of the North Abutment.....	3-25
3.17. Modeling of the Steel and South Concrete Structures.....	3-26
3.18. Pile Group Configurations.....	3-31
3.19. Variation of (a) Stiffness and (b) Damping Coefficient with Frequency for Vertical and Horizontal Translation .....	3-32
3.20. Variation of (a) Stiffness and (b) Damping Coefficient with Frequency for Rocking and Torsion .....	3-32
3.21. Model of Soil-Structure Interaction.....	3-34
3.22. Response Spectra and Target Spectra for Synthetic Rock Input Motions at the 72- Year, 475-Year, and 2,475-Year Hazard Levels .....	3-37
3.23. Computed Ground Surface Response Spectra for the 72-Year, 475-Year, and 2,475- Year Hazard Levels .....	3-38
3.24. Displacement Response Spectrum for 6.5 Percent Damping .....	3-40
3.25. Gap Closures in Model Due to 72-Year Earthquake.....	3-41

4.1. Opening and Closing Moments on Test Specimens.....	4-4
4.2. Typical Theoretical Moment-Curvature Response (WSU Short Beam, Opening Moment).....	4-6
4.3. Actuator Force-Horizontal Displacement History for the As-Built Short Specimen Subjected to In-Plane Loading .....	4-9
4.4. Actuator Force-Horizontal Displacement History for the As-Built Long Specimen Subjected to In-Plane Loading .....	4-10
4.5. Joint Shear Damage in WSU “Long Outrigger,” In-Plane Loading.....	4-11
4.6. Horizontal Joint Shear Stress Determination Under Closing Moment.....	4-12
4.7. Radial Tension in Outrigger Joint: Forces on Bars .....	4-14
4.8. Radial Tension Damage to WSU Short Outrigger, In-Plane Loading .....	4-15
4.9. Definition of Variables for Radial Tension .....	4-15
4.10. Crack Pattern in WSU Short and Long Outrigger, In-Plane Loading .....	4-18
4.11. Calculation of Plastic Seismic Shear Demand .....	4-23
4.12. Torsion Cracks in “Short” Outrigger, Out-of-Plane Loading.....	4-26
4.13. Actuator Force-Horizontal Displacement History for the As-Built Short Specimen Subjected to Out-of-Plane Loading .....	4-29
4.14. Outrigger Bent 9 Displacement Histories (ft).....	4-31
4.15. Beam Shear Demand .....	4-47
4.16. Beam Torsion .....	4-51
4.17 Representation of Torque-Twist Angle Curve from Rahal-Collins.....	4-52
4.18 Representation of Torque-Twist Angle Curve for an As-Existing Outrigger Beam .....	4-53
5.1. Column Modification .....	5-3
5.2. Joint Retrofit Options .....	5-7
5.3. Beam Retrofit Options .....	5-10
5.4. Five-Part Column Representation .....	5-14
5.5. Column Isolation Retrofit Schemes .....	5-19

## TABLES

<u>Table</u>	<u>Page</u>
2.1. Measured Material Properties for WSU Test Specimens .....	2-11
3.1. North Concrete Structure Outrigger Bent Dimensions.....	3-5
3.2. Deck Model Lateral Displacements and Fundamental Periods .....	3-16
3.3. General Soil Units .....	3-28
3.4. Average Standard Penetration Test (SPT) Resistance.....	3-29
3.5. Shear Wave Velocity of Soil Layers .....	3-29
3.6. Maximum Structural Displacement (ft) Using Different Foundation Models .....	3-35
3.7. Period of Fundamental Modes for Individual Frames.....	3-39
4.1. Critical In-Plane Moments of Test Beams and Columns .....	4-7
4.2. Maximum Bar Stresses and Stress Ratios for In-Plane Specimens.....	4-8
4.3. Maximum Displacement Ductilities Achieved in the In-Plane Experiments.....	4-10
4.4. Normalized Horizontal Shear Stress on Test Specimens, ( $v_{jh} / \sqrt{f'_c}$ psi), at Peak Load.....	4-13
4.5. Normalized Radial Tension Stresses on WSU Outrigger Joints .....	4-17
4.6. Normalized Average Bond Stress, $\tau_{bond} / \sqrt{f'_c}$ (psi) on Test Beam and Column Bars in Tension.....	4-19
4.7. Beam Shear Demand on and Theoretical Capacity of Specimens (kips).....	4-23
4.8. Summary of Torsion Demands on WSU “Short” Outrigger Beam.....	4-28
4.9. Maximum Displacements (ft) at Outrigger Joints (72- and 475-Year Earthquakes) .....	4-32
4.10. Maximum Drift Ratios at Outrigger Bents (%) .....	4-32
4.11. Yield Displacement (ft.) of the Outrigger Beams and Columns .....	4-35
4.12. Maximum Displacement Ductility Demands on Outrigger Beams and Columns.....	4-35
4.13. In-Plane Yield, Maximum, and Demand Moments of As-Existing Outrigger Beams and Columns .....	4-39
4.14. As-Existing Outrigger Beam and Column Reinforcing Steel Yield, Ultimate, and Demand Stresses.....	4-40
4.15. Normalized Shear Stress Demands on Outrigger Joints Under Opening and Closing Moments ( $v_{jh} / \sqrt{f'_c}$ ) .....	4-41
4.16. Normalized Radial Tension Stress Demands on Outrigger Joints Based on Beam and Column Bar Stresses ( $\sigma_{rad} / \sqrt{f'_c}$ ) .....	4-43
4.17. Evaluation of Beam Bar Anchorage in Outrigger Joints .....	4-44
4.18. Evaluation of Column Bar Anchorage in Outrigger Joints .....	4-45
4.19. Outrigger Beam Shear (kips) and Demand/Capacity Ratios .....	4-49
4.20. Outrigger Beam Torsion Evaluation.....	4-51
4.21. Potential Response Mechanisms for Outrigger Bents Subjected to Opening Moments.	4-56
4.22. Potential Response Mechanisms for Outrigger Bents Subjected to Closing Moments..	4-57
5.1. Maximum Displacement Ductility Demands for Element Strengthening Schemes, Longitudinal Direction .....	5-15

5.2. Maximum Displacement Ductility Demands for Element Strengthening Schemes, Transverse Direction .....	5-15
5.3. Maximum Isolator Displacement (ft) and Column Base Moments (k-ft) for Top Isolation.....	5-20
5.4. Outrigger Column Moments (k*ft) for Column Isolation Retrofit Scheme.....	5-21

## LIST OF SYMBOLS

$A_{\text{bar}}$	=	area of bar
$A_{\text{cp}}$	=	area enclosed by outside perimeter of concrete cross section
$A_{\text{g}}$	=	gross area of member section
$A_{\text{o}}$	=	gross area enclosed by shear flow path
$A_{\text{s}}$	=	area of reinforcing steel
$A_{\text{t}}$	=	area of 1 leg of closed stirrup resisting torsion
$A_{\text{v}}$	=	area of transverse reinforcing steel
$A_{\text{v-dem}}$	=	area of transverse reinforcing steel required to resist shear demand
$b$	=	width of beam
$b_{\text{jt}}$	=	width of joint
$C_{\text{bm}}$	=	beam compression force resultant
$c$	=	neutral axis distance
$c_1, c_2, c_3$	=	constants defined in section A.3
$D/C$	=	demand-capacity ratio
$d$	=	distance from extreme compression fiber to centroid of longitudinal tension reinforcement
$d_{\text{b}}$	=	diameter of bar
$E$	=	elastic modulus
$E_{\text{c}}$	=	elastic modulus of concrete
$E_{\text{cr}}$	=	cracked section elastic modulus
$E_{\text{s}}$	=	elastic modulus of reinforcing steel bars
$E_{\text{s,eff}}$	=	reduced elastic modulus for a steel segment representing the unjacketed column length
$EI_{\text{cr}}$	=	cracked section flexural rigidity
$EI_{\text{eff}}$	=	effective flexural rigidity
$(EI_{\text{eff}})_{\text{unj}}$	=	flexural rigidity of the unjacketed section
$EI_{\text{g}}$	=	gross section flexural rigidity
$EI_{\text{prism}}$	=	flexural rigidity of equivalent prismatic member
$F_{\text{act}}$	=	applied actuator force
$f_{\text{bar}}$	=	compression bar stress demand
$f'_{\text{c}}$	=	concrete compressive strength
$f_{\text{s-dem}}$	=	bar stress demand
$f_{\text{s,max-exp}}$	=	bar stress corresponding to the maximum experimental moment

$f_{sy}$  = bar stress at yield  
 $f_{su}$  = bar stress at ultimate or maximum load  
 $f_y$  = yield strength of reinforcing steel bars  
 $f_{yv}$  = yield strength of transverse reinforcement  
 $f_u$  = ultimate strength of reinforcing steel bars  
 $g$  = length of the gap between the end of the jacket and the footing or joint face  
 $H$  = column height  
 $H_{act}$  = height of actuator  
 $h_b$  = depth of beam  
 $h_c$  = depth of column  
 $h_{jt}$  = depth of joint  
 $I$  = moment of inertia  
 $I_{prism}$  = moment of inertia of equivalent prismatic member  
 $K_y$  = secant stiffness at yield from Prestley, et al. (1994)  
 $k_{lat}$  = lateral bending stiffness  
 $k_{lat,prism}$  = bending stiffness of prismatic column  
 $k_{t-cr}$  = final cracked torsional secant stiffness  
 $k_{(t-el)2}$  = elastic torsional secant stiffness from second iteration  
 $k_{(t-el)RC}$  = elastic torsional stiffness from approximated Rahal-Collins curve  
 $k_{(t-el)SR-99}$  = elastic torsional stiffness of SR-99 outrigger beam  
 $k_{(t-pl)RC}$  = plastic torsional stiffness from approximated Rahal-Collins curve  
 $k_{(t-pl)SR-99}$  = plastic torsional stiffness of SR-99 outrigger beam  
 $k_{\theta}, k_{\theta 1}, k_{\theta 2}$  = rotational spring stiffness  
 $L$  = length of member  
 $L_{cant}$  = length of a cantilever column  
 $L_{clear}$  = clear length of member  
 $l_{cr}$  = length of cracked section  
 $l_d$  = bar embedment length  
 $l_p$  = plastic hinge length  
 $l_{p1}$  = portion of plastic hinge length attributed to curvature of the member  
 $l_{p2}$  = portion of plastic hinge length attributed to strain penetration  
 $l_{sp}$  = length of splice  
 $M_1, M_2$  = column end moments  
 $M_{bm}, M_{bm1}, M_{bm2}$  = beam moment

$M_{col}$  = column moment  
 $M_{cr}$  = cracking moment  
 $M_{dem}$  = moment demand  
 $M_{dem-base}$  = moment demand at base of column  
 $M_{FE}$  = moment from FE analysis  
 $M_{FE-long}$  = moment from FE analysis due to longitudinal loading  
 $M_{FE-trans}$  = moment from FE analysis due to transverse loading  
 $M_{max}$  = maximum moment from moment-curvature analysis  
 $M_{max-exp}$  = maximum experimental moment  
 $M_{p1}, M_{p2}$  = plastic moment  
 $M_u$  = ultimate moment or maximum moment on moment-curvature diagram  
 $M_y$  = yield moment  
 $M_{y-base}$  = yield moment at base of column  
 $M_{ycol}$  = column yield moment  
 $P_{bm}$  = beam axial force  
 $P_{col}$  = column axial force  
 $PI$  = plasticity index  
 $p_{cp}$  = outside perimeter of concrete cross section  
 $r$  = radius of curved bars  
 $S_d$  = spectral displacement  
 $s$  = spacing of stirrups or closed hoops  
 $T$  = structural period of vibration  
 $T_{cr}$  = cracking torque  
 $T_{bm}$  = tension force in beam bars  
 $T_{dem}$  = torque demand  
 $T_{FE-el}$  = elastic torque demand on outrigger beam from FE analysis  
 $T_n$  = nominal torsion strength at yield of transverse reinforcement  
 $T_{max-exp}$  = maximum experimental torque  
 $T_{pl}$  = plastic torque  
 $T_{rad}$  = radial tension force resultant  
 $T_y$  = yield torque  
 $V$  = shear  
 $V_{bm}$  = beam shear  
 $V_c$  = shear strength attributed to the concrete

$V_{col}$	=	column shear
$V_{dem}$	=	experimental shear demand
$V_{eq}$	=	shear force due to earthquake loading
$V_{exp}$	=	measured experimental shear
$V_{FE}$	=	shear force from FE analysis
$V_{grav}$	=	shear force due to gravity loading
$V_{jh}$	=	horizontal joint shear force
$V_n$	=	nominal shear strength
$V_{pl}$	=	plastic shear
$V_s$	=	shear strength provided by reinforcing steel
$V_s$	=	shear wave velocity
$V_y$	=	shear at yield from Priestley et al. (1994)
$v_{jh}$	=	average horizontal joint shear stress
$z$	=	depth of soil layer
$\alpha$	=	scale factor on the length of the column used to represent the unjacketed section
$\beta$	=	rotation angle defined in Section B.1
$\chi$	=	variable for steel grade from Priestley et al. (1994)
$\Delta$	=	lateral displacement of the top of the column relative to the bottom
$\Delta_{axial}$	=	axial elongation of column due to rotation of one hinge
$\Delta_{dem}$	=	horizontal displacement demand of the outrigger
$\Delta_{FE}$	=	displacement from FE analysis
$\Delta_{FE-long}$	=	displacement from FE analysis due to longitudinal loading
$\Delta_{FE-trans}$	=	displacement from FE analysis due to transverse loading
$\Delta_{iso}$	=	elastic displacement from FE analysis for isolation retrofit scheme
$\Delta_{ph}$	=	horizontal displacement demand on the outrigger due to plastic hinge rotation
$\Delta_{pl}$	=	plastic displacement from reduced torsional stiffness FE analysis
$\Delta_{pv}$	=	differential vertical deflection between plastic hinge and beam to deck connection
$\Delta_{u-exp}$	=	measured displacement at loss of load carrying capacity
$\Delta_y$	=	yield displacement
$\Delta_{yh}$	=	horizontal displacement demand on the outrigger prior to yielding
$\Delta_{y-exp}$	=	measured yield displacement
$\delta_s$	=	elongation of rebar due to the unjacketed section of the column
$\delta_{tot}$	=	total elongation of rebar

- $\epsilon_{\text{avg}}$  = average strain
- $\epsilon_y$  = yield strain
- $\phi_{\text{dem}}$  = curvature demand
- $\phi_p$  = plastic curvature
- $\phi_{\text{tot}}$  = total curvature
- $\phi_y$  = yield curvature
- $\gamma$  = scale factor on development length due to strain penetration
- $\varphi_{\text{FE-el}}$  = twist angle of outrigger beam from FE analysis
- $\varphi_y$  = twist angle of outrigger beam at yield
- $\kappa$  = rotation angle of beam
- $\lambda$  = angle between inclined stirrups and longitudinal axis of member
- $\mu_{\Delta}$  = displacement ductility demand
- $\mu_{\Delta\text{-exp}}$  = displacement ductility at loss of load carrying capacity
- $\sigma_{\text{rad}}$  = radial tension stress
- $\tau_{\text{bond}}$  = average bond stress
- $\theta$  = angle of compression diagonals in truss analogy for torsion, equal to  $45^\circ$  for non-prestressed members
- $\theta_1, \theta_2$  = column end rotations
- $\theta_p$  = plastic hinge rotation
- $\theta_{\text{rt}}$  = angle between radial tension force resultant and the horizontal
- $\theta_y$  = member end rotation at yield
- $\xi d$  = distance from the extreme tension bar to the neutral axis



## **EXECUTIVE SUMMARY**

This report describes a detailed analytical study of the seismic vulnerabilities of the SR99–Spokane Street over-crossing in the City of Seattle. The study was undertaken for the Washington State Department of Transportation (WSDOT) because the structure contains significant irregularities, most notably outrigger bents, and the reinforcement in the RC sections of these bents does not satisfy modern ductile detailing requirements. For both reasons the structure poses a potential hazard. In this study, the seismic demands on the structure and its vulnerable elements were investigated, and several retrofit schemes were developed. In a parallel study conducted at Washington State University (WSU), the capacities of the outrigger bent joints were studied experimentally.

A detailed analytical model of the north half of the structure was developed and was subjected to site specific synthetic ground motions representing a 2 percent, 10 percent, and 50 percent probability of exceedence in 50 years. The soil conditions represented in the model and the ground motions used as dynamic input were developed through rigorous analysis of the soil at the site. The model of the foundations contained spring and dashpot elements to simulate the nonlinear soil response. Most of the structural components were linear elastic elements, but special nonlinear modeling techniques were required for the expansion joints and jacketed columns.

The largest response was found with the 10 percent and 50 percent in 50 years ground motions, because the large soil strains caused by the 2 percent in 50 years motion resulted in significant softening of the soil and consequent reductions in the accelerations transmitted to the structure. Almost all of the columns in the structure have been jacketed, but the outrigger beams have not. The overall displacement response was found to be controlled by the main line (i.e., non-outrigger) columns, which are relatively numerous, so changing the properties of the outrigger elements had little effect on global displacements. The outrigger knee joints were found to be particularly vulnerable, which as exacerbated by having columns directly below them stiffened by jacketing, thereby

forcing almost all of the deformation into the joint region. The vulnerability of the joints was confirmed by the test program at WSU. The outrigger beams were also shown to be vulnerable to longitudinal ground motion, which induces inelastic torsional response. Some of the beams contain only open stirrups, which are ineffective at resisting torsional moment.

Several retrofit methods were developed and evaluated. They included column, joint, and beam retrofits or a combination of the element modifications, as well as isolation methods. Some of the schemes attempted to reduce demands, others attempted to increase capacity, and still others combined both approaches.

# 1 INTRODUCTION

## 1.1 Background

Washington State Route 99 runs through the city of Seattle. Before the construction of I-5, it was the main north-south thoroughfare in the western part of the state, and it now carries some 80,000 vehicles per day, or about one third of the total north-south traffic, through the city. At the southern end of the city, it crosses over Spokane Street, with which it also intersects. That over-crossing is the subject of this report. Its location is shown in Figure 1-1.

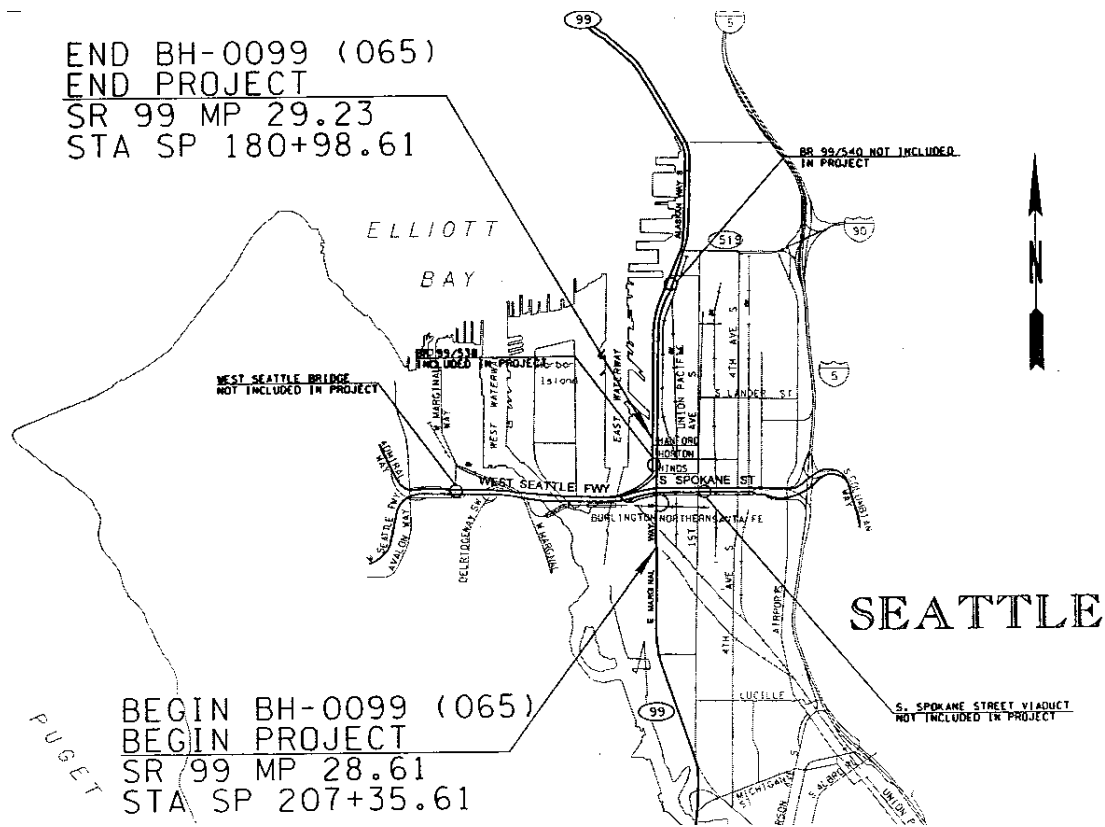


Figure 1-1: Site Map of SR 99–Spokane Street Over-Crossing

The over-crossing was designed and constructed in the late 1950s and opened to traffic in 1959 (Zhang et al. 1996). It consists of four separate parts. The most northerly is a concrete box section supported by concrete columns. The next section crosses Spokane

Street itself and is a steel structure with a cast-in-place concrete deck. The third section is another concrete box, similar to the northernmost, and the fourth and southernmost section is a timber trestle. The structure is supported on pile foundations. The surface soils are generally poor and consist of loose fill or loose marine deposits. The structure was built over a series of Burlington Northern railroad tracks, which precluded placement of some of the columns in their ideal locations.

A Phase I retrofit of the structure has already been conducted (Zhang et al. 1996). It consisted of applying full-height steel jackets to almost all of the columns of the two concrete structures. Two columns of the southern concrete structure were not jacketed because the clearance to the railroad tracks was insufficient. One of the columns of Bent 25, which is the southernmost bent of the northern concrete structure, was also not jacketed because of clearance issues.

The north section of the structure consists of seven frames, each of which consists of three or four bents. The frames are separated by expansion joints, at which the columns are split to accommodate longitudinal expansion or contraction of the deck. At seven of the bents in the northern structure, the outermost column is located away from the box girder to allow passage of the railroad tracks, and the inner columns are displaced from their standard alignment. The vertical load is transmitted from the box girder to the column by a beam, referred to herein as an outrigger beam. This arrangement results in asymmetry in the structure and, under earthquake loading, it could lead to the occurrence of internal forces that differ from those normally found in a symmetric structure. In particular, longitudinal motion (north-south motion for this structure) induces torsion in the outrigger beams.

The two reinforced concrete structures also contain reinforcement detailing that is typical of the construction practices of the 1950s but that has subsequently been shown to lead to non-ductile seismic response. In particular, the beams, columns, and joints contain little transverse reinforcement, and the ties that do exist are either closed with 90-degree bends or consist of an open U-stirrup and a closure bar. Neither arrangement provides reliable

confinement. This deficiency has been rectified in most of the columns by fitting them with elliptical steel jackets during the Phase I retrofit. However, the seismic performance of the outrigger joints and beams, which remain in their original as-built condition, is uncertain.

## **1.2 Objectives and Scope**

The Washington State Department of Transportation (WSDOT) initiated two research projects to determine the likely seismic response of the structure. A program of laboratory experiments was sponsored at Washington State University (WSU), while an analytical study was undertaken at the University of Washington (UW). This report describes the latter study.

The analytical study comprised the following tasks:

- Review past research on outrigger systems.
- Develop performance and seismic hazard levels for evaluating the as-existing structure and designing the retrofit measures.
- Develop site-specific ground motions and response spectra for the bridge site, taking into account the local geology, soil conditions, and different levels of seismic risk.
- Identify the performance and force-deformation response of critical elements in the structure by using the results of previous research and the WSU experimental study.
- Develop a model of the structure, its foundations, and the soil-structure interface that includes all the components that influence the response significantly, and determine suitable member properties.
- Identify important modes of response.
- Establish capacity/demand ratios for critical elements of the as-existing structure.
- With WSU, develop and evaluate suitable retrofit strategies for outrigger bents in general and the SR 99–Spokane Street structure in particular.

### **1.3 Outline of the Report**

The report is organized by chapters. In Chapter 2, past research on outrigger systems is reviewed. Chapter 3 describes the development of the analytical model. A number of subsidiary studies were needed to determine the best way to model certain components, such as the soil-foundation-structure interaction and the jacketed columns, and they are included in the description. Chapter 4 summarizes the results of the analyses. Chapter 5 contains a description of the proposed retrofit measures, including the vulnerabilities that they are intended to address, the way that they work, and the extent of the mitigation that they will provide. Chapter 6 contains a summary of the work, the conclusions of the analytical studies, and recommendations for both implementation and further research.

## 2 PREVIOUS WORK

Previous earthquakes have highlighted the vulnerabilities of outriggers subjected to lateral loading, most notably the collapse of the Cypress Street Viaduct in the Loma Prieta earthquake (Housner et al. 1990). Damage to outrigger bents in previous earthquakes prompted several departments of transportation, most notably the California Department of Transportation (CALTRANS), to initiate several research studies (Thewalt and Stojadinovic 1995, and Ingham et al. 1997) to understand and improve the response of outrigger bents. Several other studies on outriggers have also confirmed the potential for damage under seismic loading.

Several features of structures containing outrigger bents suggest that their response might differ from that of conventional bridge bents. First, the structure is inherently asymmetric, so rotation about a vertical axis is likely. This behavior induces additional displacements at columns distant from the center of rotation. Second, longitudinal motion of the superstructure induces torsional moments in the outrigger beams. Outrigger beams in older structures are particularly vulnerable because the transverse reinforcement often consisted of open stirrups, rather than the closed hoops that are best suited to resist torsion. Third, the knee joints in older structures were often poorly confined, rendering them vulnerable to joint shear and anchorage damage.

The previously conducted studies and the potential vulnerability of the SR 99 structure based on its age and the nature of its reinforcing details provided the impetus for both the research study described herein and the companion experiment research study (McLean and Shattarat 2004).

This chapter reviews some of the previous studies on outriggers and introduces the program of physical tests conducted at Washington State University (WSU). A previous analytical evaluation of the SR 99–Spokane Street over-crossing was conducted by WSDOT (Zhang et al. 1996). In the latter part of the chapter, that study is reviewed to provide a basis for, and comparison with, the current research effort.

## 2.1 Experimental Evaluation of Outrigger Bents

Experimental research has been conducted to establish the seismic response and vulnerability of outrigger bents. In addition, various retrofit options have been studied. However, because detailing practices vary from region to region and bridge to bridge, the findings of the previous experimental studies may not be directly applicable to all outriggers. Nonetheless, they provide insight into the behavior of outrigger systems in general and are reviewed here for that purpose.

In response to the poor behavior of outrigger joints in the Loma Prieta earthquake, CALTRANS initiated a study to evaluate the response of and develop retrofit measures for outrigger bents. Thewalt and Stojadinovic (1995) performed a series of tests on half-scale models of existing and retrofitted outrigger systems. The objective was to study the behavior of existing outriggers under bi-directional loading and develop retrofit strategies as needed. The two specimens were sub-assemblages that represented a part of a typical outrigger bent, and they consisted of part of a beam, a joint, and part of a column (see Figure 2-1). Bi-directional loading histories were used to simulate a wide range of effects, including beam torsion. The bar details included longitudinal beam top reinforcement hooked at the outer perimeter of the joint and spliced with longitudinal straight column bars. There was no transverse joint reinforcement. These details are similar to the ones in the SR 99 structure. During in-plane loading, diagonal cracks appeared in the joints under both opening and closing moments, and combined shear and torsion cracks appeared in the beam under out-of-plane loading. The researchers reported that lateral load carrying capacity was lost as a result of failure of the column and beam bar splices around the perimeter of the joints. The measured joint shear stress at the observed “failure point” for the first specimen was  $4.43\sqrt{f'_c}$  and for the second specimen was  $5.90\sqrt{f'_c}$ ; the associated displacement ductility was 1.5 for the first specimen and 2.0 for the second. This is assumed to be at or near the peak load.

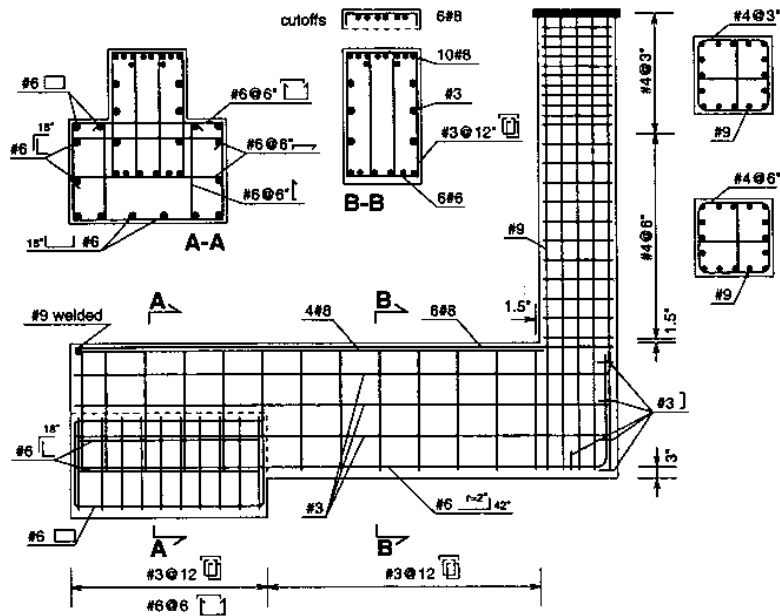


**Figure 2-1: Details of As-Built Test Specimen (Courtesy of Thewalt, Stojadinovic, 1995)**

Thewalt and Stojadinovic proposed two retrofit schemes, which they called the “ductile” upgrade strategy and the “strong” upgrade strategy. The ductile strategy attempted to provide larger displacement ductility capacity without necessarily increasing the strength of the system. To do this, a reinforced concrete jacket was placed around the outrigger beam and joint. The strong strategy attempted to force plastic hinging into the column while strengthening the other elements. This strategy was executed by bolting steel plates around the perimeter of the beam and joint, as well as welding a wide flange beam in the area of the joint, which the researchers deemed critical. The same loading pattern that was applied to the as-existing specimens was applied to the retrofitted specimens. The displacement ductility on the ductile system increased to 8.2 in the transverse direction and 6.0 in the longitudinal direction. Quantitative displacement ductilities were not provided for the strong system, but larger displacements were achieved because the steel plates provided confinement, which led to good anchorage of the column bars.

CALTRANS simultaneously sponsored a research effort conducted at the University of California, San Diego (Ingham et al. 1997) to evaluate the vulnerability of the outriggers in the I-980 Southbound Connector Bridge in Oakland, California, which collapsed in the Loma Prieta earthquake. The researchers performed tests on a 1/3-scale outrigger that consisted of a relatively short beam supporting a box girder deck. The “as-built” joint contained longitudinal beam top reinforcement hooked at the perimeter of the joint and spliced with the longitudinal straight column bars (see Figure 2-2). Very little transverse reinforcement was provided within the joint ( $\rho_s = 0.07$  percent extending from the column, and no transverse reinforcement extending from the beam), and the researchers suggested that the joint was effectively unconfined. The test joint was subjected to cyclic in-plane loading, and the damage was noted. Under closing moments, diagonal splitting occurred within the joint during the first cycle at the yield strength of the specimen. The researchers reported that the corresponding strength deterioration resulted from damage to the lap splice of the beam and column bars around the perimeter of the joint.

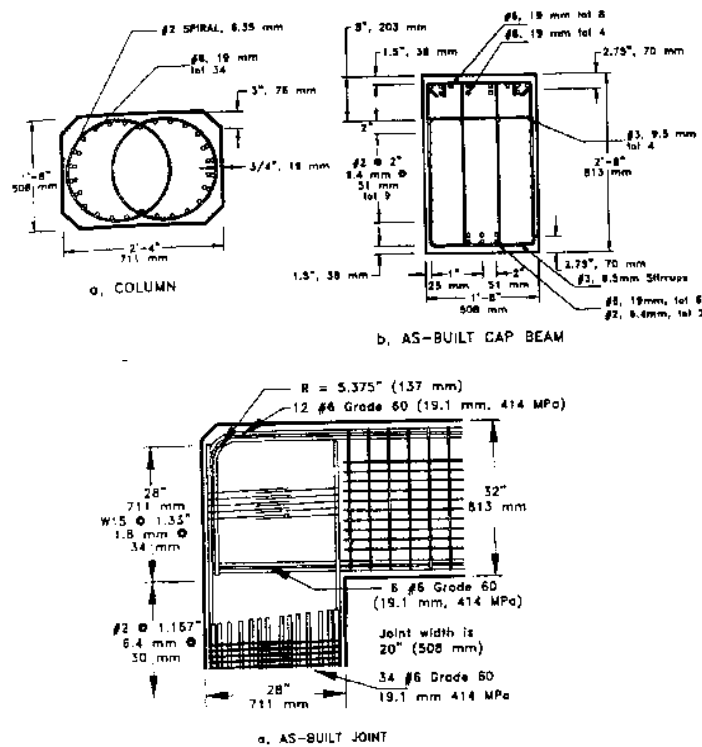
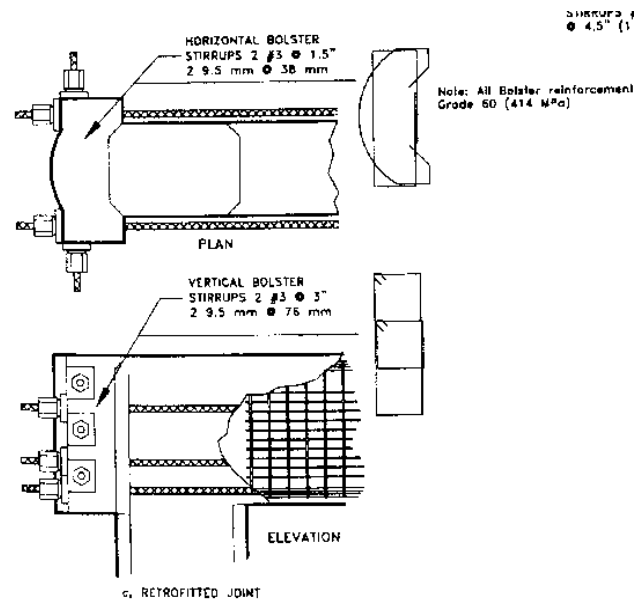


Figure 2-2: Details of As-Built Test Specimen (Courtesy of Ingham et al. 1997)

Ingham et al. also tested a retrofitted outrigger that consisted of adding a bolster to the end of the joint with external prestressing tendons extending from the joint along the sides of the beam (see Figure 2-3). Additional tendons were provided in the perpendicular direction in the bolster. The objective of the retrofit was to prevent inelastic action in the joint and cap beam, as well as failure of the lap splice around the perimeter of the joint. The specimen was subjected to the same loading as the as-built specimen and was able to achieve a displacement ductility of 2.0 before strength degradation occurred as a result of opening moments. Significant loss of strength due to closing moments did not occur until a displacement ductility demand of 3.0. The test results showed that the beam remained elastic, and the loss of strength was due to degradation caused by high joint shear stresses while the lap spliced remained intact. The prestressed bolster provided some confinement and presumably aided in preserving the splice.



**Figure 2-3: Details of Retrofitted Test Specimen (Courtesy of Ingham et al. 1997)**

Griezic, Cook, and Mitchell (2001) conducted cyclic in-plane tests on a 1/4-scale outrigger bent, including the beam, column, and joint, to evaluate the performance of a typical outrigger in an existing Montreal bridge structure. No transverse reinforcement was

provided in the joint, and the beam bottom bars were straight and had a shorter embedment than required by current code (see Figure 2-4). In contrast to Ingham's and Thewalt's tests, the reinforcement extending around the outside of the joint was not spliced. Rather, continuous bars ran along the beam, around the perimeter of the joint and down the column. Axial load representing gravity load on the column and a lateral load was applied to the tip of the column of the inverted specimen. Diagonal cracking was observed in the joint, as well as flexural and shear cracking in the beam and eventually the column, before yielding occurred in the column. Loss of lateral load capacity occurred for two reasons: anchorage failure and pullout of the poorly embedded beam bottom bars (which were on the top in the inverted specimen) under opening moments, and excessive joint shear and anchorage failure of the intermediate column bars under closing moments. Significant spalling was observed around the outside of the joint; however, no noticeable circumferential cracking was observed.

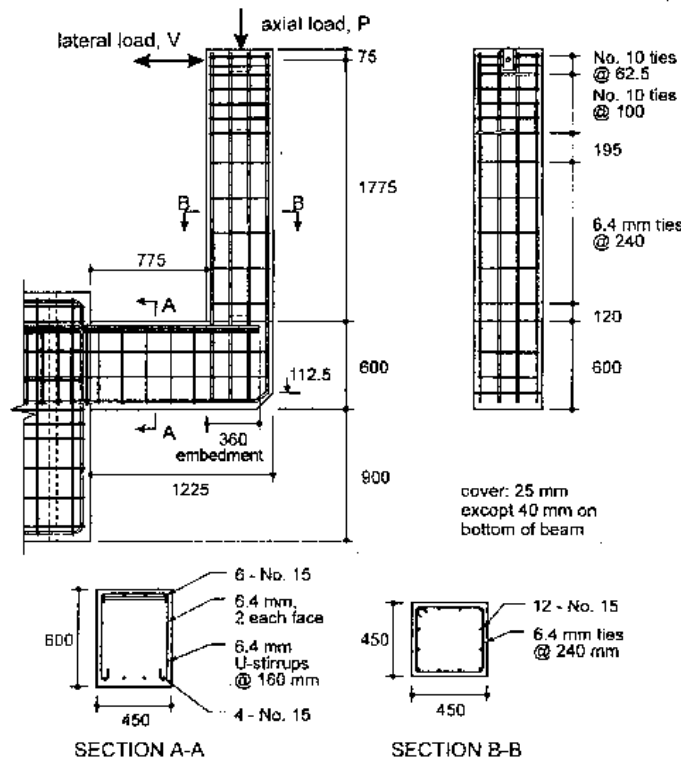


Figure 2-4: Details of As-Built Test Specimen (Courtesy of Griezic et al. 2001)

A retrofitted specimen was also tested by Griezic et al. It consisted of a circular concrete-filled steel jacket around the as-built column and a rectangular reinforced concrete sleeve around the as-built beam and joint. The objective of the retrofit was to provide confinement around the column, increase the strength of the beam, and increase the strength and confinement of the joint. The retrofit would be judged a success if ductile hinging occurred in the column while the beam and joint remained elastic. The specimen was subjected to cyclic loading and was able to achieve a displacement ductility of 8.0 without significant loss of load carrying capacity. Energy was dissipated through plastic hinging of the column, and the eventual loss of lateral load capacity was caused by fracture of the column bars at a displacement ductility of 10. No brittle response mechanisms were observed in the joint and beam.

## **2.2 Experimental Evaluation of SR 99 Outrigger Bents**

To evaluate the as-existing capacity of, and potential retrofit strategies for, the outrigger bents of the SR 99–Spokane Street over-crossing, WSDOT initiated an experimental research study. This study, conducted at WSU (McLean and Shattarat 2004), served as a companion project to the research study described herein. The experimental research findings were used by the UW research team to establish the global and local capacities of the outrigger elements. Those capacities, and the methods used to evaluate them, are presented in Chapter 4. A brief description of the experimental research program follows. A full description of the experimental findings may be found in McLean and Shattarat (2004).

The experimental research consisted of three, 1/3-scale outrigger specimens from the SR 99–Spokane Street over-crossing representing the as-existing conditions, and four retrofitted specimens (McLean and Shattarat 2004). The as-existing specimens reflected conditions in the field, and therefore the columns were fitted with concrete-filled steel jackets, but the beams and joints were as originally built. Two of these specimens (labeled “short”) consisted of a short outrigger beam and represented a scaled version of Bent 20, as described in Chapter 3. The third specimen (labeled “long”) consisted of a

long outrigger beam that was designed to represent the Bent 36 outrigger on the south concrete structure.

Each specimen consisted of part of the beam, part of the column, and a joint but was tested “upside down” relative to its orientation in the bridge, i.e., the beam was near the floor and the column projected upwards, as indicated in Figure 2-5. The specimens were cast upright in two pours, and a large concrete block was used to represent a fixed connection between the beam and the deck. The part of the column adjacent to the joint was enclosed in a steel jacket, with a gap between the end of the jacket and the face of the joint. To reduce the weight of the specimen, the remainder of the column was represented by a steel section designed to remain elastic at the approximate failure load of the specimen and to provide the same stiffness as the jacketed concrete column that it replaced. The steel section was connected to the top of the column through six high-strength bolts embedded into the concrete. A constant axial load representing the self-weight, as well as anticipated seismic loads due to closing moments, was applied to the top of the column. Cyclic lateral loads were then applied to the top of the column, which approximated the inflection point.



**Figure 2-5: Washington State University Test Set-Up for the “Short” Specimen**  
*(Courtesy of Washington State University)*

The reinforcement details in the test specimens were chosen to simulate the details used in the bridge (see Figure 2-6 for the “short” specimen and Figure 2-7 for the “long” specimen). Some of the details were similar to those used in the specimens in the studies described previously. The outside column and beam bars (top beam bars in the prototype but bottom bars in the as-tested orientation) were bent around the perimeter of the joint, thereby creating a lap splice within the joint. In the long specimen, the inside beam bars (bottom in the prototype) terminated in 180-degree hooks. All of the other beam and column longitudinal reinforcing bars in both specimens were detailed with straight anchorage lengths in the joint. A minimal amount of column transverse reinforcement was extended into the joint but provided very little confinement.

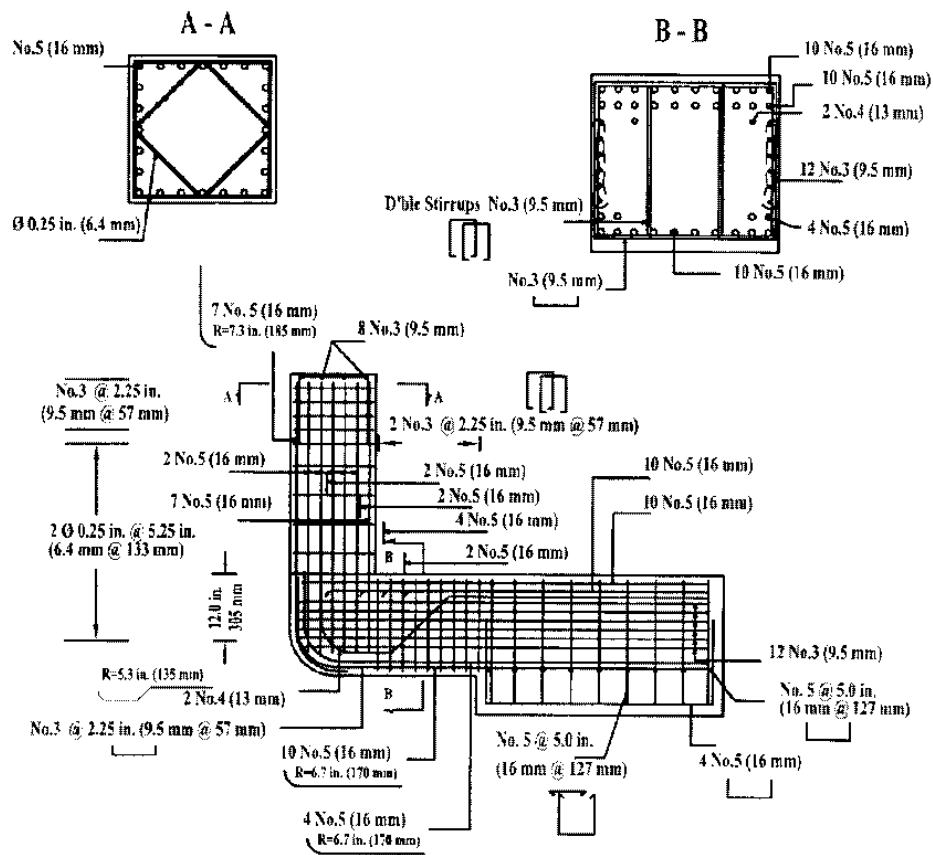


**Figure 2-6: Washington State University “Short” Specimen Details** (Courtesy of Washington State University)

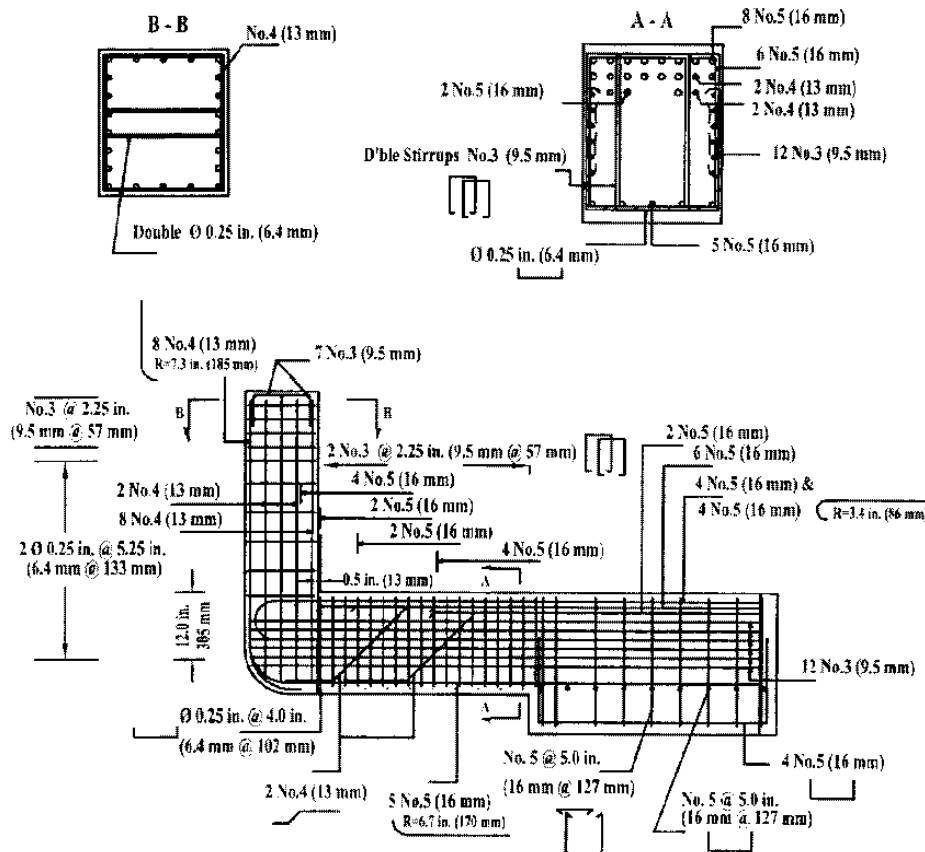


**Figure 2-7: Washington State University “Long” Specimen Details (Courtesy of Washington State University)**

The measured concrete compressive strengths and reinforcement yield and ultimate strength for the test specimens are shown in Table 2-1. As seen in figures 2-6 and 2-7, the top and bottom longitudinal beam reinforcements were No. 5 bars for both specimens, and for the column, the short specimen consisted of No. 5 longitudinal bars, while the long specimen consisted of No. 4 longitudinal bars. In the short specimen, the column transverse hoops were made from 0.25-in.-diameter wire, while the beam contained No. 3 transverse ties and stirrups. The long specimen column consisted of 0.25-in.-diameter transverse hoops, while the beam consisted of No. 3 transverse stirrups and 0.25-in.-diameter ties.

**Table 2-1: Measured Material Properties for WSU Test Specimens**

	f'c (psi)		fy (ksi)				fu (ksi)			
	Beam	Column	0.25	#3	#4	#5	0.25	#3	#4	#5
As-Existing	5400		44				77			
Short	4240	4168	51.2	49.3	53.4	53.6	51.2	49.3	87.5	79.6
Long	4240	4168	51.2	49.3	53.4	53.6	51.2	49.3	87.5	79.6

The corresponding material strengths for the as-existing bridge structure were also tabulated. These values were estimated by WSDOT engineers and were based on material strengths typical of those in use when the over-crossing was constructed, modified to reflect the effects of aging. They are discussed in further detail in the following chapter.

Of the as-existing specimens, in-plane loading was applied to one short and one long specimen, and out-of-plane loading was applied to one short specimen. Test observations suggested that the details of the outer longitudinal reinforcement, spliced around the perimeter of the joint, played a major role in the failure of the system. In both specimens subjected to in-plane load, significant circumferential cracking occurred around the perimeter of the joint at the hooked lap splice, as shown in figures 2-8 and 2-9. In addition, for the long specimen, diagonal joint shear cracking due to closing moments accompanied the radial circumferential caused by opening moments. Splitting in the plane of the exterior column bars was also observed in the short specimen.

In the short specimen subjected to out-of-plane load, shear and torsion cracks occurred on the bottom and sides of the beam (Figure 2-10), and splitting initiated in the plane of the exterior column bars. A more detailed description and evaluation of the test results are presented in Chapter 4.



**Figure 2-8: Damage to the “Short” Specimen Under In-Plane Loading** (*Courtesy of Washington State University*)



**Figure 2-9: Damage to the “Long” Specimen Under In-Plane Loading** (*Courtesy of Washington State University*)



**Figure 2-10: Damage to the “Short” Specimen Under Out-of-Plane Loading**  
*(Courtesy of Washington State University)*

The retrofit scheme proposed by WSU consisted of providing a continuous concrete-filled circular steel jacket around the beam and joint. The new jacket was not made continuous with the existing column jacket, so that inelastic rotation could occur at the top of the column. The objective of the retrofit was to prevent the degradation of the beam and joint of the outriggers that had been observed in the as-existing tests. The four specimens included two “short” retrofitted specimens, one “long” retrofitted specimen, and a retrofitted split column specimen with a long outrigger beam, representative of Bent 34 at the south end of the as-existing structure.

The first “short,” “long,” and “split” specimens were subjected to in-plane cyclic loading, while the second “short” specimen was subjected to out-of-plane loading. All load patterns were the same as the ones applied to the as-existing specimens. All four of the retrofitted specimens achieved significantly higher displacement ductilities than their as-existing counterparts. The stroke limit of the actuator was reached before lateral load carrying capacity was lost, and none of the failure mechanisms observed in the as-existing specimens occurred for the retrofitted specimens.

### **2.3 WSDOT Seismic Evaluation of the SR 99–Spokane Street Over-Crossing Structure**

To determine the seismic vulnerability of the as-built SR 99–Spokane Street over-crossing, WSDOT conducted an in-house study (Zhang et al. 1996). The objective of the study was to establish the seismic demands on the structure and compare them to established capacities to evaluate the need for retrofitting the structure. To simulate the seismic response of the structure, WSDOT conducted three-dimensional, elastic dynamic analyses. Three separate models were used to represent the structure: the north concrete structure including the west off-ramp, the south concrete structure, and the intermediate three-span steel structure.

The models of the concrete structures consisted of a single spine girder frame element to model the deck in the longitudinal direction and frame elements to represent the beams and columns. Cross-section properties of the rectangular frame element used for the spine girder were chosen to provide stiffness properties comparable to those of the box girder deck. The split columns between each of the frames were modeled, and the frames were allowed to move independently without any pounding interaction.

For all concrete elements, the moment of inertia increased by 50 percent of the gross value to account for cracked section properties. The concrete compressive strength was assumed to be 150 percent of its specified value of 3600 psi to account for the effects of aging. The yield strength of the reinforcing steel was assumed to be 110 percent of its nominal value (this was not mentioned in the report but is assumed to be 40 ksi). The resulting assumed strengths were 5400 psi and 44 ksi, respectively.

The pile cap and pile foundation system were modeled with linear spring elements. A generic response spectrum from ATC-6-02 (ATC 1983) was used for the spectral analysis. Neither soil structure interaction nor site-specific ground motions were included. A total viscous damping of 5 percent was used for all modes of vibration of the system.

A detailed model that used quadrilateral elements for the deck was also developed for one of the frames of the bridge so that the influence of the modeling of the deck could be determined. It was determined that the column axial forces differed for each model. Therefore, a scaling procedure was used in the global model to account for the discrepancies due to the simplifications introduced by use of the single spine beam. Details of the scaling procedure were not presented.

A detailed finite element model of the steel structure was generated by using quadrilateral elements for the webs of the plate girders and cross beams supporting the bridge deck. The flanges of the girders and cross beams, the columns, and the braces were all modeled by using frame elements. The southernmost frame of the north concrete structure and the northernmost frame of the south concrete structure were also included in this model since they share mid-height split columns with the steel structure. Although not specifically mentioned by Zhang et al. (1996), it is assumed that a response spectrum analysis was also performed on this structure.

A demand-capacity analysis was performed on some of the elements of the structure. The column analysis was based on ATC 6-02 (ATC 1983) and considered flexure, shear, anchorage, and lap splice failure as potential response mechanisms. From the analyses, the investigators determined that many of the columns had potential for failure under one or more of the response mechanisms. An analysis on the foundation system also showed that the footing and pile system had potential for failure. Finally, an analysis of the outrigger beams was performed. A demand-capacity evaluation on beam and joint torsion was performed with capacities determined from a procedure presented by Collins and Mitchell (1991). The analysis method was not presented in detail, but Zhang et al. concluded that the outriggers were vulnerable under seismic loads.

A four-step retrofit plan was prepared that included fitting the concrete columns with steel jackets, retrofitting the outriggers and foundations, replacing the intermediate steel framed structure, and eventually replacing the structure in its entirety. Since the report's publication in 1996, only the concrete column retrofit has been implemented.

## 2.4 Field Observation of the SR 99–Spokane Street Over-Crossing

A field observation of the structure was performed on October 22, 2002. Although the structure is approximately 50 years old and has experienced two moderate earthquakes (in 1965 and 2001), the outrigger beams and joints showed relatively little seismic damage. In fact, the most extensive cracking was in the box girder and was due to flexure and shear under gravity loading.



**Figure 2-11: Outrigger at Bent 11**

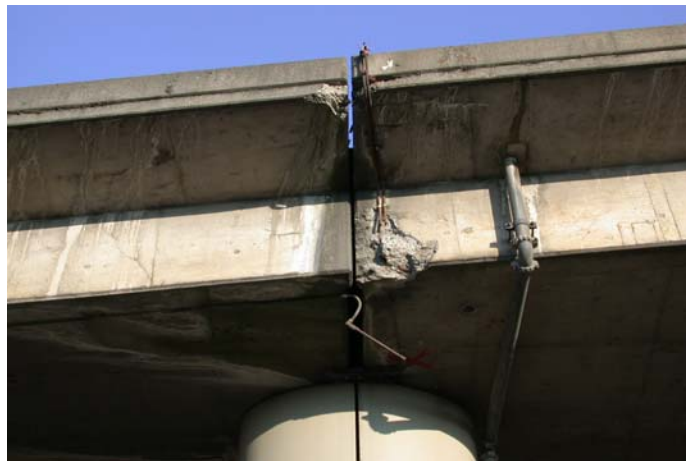


**Figure 2-12: Pounding Damage Observed at the Expansion Joint at Bent 13**

Figure 2-11 shows spalling around the exterior of the joint at Bent 11 and cracks in the beam at the underside of the deck. This amount of damage is typical of that seen in the outrigger joints. In addition, pounding damage was observed at some of the expansion joints between the split columns, as seen in Figure 2-12.

## 2.5 Summary

Only a small number of studies have been conducted on the seismic behavior of outrigger bents. Those studies show that damage generally concentrates in the joints rather than the members. Joints with bars spliced around the exterior corner of the joint seem particularly vulnerable, especially when the joints contain little or no transverse reinforcement. If the splice is the critical component of the outrigger, it is possible that other, non-outrigger joints that contain the same detail may be vulnerable to this failure mechanism. These joints may present the added problem of being difficult to retrofit, depending on the geometry of the surrounding structural and non-structural elements.

The interaction of different response mechanisms, particularly with regard to the progression of degradation and the accumulation of damage, presents additional challenges. It appears that damage due to one action may weaken the capacity in other response mechanisms, and this becomes apparent either in cyclic in-plane loading or bi-directional loading. One example, occurring during in-plane motions, is the development of joint circumferential splits caused by opening moments that weaken the exterior splice and thereby reduce the capacity of the joint under closing moments. Another example is beam diagonal cracking due to high in-plane shear demands which reduces the capacity of the beam in combined torsion and out-of-plane shear as a result of out-of-plane loading.

The reinforcing details in the outriggers of the SR 99 structure vary among bents and differ from those used in other structures of the same era. However, the common features of poor confinement (especially in the joints), inadequate embedment lengths, and unconfined curved splices around the outside of the joints suggest that all of these structures have vulnerabilities that are specific to outrigger systems. In particular, the

experimental research studies of Thewalt and Stojadinovic (1995) and of McLean and Shattarat (2004) are helpful in understanding the nature of the potential failure mechanisms and the strength and ductility capacities of the as-existing systems.

## **3 MODELING OF THE AS-EXISTING STRUCTURE**

### **3.1 Introduction**

Seismic evaluation of a bridge requires computation of the demands on, and capacities of, the components. To determine the demands on the SR 99–Spokane Street over-crossing structure, a dynamic structural analysis was performed. To ensure valid results, an accurate simulation of the structural configuration, element properties, soil properties, and ground motions was needed. This chapter describes the development and details of these features of the model.

Ideally, the elements would all be nonlinear and would be capable of tracking the strength and stiffness changes that occur with concrete cracking and steel yielding. However, such a full nonlinear analysis with a 3-D model was deemed to be too computationally demanding so, as a compromise between computational efficiency and accurate representation of the physical structure, a limited nonlinear analysis was conducted with SAP 2000 (Computers and Structures Inc). That program permits the use of a small number of nonlinear elements while retaining most of the computational efficiency of a linear analysis. Thus, nonlinear elements were used only where necessary, for purposes such as the contact elements between individual frames. The numerical results of the analyses and their use in the seismic evaluation procedure are presented in Chapter 4.

The modeling approach used here differed from that used in previous analyses of the structures (Zhang et al. 1996). The principal differences were as follows:

- Compression-only gap elements were used between the individual frames to simulate the behavior of the expansion joints.
- The adjacent structures were modeled, albeit at a simplified level, in order to include their effects on the behavior of the main structure.

- The deck was modeled as a distributed structure, rather than as a single beam. (This required many more elements than had been used previously but provided more realistic modeling of the interaction between the deck and supporting frames.)
- The columns were represented in detail to reflect the effect of the jacket on their stiffness and yield displacement.
- Soil-foundation-structure interaction was simulated by using springs and dampers whose values were determined specifically for the site conditions.
- Site-specific ground motions, for three hazard levels, were developed and used.
- The structure was subjected to a comprehensive seismic evaluation by using experimental results specific to the bridge.

For convenience, the model description is broken into sections. The overall geometry of the structure is defined in Section 3.2; the soil properties, soil-foundation-structure interaction, and ground motions are described in Section 3.3; and a comprehensive description of the structural model is given in Section 3.4. The structure had been partially retrofitted when the project started, so in that state it is referred to as the “as-existing” structure. The topology and member sizes of the north concrete structure and the adjacent peripheral structures in their as-existing form were defined from structural drawings and a visual inspection of the bridge. The material properties were estimated from available resources.

The ground conditions were studied extensively to generate the appropriate soil properties and site-specific ground motions. Soil-foundation-structure interaction elements were used in the model.

To validate the model, the time history results were compared with the results of spectral analyses of each frame individually, and the predicted impacts between adjacent frames were compared with the evidence of pounding that was visible in the field.

## 3.2 Overview of the As-Existing Structure

### 3.2.1 Bridge Configuration

The SR 99–Spokane Street over-crossing structure consists of four main-line structures. Starting from the north end, they are a 25-bent north concrete approach structure, a three-bent steel structure that carries traffic over the Spokane Street Viaduct, a 16-bent south concrete approach structure, and a 457-foot-long timber trestle structure. Each structure is constructed independently and, apart from impact interactions during longitudinal ground motions, may be considered to respond independently.

To maintain acceptable run times for the analyses (i.e., no more than about 8 hours) either the whole structure could be modeled at a coarse level or a portion of it could be modeled in greater detail. Initial experiments (for example, with the different deck models described in Section 3.4.3) showed that a large number of elements was needed to represent properly the behavior of the superstructure, even in one frame. The weak interconnectivity between the north and south concrete structures also suggested the possibility of analyzing only half of the bridge. Thus a decision was made to model only the north concrete structure and those others that are contiguous with it. The concrete structure was simulated in considerable detail, while the adjacent abutments, off-ramps, and steel structure were modeled at a less refined level.

The bridge deck rises from an elevation of 22.91 feet at the north end to 57.37 feet at the steel section and then gradually decreases in elevation to 38.80 feet at the south end of the south concrete structure.

Figure 3-1 shows the north concrete structure, which is the focus of this study, and surrounding structures. The north and south concrete structures consist of an 80-foot-wide by 4-foot 6½-inch-deep box girder deck that spans between transverse frames composed of rectangular concrete beams and columns. Each column is constructed on a concrete pile cap supported by a group of piles. At several locations along each structure,

the outer column in the frame has had to be located away from the edge of the deck to avoid interference with the railroad that passes under the structure at an oblique angle. In those cases, outrigger beams are used to carry the gravity loads from the deck to the columns. Although almost all of the main-line and outrigger columns have been retrofitted with steel jackets, the outrigger beams and beam-column joints remain in their original state and formed the primary focus of the study. A detailed description of the model of the north structure, which emphasized the outrigger bents, is presented in Section 3.4.

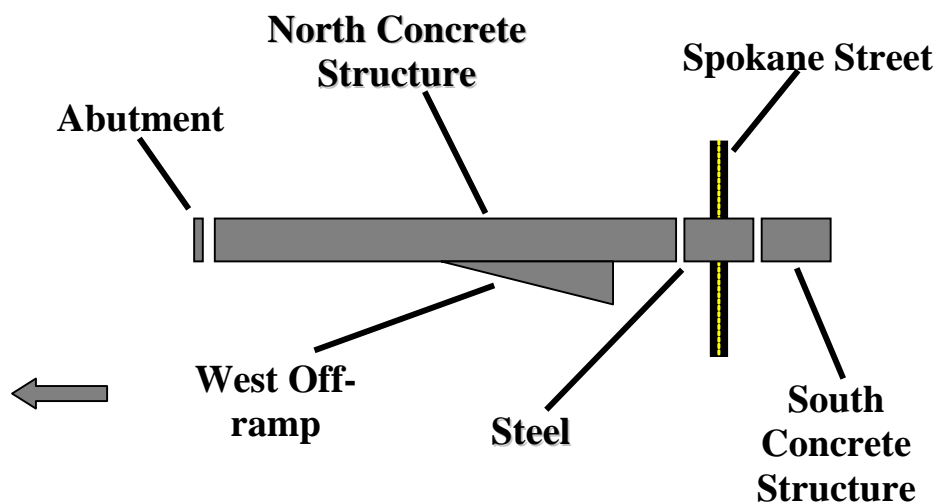


**Figure 3-1: Layout of North Concrete Structure**

At the north end of the concrete structure, an expansion joint separates the box girder from a concrete abutment. At its south end, another expansion joint separates it from the steel structure, which consists of a concrete deck on built-up steel beams and plate girders, supported by wide-flange steel columns. The columns rest on pile foundations, each of which consists of a concrete pile cap and a group of piles.

The north structure contains seven frames with four or five bents per frame. Each frame is given a number (1 to 7), and the frames are numbered sequentially from north to south. There are 25 bents in all, also numbered sequentially from north to south. Each frame is separated from the adjacent one by a 1.5-inch gap. At the gaps, split columns support the

deck and permit thermal expansion, as shown in Figure 3-2. At some of the taller bents (16, 19, and 25), the rectangular split columns merge into a single rectangular column at approximately mid-column-height, while at bents 5, 9, 13, and 22, they are split over the whole height above the pile-cap. At Bent 1, the columns share a footing with the abutment. At the southernmost bent, Bent 25, the deck is supported by rocker bearings placed on top of the transverse frame beam.

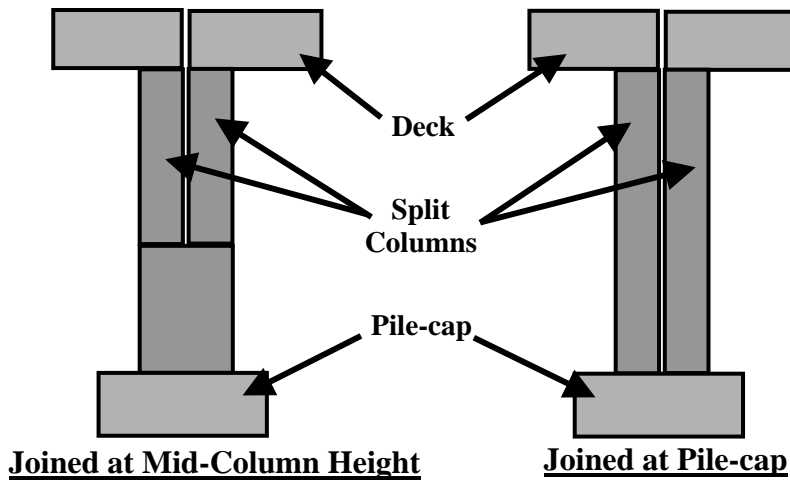


**Figure 3-2: Split Column Details**

Seven bents of the north concrete structure contain outriggers. Table 3-1 provides details of their locations and member dimensions. No beam length is provided for Bent 21 because the outrigger column frames directly into the deck transverse beam.

**Table 3-1: North Concrete Structure Outrigger Bent Dimensions**

Bent #	Column			Beam		
	Length (ft.)	Width (ft.)	Depth (ft.)	Length (ft.)	Width (ft.)	Depth (ft.)
9	34.29	3.0	3.75	29.75	2.25	4.5
10	35.46	3.25	4.0	16.5	3.75	4.5
11	37.14	3.25	3.25	5	3	4.5
12	38.33	3.75	3.25	7.25	4.25	4.5
20	49.20	3.75	3.75	6.67	4.75	4.5
21	50.51	3.75	3.75	-----	3.75	4.5
25	54.42	2.75	3.75	11.25	2.375	4.5

In addition to the north abutment and the steel structure, an off-ramp exists at the west side of Bent 16. The off-ramp structure was designed in 1981 and consists of a concrete slab supported by precast, prestressed girders that span between cap beams. Each beam is supported by a single column bent, supported in turn on a pile-cap and a group of piles. Because the south timber structure and the south concrete off ramps were expected to have a negligible effect on the response, they were not included in the analysis.

### 3.2.2 Phase 1 Retrofit Measures

In 2000, WSDOT designed Phase 1 of the retrofit program, which called for strengthening of the bridge columns. The retrofit of the columns was completed before the Nisqually earthquake occurred in February 2001. Circular and elliptical steel jackets were placed around the square and rectangular columns, and the voids between the steel jackets and existing columns were filled with grout. The original column dimensions, and therefore the jacket dimensions, varied from column to column. The jackets were placed over the full height of the column with gaps of 2 to 4 inches at the top and bottom. The split columns, located between frames, were jacketed with either semi-circular or half-elliptical jackets. Figure 3-3 shows cross-sections of the retrofitted rectangular and split columns. Columns 25 in the north structure and 38 in the south structure, which are both outrigger columns, remained unjacketed because of railroad clearance requirements.

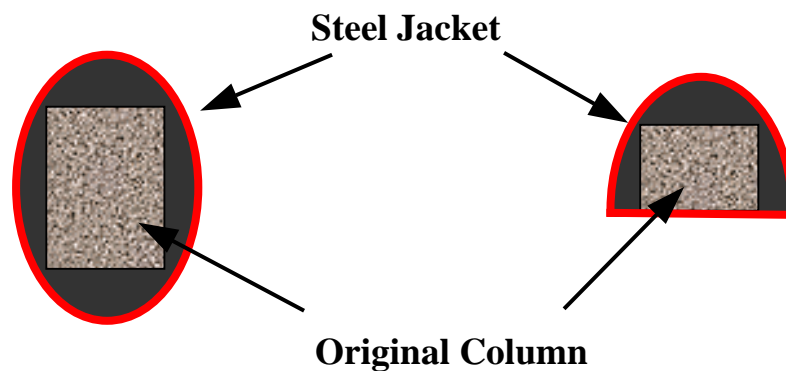


**Figure 3-3: Elliptical and Semi-Elliptical Steel Column Jackets**

### 3.3 Numerical Model of North Concrete Structure

To develop an analytical model of the north concrete structure, elements were needed to model the foundation, columns, beams, deck, and expansion joints. To facilitate development of these elements, several studies were performed to optimize processing time and ease of output review without compromising accuracy. The objective of these studies was to determine the type and connectivity of the elements to be used in the final model. Descriptions of these studies and the resulting modeling decisions are presented below. First an overview of the model is introduced. Next, the material properties are described. A significant effort was expended on developing an accurate representation of the deck, and the results of these detailed analyses of different deck representations are presented. A description of the modeling decisions regarding the beams, columns, and expansion joints follows. Finally, the structural damping and the effects of joint flexibility are discussed.

#### 3.3.1 Overview

The northern section of the SR 99–Spokane Street over-crossing was modeled by using the finite element analysis (FEA) program SAP2000 (Computers and Structures, Inc). The model includes the north mainline concrete structure, the abutment to the north of it, the steel structure to the south, and the west off-ramp (see Figure 3-4).

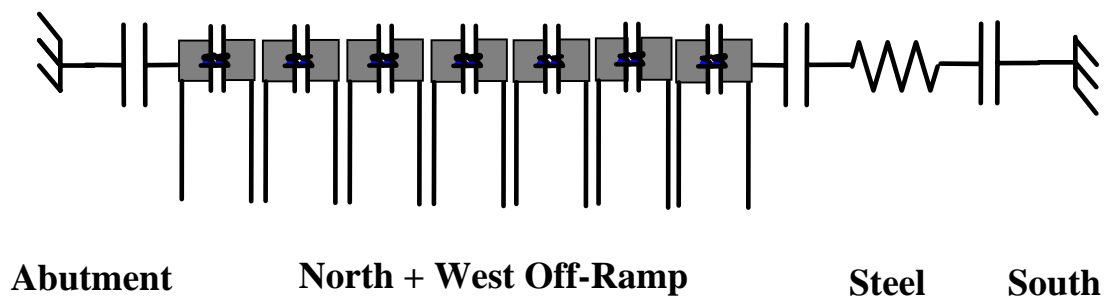


**Figure 3-4: Functional Representation of North Concrete Model and Peripheral Structures**

The north abutment and the south concrete structure were both represented as rigid blocks. Compression-only gap elements were used to model the expansion joints

between the individual frames and peripheral structures (shown as gaps in the figure). The complete computer model of the north and adjacent structures is shown in Figure 3-5.

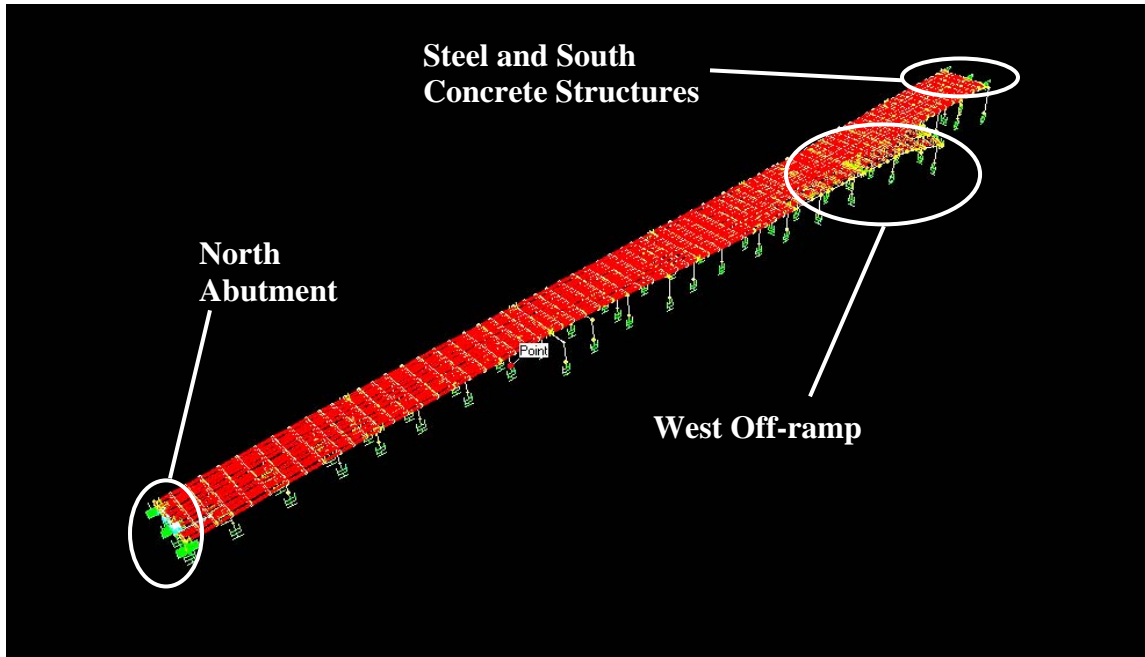


**Figure 3-5: Computer Model of North Concrete and Peripheral Structures**

### 3.3.2 Material Properties

Material properties are needed to define the stiffness of each of the structural elements. The as-existing concrete compressive strength and yield strength of steel were determined on the basis of the previous WSDOT study (Zhang et al. 1996). On the basis of data available from Priestley et al. (1996), Zhang et al. suggested using a concrete strength of 1.5 times the 28-day specified strength of concrete typically used in the 1950s when the structure as built. Because the structural drawings did not indicate a concrete strength, the material strengths specified in drawings from the adjacent Spokane Street ramps, which were designed in 1958, were assumed. Those drawings indicated a concrete strength of 3600 psi, so 5400 psi was used here. This is significantly less than the average strength of test cores (7882 psi) taken from the adjacent Alaskan Way Viaduct, which was constructed in the early 1950s. Therefore, it may be lower than the

real strength. The elastic modulus was based on the concrete strength and was calculated to be  $E_c = 57000\sqrt{f'_c}$  (psi), (ACI 2002).

A value for the elastic modulus of the grout between the original column and the steel jacket was also needed but was not available from site records. It is significantly stronger than the column concrete, so it might be expected to have a higher modulus. However, it contains no coarse aggregate, the absence of which would be expected to reduce the modulus. Therefore, a modulus based on a uniform strength of 5400 psi was used for the entire column region enclosed by the steel jacket. While more accurate values for these properties would be desirable, they were not available. Fortunately, the error introduced did not have a large effect on the predicted displacements because the stiffness of the jacketed section of the column proved to be much larger than that of the short, unjacketed regions at the ends. The properties of the unjacketed portion largely controlled the overall column stiffness and, therefore, the global displacements.

Grade 40 steel was typically used for structures built in the 1950s. Since the yield strength of steel was not specified on the drawings, Grade 40 steel was assumed for the SR 99–Spokane Street north concrete structure. A yield strength of 44 ksi was used for both the longitudinal and transverse reinforcement. This strength was based on a 10 percent overstrength factor, as recommended by Zhang et al. (1996). The west off-ramp was assumed to have material properties similar to those of the north structure. This assumption was based on the fact that its specified concrete strength was higher than that of the main line structure, but it had undergone fewer years of age-strengthening.

### **3.3.3 Numerical Representation of the Concrete Deck**

To develop the numerical model of the deck, four models with different deck representations were analyzed and compared. One model was then selected for use in the analyses of the whole structure. The different deck models are shown in figures 3-6 through 3-9. In order of increasing complexity, they consist of a single spine girder, multiple girders, a flat plate, and a full box girder.

In the interests of limiting the computational effort during the evaluation of the deck models, a simple, isolated 3-D frame that represented a portion of the bridge was used. The overall geometry consisted of a two-span, three-bent model. The 57-foot span and 80-foot width were used to replicate the typical span length and width of the prototype structure.

Within the model, each bent consisted of a two-bay transverse frame, and each frame had 48-ft bays with 1.5- by 4.5-ft beams. At all transverse frame locations, an outrigger bent extended 8 feet beyond each side of the bridge deck. The three rectangular columns that supported the outriggers were 1.75 by 3.25 ft in cross-section and 28 feet tall, and they were pinned at their bases to reduce the influence of the column bases—and, therefore, to increase the influence of the transverse beams—on the frame’s lateral resistance. In the interest of simplicity, and because the goal of the modeling effort was to compare the effects of using different representations of the deck, the concrete strength and stiffness were assumed to be uniform throughout the structure, and gross section properties were used for the beam and column members.. Within the model, a 2.25-ft-long rigid end zone was used at the top of the column to prevent column deformations within the depth of the deck.

Two types of analyses were conducted for each of the four models. First, each model was subjected to a static lateral load that was proportional to the weight of the structure, and the corresponding deck deflection was recorded. This was done separately in the longitudinal and transverse directions and provided an opportunity to compare the static stiffnesses of the different models. Then a modal analysis of each model was performed, and the periods for the corresponding modes in each model were compared. Because the masses of the different models were nearly the same, the modal periods reflected most strongly the models’ modal stiffnesses. They provided information that was slightly different from the static stiffnesses, because the latter were identified for the two directions independently, whereas the modal stiffness corresponded to a generalized coordinate rather than a specific direction.

The following paragraphs describe the deck elements and analysis procedures used for each of the models. A comparison of the results of the static and dynamic analyses follows.

In the first test model (referred to as Model 1), a single spine girder was used to represent the bridge deck, as shown in Figure 3-6. The stiffness of the entire deck was concentrated in one line element to represent the girder, and the mass was lumped at the nodes. This is the same representation that was used in the previous analysis performed by WSDOT (Zhang et al. 1996).

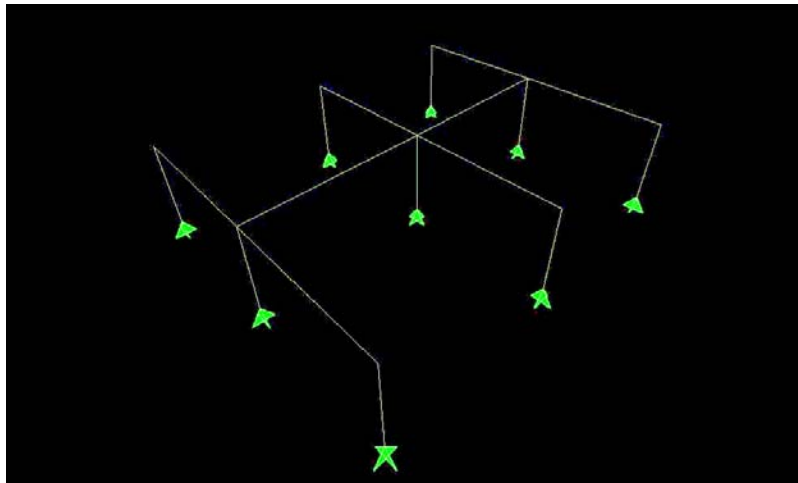


**Figure 3-6: Model 1 – Single Spine Beam**

The spine girder was represented as a single frame element, with the same bending stiffness as the real box girder deck. (The FEA program requires the user to input the cross-section dimensions, from which it automatically computes the section properties. However, the properties are applied to a single line element and do not account for finite dimensions of the zones where members intersect, unless the user specifically requires that.) This was achieved by computing the moments of inertia of the real deck, finding the rectangular shape that had the same properties, and using this shape for the frame element. Frame elements were also used to model the beams and columns.

For the static analysis, lateral loads were applied as a uniform line load along the length of the frame both parallel to the girder for the longitudinal direction and perpendicular to the girder for the transverse direction. The program automatically computes inertial loads from the cross-section dimensions, so the density of the concrete had to be artificially adjusted from its true value to account for the difference between the cross-sectional areas of the real box and the equivalent rectangular section used in the analysis.

In the second model (Model 2), each vertical web of the real box girder deck was represented by a separate girder using frame elements (see Figure 3-7). For the purpose of computing section properties, the exterior and interior webs were modeled as “C” and “T” sections, respectively, and the exact cross-section dimensions were input into the program. In each case, the effective flange width was assumed to be the distance between panel centerlines. The beam webs were 1 ft thick and 4.5 ft deep overall, and the deck elements were 6.5 in. thick to match the dimensions of the real deck. In each direction, static lateral loads were applied as uniform line loads to each beam in proportion to the associated tributary area. Because the cross-section dimensions of each component of the box girder were represented correctly by the girders, scaling the material density in the analysis was unnecessary.

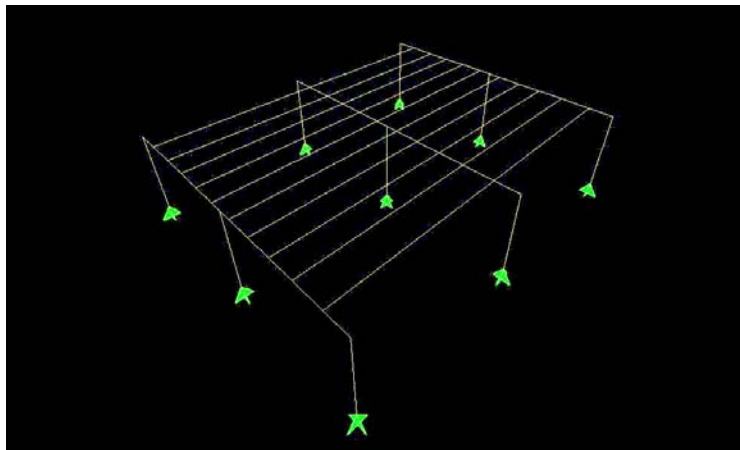


**Figure 3-7: Model 2 – Multiple Girders**

The third model (Model 3) consisted of a mesh of flat shell elements to model the deck, as shown in Figure 3-8. The shell elements were 4.29 ft. thick so that the deck model had

a bending stiffness equal to that of the real deck. In the static analysis, lateral loads were applied as a surface horizontal load (with units of force per unit area) on the shell elements in each direction. For the dynamic analysis, the density of the concrete was adjusted for the same reasons as in Model 1.

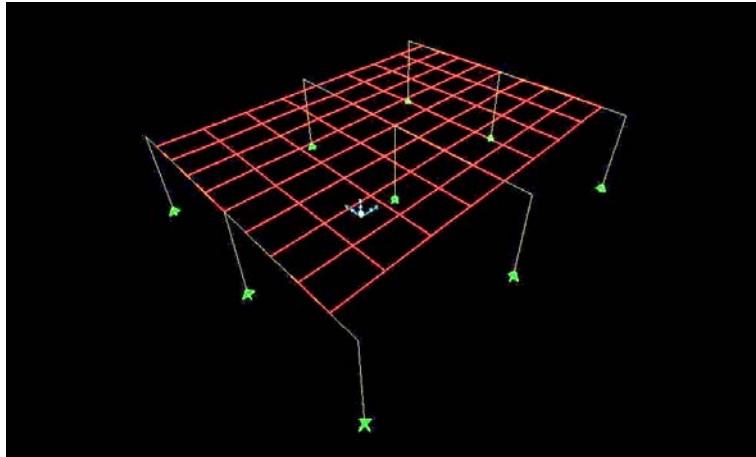


**Figure 3-8: Model 3 – Horizontal Flat Plates**

In the fourth model (Model 4), the deck was composed of horizontal and vertical shell elements that were dimensioned and positioned to represent the geometry of the real box section (see Figure 3-9). The thicknesses of the horizontal and vertical shell elements were equal to those of the real slab and webs, respectively. The flange elements were located at the mid-thicknesses of the real flanges. The transverse bent beams, which are the same depth as the box, were also modeled with shell elements (each was two elements deep), and the projecting outrigger beams and all columns were modeled by using frame elements. The columns and outrigger beams were connected to the shell elements of the transverse bent beam at the node connecting the two shell elements that represented the transverse bent beams. For the static analysis, lateral loads were applied to the horizontal shell elements as surface loads, with the load divided equally between the top and bottom slabs. Again, no scale factor was used for the concrete density.

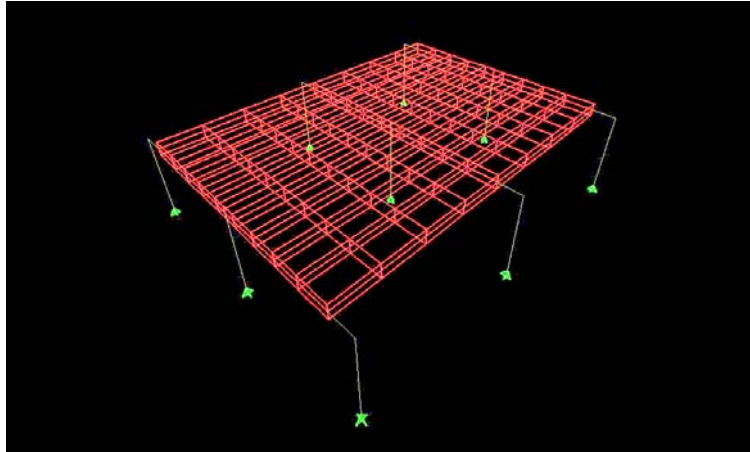


**Figure 3-9: Model 4 – Box Girder**

The displaced shape of Model 4 in the transverse direction showed that large local rotations were occurring at the node where the frame element of the outrigger beam joined the shell element of the deck. These rotations made the structure much more flexible in the transverse direction than a comparable structure in which the entire frame was composed of beam-column elements. The problem was attributed to the “drilling” stiffness of the plate elements and is illustrated in Figure 3-10. (This is the rotational stiffness of the plate about an axis normal to the plane of the plate. No rationale exists for computing this stiffness, and there is no consensus over the value to be used, so the problem is common in 3-D modeling using plate elements).

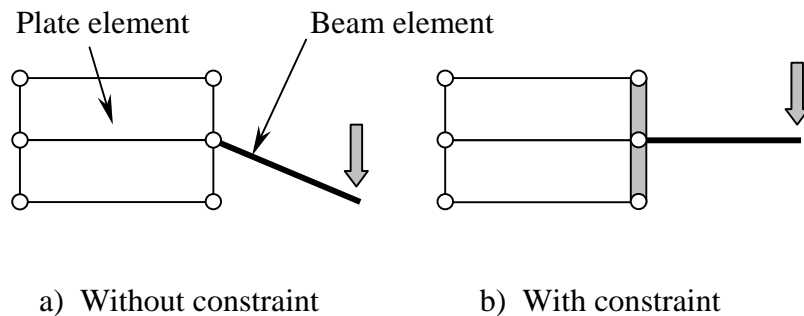


**Figure 3-10: Application of Beam (Rotational) Constraints to Connections between Plate and Beam Elements**

To overcome this problem, a detailed study of the local region was performed in which different options were evaluated. The solution chosen was to use “constraints” that

would slave the displacements of adjacent nodes. Rotational constraints (called “Beam Constraints” in the program) were introduced that forced the three nodes that lie in a straight line in the undeformed structure to remain in a straight line after loading (essentially forcing plane sections to remain plane in the part of the transverse beam that was represented by plate elements). Figure 3-11 illustrates the typical locations of this constraint. The use of vertical constraints among the three nodes in each group was also considered. Such constraints can prevent any change in the deck thickness due to loading, but in this case they also introduced spurious local stresses at the edge of the shell elements. Therefore, they were not used.

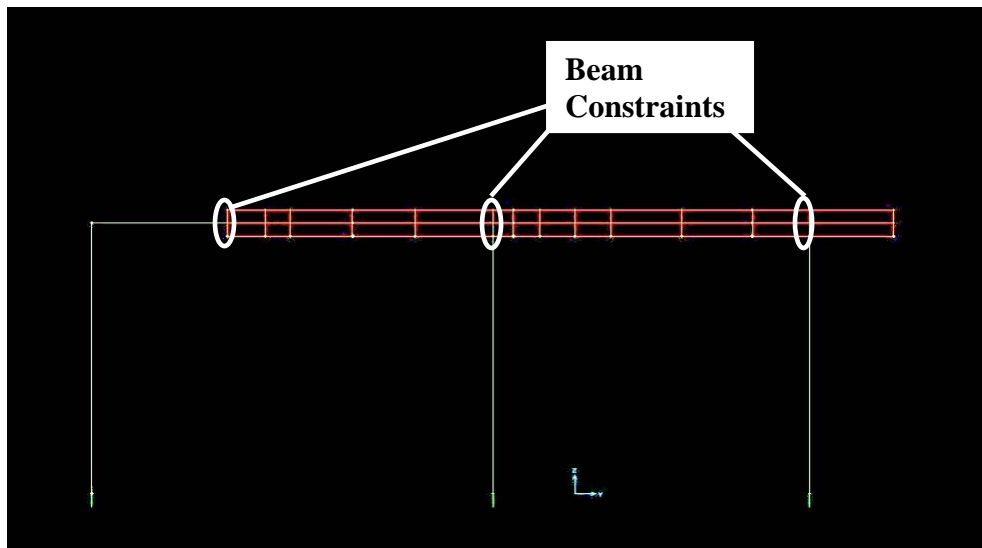


**Figure 3-11: Example of Beam Constraint Locations**

No true solution was available against which each model could be compared, so the models were evaluated by comparing them against each other. In particular, the displaced shapes were reviewed, and deformations that could not occur in the prototype structure were noted. The measures used for the comparisons were the fundamental periods and the displacements at the centerline of the deck resulting from static lateral load. The values for each model are shown in Table 3-2. The values in the transverse direction differed little among models because the stiffness in that direction depended most strongly on the modeling of the columns and transverse beams, rather than the deck. By contrast, in the longitudinal direction, results from the four models displayed

relatively large differences, primarily through the different connectivity arrangements for the deck elements.

**Table 3-2: Deck Model Lateral Displacements and Fundamental Periods**

	Displacement (in.)		1 <sup>st</sup> Mode Period (sec)	
	Longitudinal	Transverse	Longitudinal	Transverse
Model 1	1.21	0.19	2.16	0.88
Model 2	0.81	0.19	1.80	0.88
Model 3	0.71	0.17	1.70	0.83
Model 4	0.77	0.17	1.82	0.87

Model 1 provided the longest periods and the largest displacements. Because the deck was represented as a single beam connected directly to the center columns of the transverse frames, the dimensions of the regions where members intersected were poorly represented, and the structure was much more flexible than in Model 4. The deficiencies in the modeling were exemplified by the representation of the transverse beams under longitudinal loading. In Model 1 the transverse beams were free to twist, whereas in the real structure and in Model 4 they were embedded within the deck, and little twisting could occur. The coarseness of Model 1 resulted in deformations that were larger than those of Model 4, particularly in the longitudinal direction. The modal analysis also highlighted the oversimplification of Model 1, in that many of the mode shapes (not shown here) included deformations that could not occur in the real structure.

The accuracy with which the model reproduces the response of the real structure depends primarily on two features of the model: the type and distribution of members used to represent the structure (e.g., an isotropic plate or an explicit representation of the box with all of its internal webs) and the stiffnesses chosen for the individual members. Both features are likely to influence the global response, such as deck displacement under lateral load or modal period, but because the vulnerability of the structure is likely to be judged against local criteria, such as the demand/capacity ratios of individual members, the local responses will also be important. For those purposes, the models that best

reproduce those local responses will be the most useful. Simpler models, such as Model 1 with its single spine beam, do not capture the level of detail needed because, for example, the torsional conditions in the outrigger beam are so poorly modeled. On this basis, models 3 and 4 were preferable because their representation of the member distribution was closer to that of the prototype structure.

Note that, in the longitudinal direction, Model 3 (the plate) appeared to be slightly too stiff in comparison with the explicitly modeled box of Model 4. The reason for this is not known but is believed to be associated with the torsional stiffnesses of the two representations. (Recall that the plate could be characterized by only two dimensions—the width and thickness—and these were selected to represent correctly the longitudinal and transverse bending stiffnesses of the real box. It might have been possible also to match the torsional stiffness of the box by adjusting the Poisson's ratio of the material, but in the interests of simplicity,  $\nu$  was set at the standard material value of 0.2.)

The choice of model therefore depends on the balance of computer run time vs. model accuracy. Models 1 and 2 were considered unacceptable on the basis of member distribution, and Model 4 was regarded as slightly more accurate than Model 3. The run time for Model 4 was slightly longer than Model 3, but the increased accuracy was determined to be worth the trade-off in run time. Therefore, the deck representation in Model 4 was chosen for use in all subsequent studies.

The material properties used for the model of the north concrete structure deck were selected to represent cracked conditions because extensive cracking due to gravity loading was visible in the deck of the as-existing structure. The elastic modulus was set at 50 percent of the gross value, and Poisson's ratio was set to 0.2. The value of 50 percent was based on visual inspection. These values were used for the entire deck, because the available information about the distribution of cracking was not sufficiently detailed to justify a more refined modeling approach.

### **3.3.4 Transverse Beams**

The transverse beams of the outrigger bents and those within the deck were modeled with different elements. The transverse beams within the deck section were modeled as shell elements to ensure compatibility with the deck shell elements. However, the free-standing outrigger beams were modeled with beam-column elements to reduce the number of degrees of freedom in the model. If shell elements had been used for the full length of the transverse beams, not only would they have required three nodes in a vertical line at each plan location, in comparison with only one for the beam element, but the beam would require many shell elements along its length in order to avoid numerical problems when the element aspect ratio became too large.

Beam constraints were used at the connections between the outrigger frame elements and transverse beam shell elements, as well as between the column frame elements and transverse beam shell elements, to restrain the rotation at the connections. The use of these constraints followed the procedure described in the previous section and illustrated in Figure 3-10. Full, gross-section properties were used for all of the beams because minimal cracking in the beams was observed during visual field inspections.

### **3.3.5 Columns**

To represent the appropriate stiffness of the column, the effects of the column jacket and the bar strain penetration into the column and adjacent elements (e.g., pile cap, joint) must be taken into account. Jacketing the original rectangular sections significantly increased their size and moment of inertia, so most of the column flexibility resulted from deformation of the unjacketed sections (gaps) at the top and bottom of the column and from the strain penetration effects. Therefore, three primary sources of column flexibility were identified and are illustrated in Figure 3-12: deformation in the jacketed section of the column, deformation in the unjacketed sections, and penetration of the reinforcing steel strains into the adjacent elements. Neglecting these sources of deformation by modeling only the jacketed section could produce overestimates of the stiffness and underestimates of the yield displacement of the column. Therefore, these components were modeled explicitly with a procedure that included each of these sources of

deformation. The procedure is described in Appendix A and was calibrated using results from tests on steel-jacketed rectangular columns (Priestley et al. 1994a and 1994b).

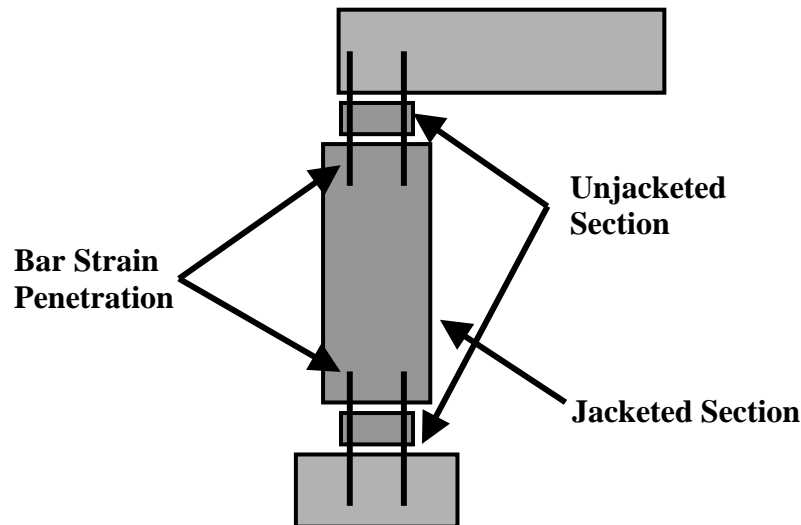


**Figure 3-12: Sources of Deformation in the Column**

Almost all of the columns were jacketed. For them, the analysis procedure was to establish the stiffness for each component (jacketed section, unjacketed section, and strain penetration) and to assemble the components into a composite column for which the yield displacement could be established. In the global model, the jacketed outrigger columns were typically modeled with four elements representing the jacketed section (two frame elements joined at an intermediate node at mid-height) and the 2-in. unjacketed sections at the top and bottom of the column, including the strain penetration effects (one frame element each). The additional node at the center of the jacketed section was introduced because the program assigns mass only at the nodes, and this arrangement provided a more realistic distribution of mass.

The column at Outrigger Bent 25 was not jacketed. A process similar to the one described above was used to account for all sources of deformation in that column. However, a five-part column was used in the global model to better represent the stiffness distribution since the deformation was not concentrated at the very top and bottom of the

column, as was the case for the jacketed columns. Appendix A presents details of the procedure and the equations used for the modeling of these five-part unjacketed columns.

Each of the interior mainline columns was represented by a single element. This was done because the orthogonal arrangement of beams within the box girder deck provided good confinement for the beam-column joints, which were therefore deemed to be much less vulnerable to joint shear failure than were the outrigger joints. Without the need to compute the joint shear demand, the column bar stresses were not needed, so the internal nodes, such as the one between the 2-in. unjacketed section and the long jacketed section, could be condensed out. This was done in the interest of computational efficiency. This procedure is also described in Appendix A.

The split columns were modeled with two beam-column elements connected to each side of the deck. The columns were joined at the appropriate elevation, and the remaining single column below the split (where applicable) was connected to its appropriate foundation element. Where the split columns extend to the foundation, both columns were connected to the foundation element. The procedures described above were also used to calculate the stiffnesses of the split columns. As before, for mainline split columns, a single frame element with equivalent stiffness was used for each column. For the outrigger split columns, the four-element column, which modeled the single jacketed and two unjacketed sections, was used. This is also further discussed in Appendix A.

### **3.3.6 Expansion Joints**

In the real structure, the seven frames in the north concrete structure are separated by expansion joints that can open freely but carry compression force when it closes. This behavior cannot be modeled in a linear analysis, so many engineers approximate it by running two linear analyses: one with the frames permanently separated and one with them permanently pin-connected together. The intent is to bracket the true behavior, but there is, in fact, no guarantee that the procedure achieves the goal. In this study, non-linear contact elements that can carry compression but not tension force were used at the expansion joints.

In the numerical model, compression gap elements with the appropriate opening size were used to model the expansion joints. These compression gap elements would have an essentially infinite stiffness when closed and have zero stiffness when open. Although use of the gap elements required use of nonlinear analysis methods, which increased the computational effort, the benefit of obtaining accurate displacement histories was significant, and these elements were used in all of the analyses.

### **3.3.7 Structural Damping**

Although the analysis procedure used was nonlinear, the majority of the elements (e.g., beams, columns, decks) were modeled with linear elements. Therefore, the nonlinearity, and consequently the damping effects, of cracking and element hysteresis were not modeled explicitly. To account for the damping contributed by these effects, a single damping ratio was used. The necessary value depended on the energy dissipation rate, which depended on the ductility demands. Preliminary analyses showed that yielding was restricted to a small number of locations and that its extent was not large, so the structural damping ratio was assumed to be 3 percent. This has been shown to be a reasonable estimate for reinforced concrete structures at low levels of yielding (Chopra 2001).

### **3.3.8 Outrigger Joint Flexibility**

The outrigger bents include a beam, column, joint, and the supporting substructure. If the joint experiences damage due to excessive shear stress, it becomes more flexible. To evaluate the influence of the joint flexibility on the response of the outrigger bent and overall bridge, a small study was performed. In the study, a single, isolated transverse bridge bent, which included an outrigger beam, was modeled, and the rotational stiffness of the joint spring that connected the beam and column was varied from the reference value, which corresponded to uncracked elastic conditions.

The results showed that the global stiffness of the bent was very insensitive to the joint stiffness, because a 95 percent reduction in joint stiffness led to only a 5 percent increase in lateral displacement of the bent. This insensitivity of the bent displacement to the joint

stiffness was attributed to the fact that the great majority of the bent stiffness was provided by the main line columns.

However, despite the small increase in the bent displacement, the forces on the outrigger elements were significantly reduced by the decrease in local stiffness. Therefore, outrigger joint spring elements were introduced in the north concrete model. Because only limited cracking was observed in the joints during a field investigation, the stiffness corresponding to the uncracked joint was used. Use of this value led to an upper bound for the forces attracted to the outrigger elements because degradation of the joint would reduce its stiffness.

### **3.4 Modeling of Adjoining Structures**

The adjoining structures, such as off-ramps, were expected to influence the response of the north structure. The north abutment and the steel over-crossing structure interact with the main structure only in the north-south direction and induce only translational effects, so they were modeled in a very simple way. The west off-ramp joins the main structure at an angle, so it can induce both translation and torsion, and it was therefore modeled in somewhat greater detail

#### **3.4.1 West Off-Ramp**

The west off-ramp was constructed in 1981 and is shown in Figure 3-13. To numerically model the response of the structure and its influence on the main bridge, the deck, precast girders, columns, and foundations were modeled. Figure 3-14 is a diagram of the west off-ramp model. The north mainline structure model is omitted from the figure for clarity. The deck was modeled with plate elements connected to frame elements that represented the girders. The girders in the structure rest on elastomeric bearings set on the ledges of the cap beam, so the girder frame elements in the model were pinned to the cap beam frame elements. The column frame elements were rigidly connected to the cap beam elements and to the foundation elements.



**Figure 3-13: Underside of West Off-Ramp**

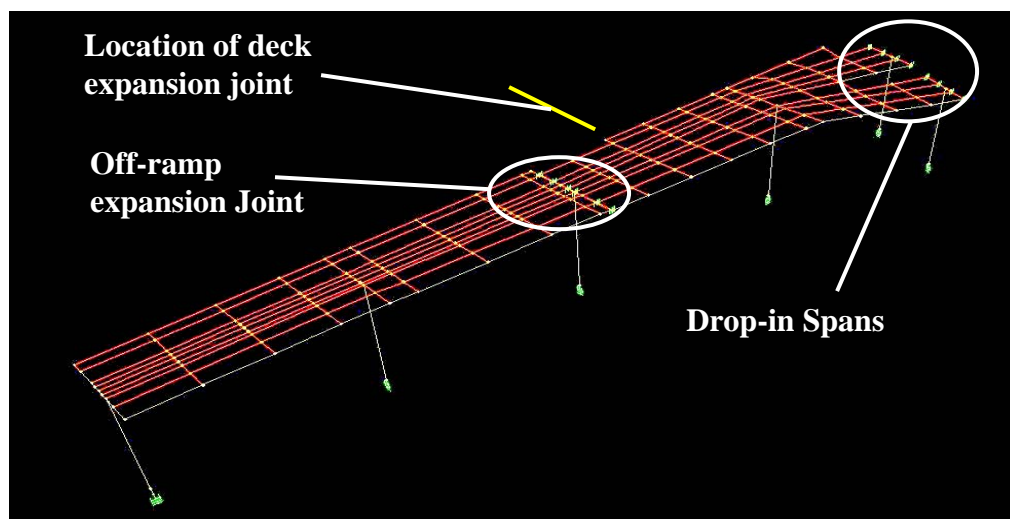


**Figure 3-14: West Off-Ramp Model**

The connectivity between the west off-ramp structure and the main north structure is slightly unusual. An expansion across the traffic lanes separates the two structures at the first bent of the off-ramp, as might be expected. However, it is not aligned with the comparable expansion joint in the mainline structure, as indicated in Figure 3-12. Between the two expansion joints, the decks abut one another, as shown in Figure 3-11, but are not continuous. Therefore, some slab elements in that region were removed from the model to allow the two structures to move independently.

The off-ramp model was discontinued at the first expansion joint beyond the point at which the deck separates from the mainline structure. The drop-in span at the expansion joint was included as a lumped mass connected to the off-ramp by vertical and horizontal springs representing the stiffness of the bearing pads (see Figure 3-15).

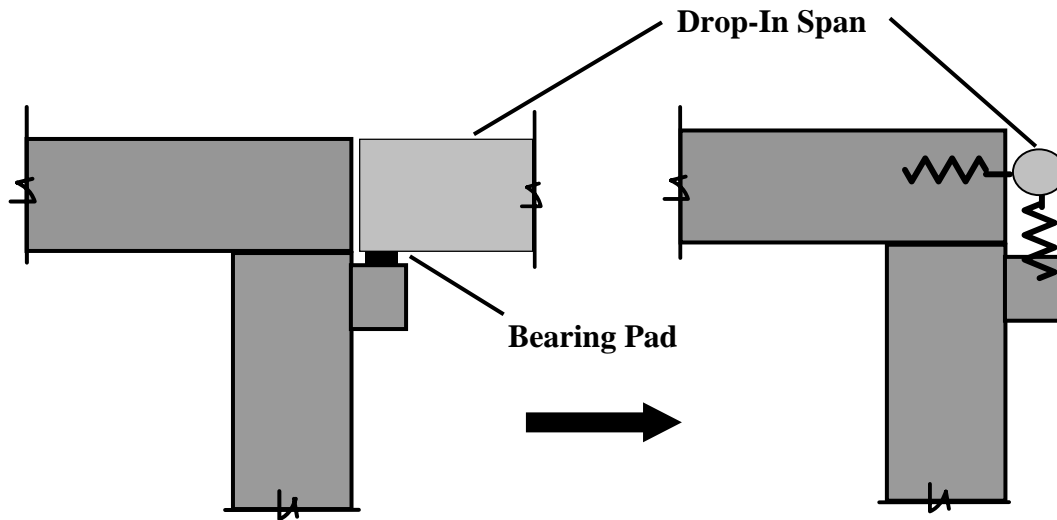


**Figure 3-15: Modeling of the Drop-In Span**

Gross section properties were used for the prestressed girders and the cap beam, and cracked section properties equal to 50 percent of gross values were used for the deck. These choices were based on the cracking visible during inspection of the structure. The columns were not jacketed, because they contained adequate spiral reinforcement, and their properties were set at 40 percent of the gross cross-sectional stiffness (Priestley et al. 1996).

### **3.4.2 North End Abutment**

The abutment to the north of the mainline structure was simulated with a compression gap element (see Figure 3-16). The compression stiffness of the abutment depends on the stiffness of the soil behind the abutment, and the properties of the spring in the gap element were calculated by using research results from California Department of Transportation (1988). The gap opening was set at 1.5 inches based on the structural drawings, which show a gap of 1.5 inches between the deck and abutment. A field

investigation revealed that the abutment has tilted. However, it appears that the 1.5-inch gap was preserved, presumably because the columns and the abutment share same footing.

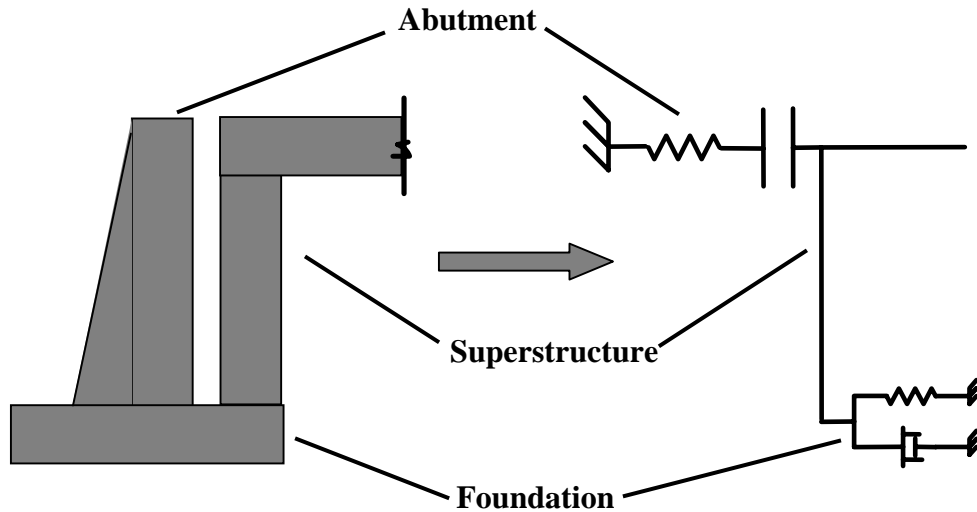


**Figure 3-16: Modeling of the North Abutment**

### 3.4.3 South End Steel Structure

The model used for the steel structure to the south of the mainline concrete structure is shown in Figure 3-17. It consisted of one translational and one rotational spring, and a rigid beam. The rigid beam allowed gap elements to be distributed across the width of the expansion joint between the steel and concrete structures. The deck was treated as rigid, and the lateral and torsional flexibilities of the steel structure were assumed to arise only from bending of the columns, which were treated as fixed against rotation at both the top and bottom. The stiffnesses of the columns were based on the steel wide flange section properties, and the translational mass and the mass moment of inertia of the structure were included in the model. The expansion joints between the steel structure and the adjoining concrete north and south concrete structures were modeled with gap elements.

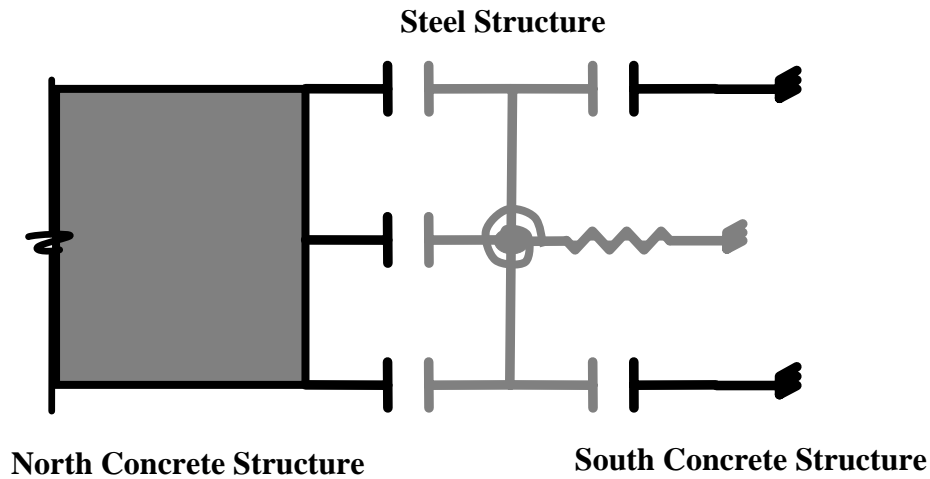


**Figure 3-17: Modeling of the Steel and South Concrete Structures**

#### **3.4.4 South End Concrete Structure**

The south concrete structure was modeled as a single degree of freedom, in the interests of simplicity. This choice was made because the south structure is separated from the north concrete structure, which was the focus of the research, by two expansion joints. The structural connectivity between the two concrete structures was therefore weak, and the properties of one were likely to have little influence on the response of the other. The expansion joints were modeled by infinitely stiff gap elements, as shown in Figure 3-17.

A study was performed to determine the effect of the stiffness used for the south concrete structure. In one run, the south concrete structure was represented as infinitely rigid, and in another, it was given a finite stiffness equal to that of the southernmost frame (Frame 7) of the north concrete structure, because the two had similar geometries. The results of the two runs were compared, and the difference in the displacements of the north structure was negligible. Therefore, all subsequent runs for the north concrete structure were conducted with the infinitely rigid model for the south concrete structure.

### **3.5 Geotechnical Characteristics of the Site**

Structural analyses are often performed by using input motions or spectra produced by free-field site response analyses, which by definition assume the absence of any structure.

Such analyses implicitly involve the use of fixed-base models, which assume that the base of the structure does not move relative to the soil on which it is supported. In reality, the soil that supports a structure and its foundation is not rigid, and relative movement between the foundation and the soil can occur. Because such soil-foundation-structure interaction effects can influence the dynamic response of some types of structures, their influence on the Spokane Street over-crossing was evaluated. In this section, the site conditions on which the soil models were based are discussed, and in Section 3.6, the analytical model for the soil and foundation system is developed.

### **3.5.1 Site Conditions**

Knowledge of the ground conditions at the site is important from two standpoints. First, the interaction of the foundations with the soil that surrounds and supports them will be strongly influenced by the characteristics of that soil. This issue is addressed in Section 3.6. Second, the response of the site to earthquakes, in particular the amplitude and frequency content of motion at the ground surface, is strongly influenced by ground conditions. The ground motions are discussed in Section 3.7.

Geologic and geotechnical conditions at the site have been investigated and detailed in previous reports (e.g., Zhang et al. 1996) and are summarized in the following paragraphs.

The Spokane Street over-crossing is located in the Puget Sound Lowland, an area whose current conditions are dominated by historical glacial activity. During Pleistocene times (1.8 million to 11,000 years ago), continental glaciation occurred across the Lowland. During the most recent period of glaciation, the Vashon Drift deposited silt, sand, and gravel throughout the area. As the glaciers advanced, these soils were compressed by the weight of the ice and as a result became dense, stiff, and strong. As the glaciers receded to the north, more silt, sand, and gravel were deposited, leaving a landscape with a series of north-south trending ridges and depressions. More recent post-glacial erosion and deposition has further altered the landscape by placing looser and softer sediments on top

of the dense, glacially overridden material. The Spokane Street site lies within the Duwamish River Valley, in which recent alluvial and estuarine soils have been deposited.

At the site, hydraulic fill, placed between 1885 and 1912, underlies the ground surface. It consists primarily of dark gray, medium dense to dense, silty to very silty, fine to coarse sand. Its thickness varies from 5 to 30 ft, with an average of approximately 10 ft.

Beneath the fill lies a 10-ft-thick layer of very soft to stiff, fine sandy estuarine silt. The estuarine silt is underlain by Duwamish River alluvium in the form of loose to dense, clean to very silty, fine to medium sand with interbedded layers of estuarine silt. These soils are underlain by dense, glacially overridden soils referred to locally as glacial till. Glacial till in this area generally consists of very dense gravelly soils and occurs at depths of approximately 160 to 180 ft.

Subsurface investigations have found groundwater at depths of about 10 ft over most of the site, with one unexplained depth measurement of about 20 ft near Bent 6.

Groundwater levels are expected to fluctuate several feet in response to tides and precipitation.

### 3.5.2 Soil Properties

In a letter dated September 1, 1995, from Tony M. Allen to M.M. Lwin, the shallow (non-glacially overridden) soils encountered in field investigations were grouped into three general soil units based on engineering properties and material classifications, as indicated in Table 3-3.

**Table 3-3: General Soil Units**

Soil Unit	Description
Unit 1 (Hydraulic fill)	Loose to medium dense, dark gray, moist, gravelly, silty to very silty, fine to coarse sand.
Unit 2 (Estuarine deposits)	Very soft to stiff, dark gray, wet, fine sandy silt.
Unit 3 (Alluvium)	Loose to dense, very dark gray, wet, clean to very silty fine to medium sand.

A review of the data on which this idealized soil profile was based indicates that it provides a reasonable representation of the pertinent soil conditions at the site.

A review of available boring data showed that the Standard Penetration Test (SPT) resistance could be used to develop a generalized soil profile for the site with the characteristics shown in Table 3-4.

**Table 3-4: Average Standard Penetration Test (SPT) Resistance**

Depth (ft)	Description	Average SPT resistance
0 – 10	Unit 1	11
10 – 21	Unit 2	4
21 – 35	Unit 3	19
35 – 173	Unit 3	$17.25 + 0.1235z$ where $z =$ depth in ft

For the purposes of performing site response analyses, Cone Penetration Test (CPT) and shear wave velocity data were reviewed. These data allowed evaluation of a representative shear wave velocity profile for the site, the details of which are shown in Table 3-5.

**Table 3-5: Shear Wave Velocity of Soil Layers**

Description	Layer	Thickness (ft)	$V_s$ (ft/sec)
Unit 1	1	10	450
Unit 2	2	11	350
Unit 3	3	14	442
Unit 3	4	8	505
Unit 3	5	10	548
Unit 3	6	20	611
Unit 3	7	30	698
Unit 3	8	30	784
Unit 3	9	40	870
Glacial Till	10	50	1301
Glacial Till	11	50	1750
Glacial Till	12	50	2100
Glacial Till	13	50	2350
Glacial Till	14	$\infty$	2500

## **3.6 Modeling of Soil-Foundation-Structure Interaction**

### **3.6.1 Foundations**

Because of the soft, loose surficial soils, the Spokane Street over-crossing is supported on pile foundations. Each column of the structure is supported on a group of piles connected by a common pile cap. A variety of different pile group configurations and different pile cap geometries were used to support this structure. Those supporting the portion of the structure considered in this study were designated as Details A, D, E, G, I, and L, and their configurations are shown in Figure 3-18.

### **3.6.2 Foundation Impedances**

The stiffness and damping characteristics of each pile group configuration were determined to permit inclusion of soil-foundation-structure interaction (SFSI) effects in the dynamic analysis of the structure. The stiffness and damping characteristics were determined with the computer program DYNA4 (Novak et al. 1993), which allows consideration of the contributions of both the piles and pile caps. DYNA4 assumes linear elastic behavior of the soil and the foundation elements, and it computes stiffness and damping coefficients as functions of frequency. The DYNA4 models included the masses of the pile-caps for the different pile group configurations; however, an evaluation determined that removing the mass of the pile caps did not change the values of the foundation stiffness and damping, and these were the only products from DYNA4 that were used in the structural analyses of the over-crossing.

The primary effects of soil nonlinearity were accounted for by a 20 percent reduction in the low-strain shear modulus for the soils surrounding the pile cap, which is consistent with the development of average shear strains on the order of 0.5 to 1.0 percent in those soils. Low-strain shear moduli were used for the deeper soils.

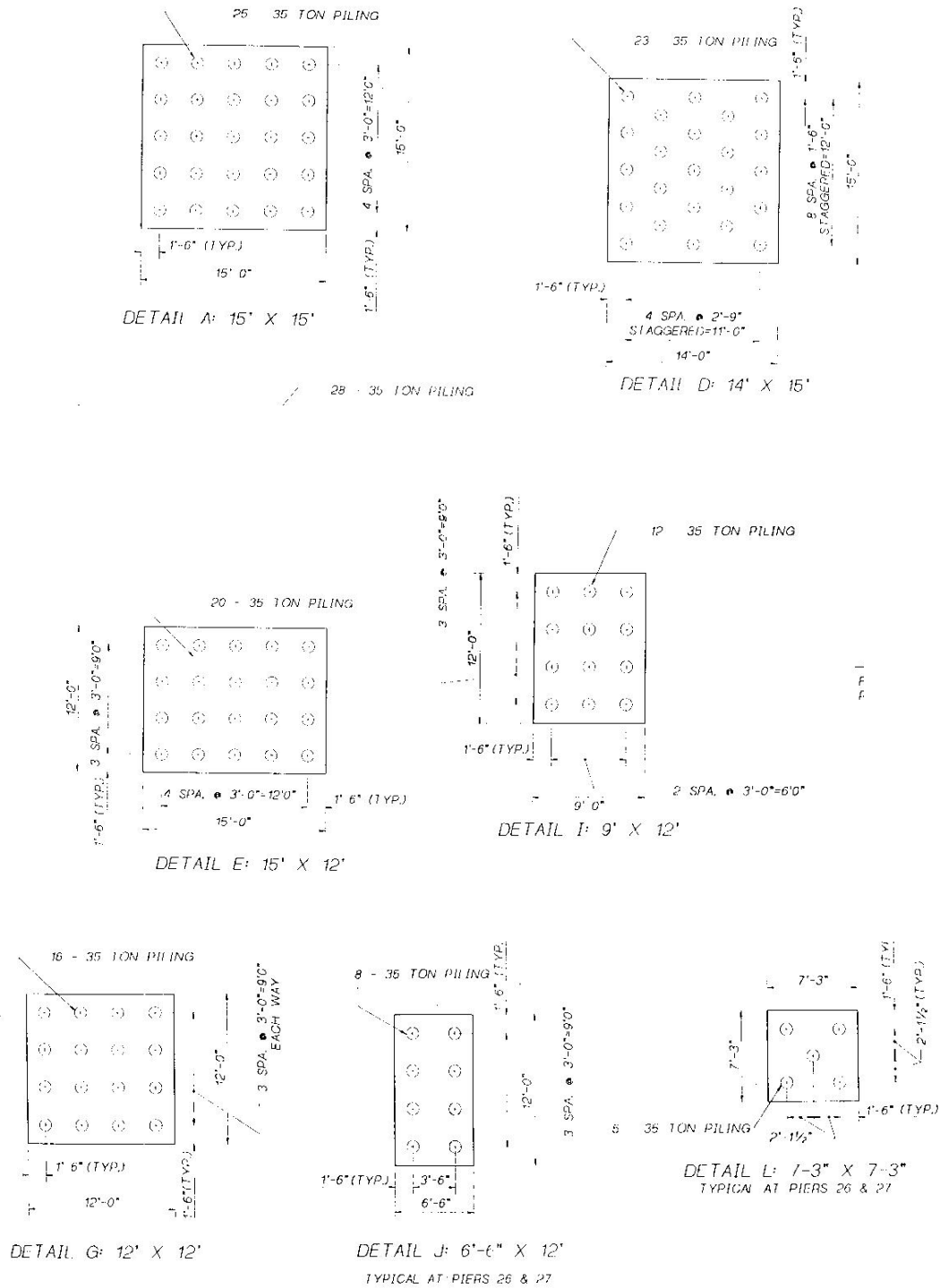


**Figure 3-18: Pile Group Configurations**

The results of these analyses are shown for a typical foundation (Detail A) in figures 3-19 and 3-20. Figure 3-19 illustrates the variation of stiffness and damping with frequency

for the cases of vertical and horizontal translation. The stiffness values are weakly dependent on frequency, but the damping coefficient is sensitive to frequencies below approximately 1 Hz. Similar behavior is seen for the rotational modes of deformation—rocking and torsion—in Figure 3-20.

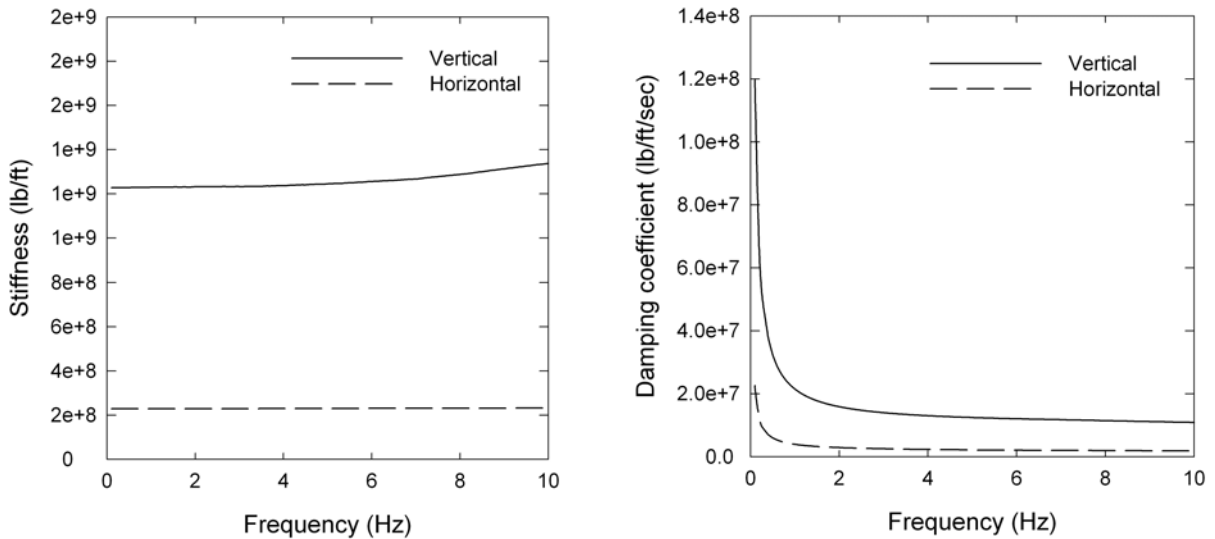


**Figure 3-19: Variation of (a) Stiffness and (b) Damping Coefficient with Frequency for Vertical and Horizontal Translation**

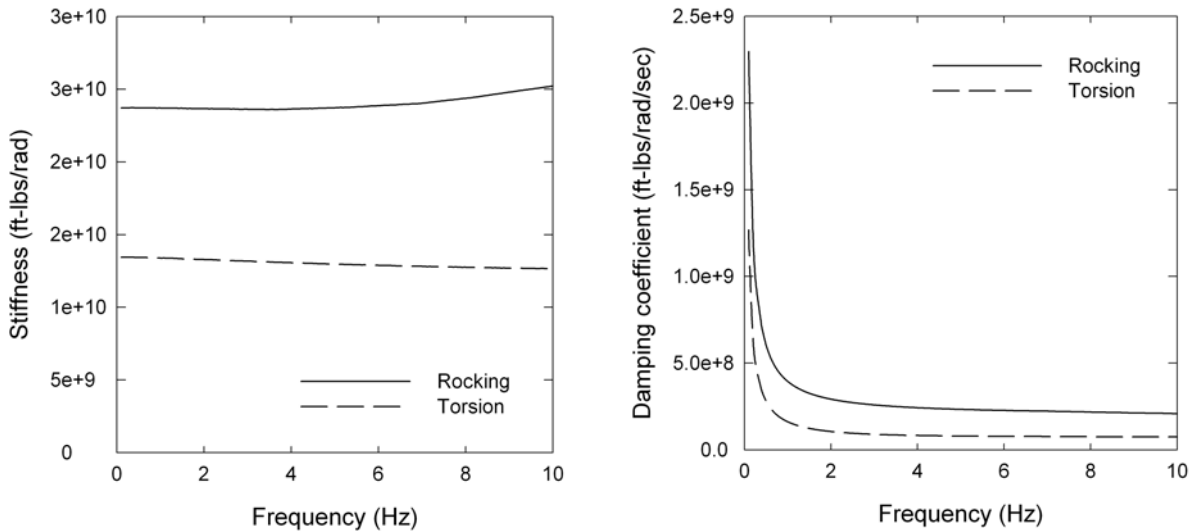


**Figure 3-20: Variation of (a) Stiffness and (b) Damping Coefficient with Frequency for Rocking and Torsion**

These analyses were performed for each of the pile group configurations supporting the study portion of the Spokane Street over-crossing.

### **3.6.3 Numerical Representation of Soil-Foundation-Structure Interaction**

The stiffness and damping values resulting from the soil analyses were used in the structural analysis of the north concrete structure. These soil characteristics were modeled with spring and damper elements, which were placed at the base of the columns.

Figures 3-19 and 3-20 show the variations in the stiffness and damping of the pile group as a result of the vibration frequency. A modal analysis of the north concrete structure showed that most of the mass participation occurred in the modes of vibration corresponding to the fundamental modes of the individual frames for both translation and rotation. The results of the modal analysis presented in Section 3.8.1 indicated that the frequencies of these translational modes range from 0.90 to 2.05 Hz. The rotational modes have higher frequencies than do the translational ones. Figures 3-19 and 3-20 indicate that the stiffness and damping are nearly constant in this range. Therefore, for each SFSI element, the stiffness and damping values used in the model were computed from the footing properties and the fundamental frequency of the frame in question and were kept constant during the analysis.

The SAP2000 element designated as “NLlink” was used to model the SFSI effects. The element consists of a mass, a spring, and a dashpot, and its use is illustrated in Figure 3-21. The NLlink elements included the pile-cap mass, but not the mass of the surrounding soil and piles. The spring and dashpot properties were obtained from the DYNA4 analyses discussed above.

The NLlink element has two possible configurations. If it is defined as linear, the spring and dashpot are placed in parallel, but if it is defined as non-linear they are placed in series. The non-linear element includes cross-coupling terms in the damping matrix and permits all terms in the matrix to be nonlinear. The cross-coupling terms could be significant if the soil damping ratio significantly exceeds the structural damping ratio, in

which case the soil properties would dominate the energy dissipation in the whole system and the most accurate possible representation of the soil would be desirable. In the present study, the energy dissipation in the soil and structure were of the same order of magnitude, so the damping cross-coupling was included. However, the available stiffness information was insufficiently detailed to warrant the use of nonlinear terms in the matrix. The damping matrix for the linear element was diagonal.

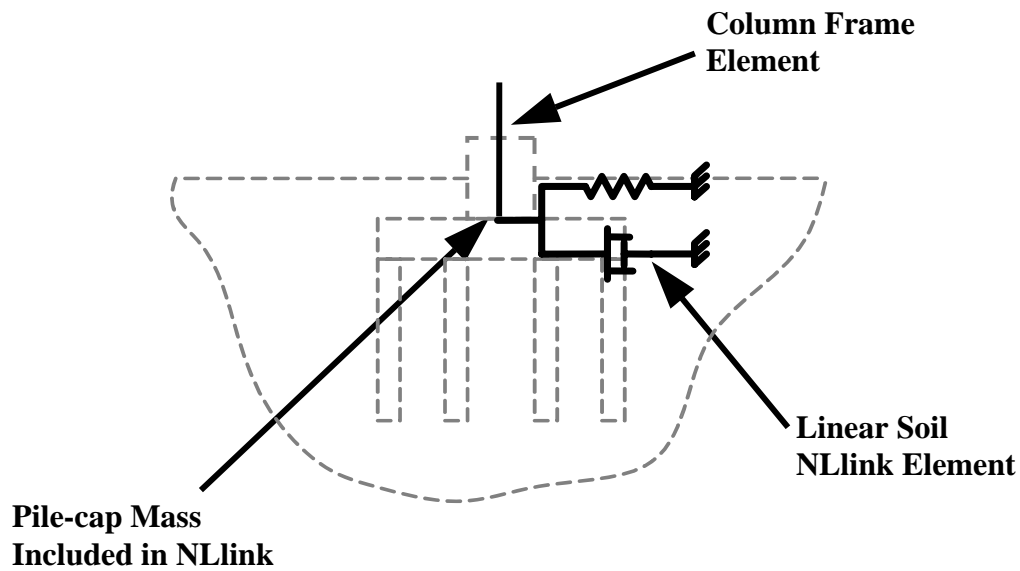


**Figure 3-21: Model of Soil-Structure Interaction**

A study was conducted to determine whether the linear representation would be adequate. Although use of non-linear NLink elements would increase analysis run time, it was necessary to know whether the extra complexity would result in significantly different response. In the study, a parallel spring-damper model was needed to simulate the required behavior. This was achieved by using a single linear NLink element or two parallel nonlinear NLink elements, one for the spring (with a zero damping component) and one for the damper (with a zero stiffness component).

For the purposes of the study, it was important to select the frame with the largest damping ratio. Since the same structural damping was assigned to each frame, any differences in total energy dissipation would come from the soil damping. The

northernmost (Frame 1) and southernmost (Frame 7) frames were isolated. They were chosen to cover the extremes of behavior. They were assigned zero structural damping so that the only energy dissipation occurred in the NLink elements in the foundations. A pullback test was performed on each frame, and the equivalent structural damping was obtained by using the half-power bandwidth method. When the non-linear NLink elements were used, damping ranged from approximately 2.3 percent for the northernmost frame (with the shortest columns) to 0.3 percent for the southernmost frame in the longitudinal direction and from 3.5 percent to 0.6 percent in the transverse direction.

Frame 1 was selected for further study because the pull-back analyses had shown that it had the highest damping. Four different foundation models were then compared: fixed base, linear springs, linear springs and dampers, and non-linear springs and dampers. Dynamic analyses using the 475-year ground motion (described in Section 3.7) were run in both the longitudinal and transverse directions for these three linear models and one nonlinear model and the maximum displacements of each are presented in Table 3-6. Use of the linear and non-linear springs and dampers led to the same displacements, and they were larger than those of the fixed-base and spring-only models.

**Table 3-6: Maximum Structural Displacement (ft.) Using Different Foundation Models**

<b>Model</b>	<b>Longitudinal</b>	<b>Transverse</b>
Fixed Base	0.033	0.024
Springs Only	0.040	0.029
Springs and Dampers (Linear)	0.039	0.028
Springs and Dampers (Non-linear)	0.039	0.028

A final study was performed on the complete structural model (rather than just Frame 1) to compare the linear and non-linear analyses. Again, ground motions were used for the loading and the computed responses were similar for the linear and nonlinear NLink

models. It was therefore determined that linear properties were adequate for defining the soil stiffness and damping of the NLink elements.

### **3.7 Ground Motions**

Evaluation of the outrigger bents required an estimate of the level of loading to which the Spokane Street over-crossing structure would be subjected in a strong earthquake. Site-specific ground motions were developed for this purpose. To cover a range of hazard levels, site response was computed for three different hazard levels – those with return periods of 72, 475, and 2,475 years. These represent probabilities of exceedence of 50 percent, 10 percent, and 2 percent in 50 years, respectively.

The results of a probabilistic seismic hazard analysis (PSHA) for a nearby site were applied to the Spokane Street over-crossing site, after they were checked against PSHA data from the U.S. Geological Survey (USGS) for different geographic regions. The PSHA provided a uniform hazard spectrum (UHS) at typical bedrock outcrop sites for each of the foregoing return periods. In order to estimate the effects of the local site conditions on ground surface shaking levels for these return periods, a series of site response analyses was performed. Those analyses consisted of a number of frequency-domain analyses of the site in which the soil was divided into layers with dynamic properties that corresponded to the shear wave velocities in Table 3-5. The input motions were bedrock accelerations compatible with the UHS that had been derived from the PSHA.

For each hazard level, synthetic ground motions were developed by combining the phase spectrum from a representative recorded ground motion with a Brune amplitude spectrum that was iteratively adjusted for compatibility with the uniform hazard spectrum across a wide range of frequencies. The 5 percent damped spectra for each of the rock input motions are shown, along with the target spectra, in Figure 3-22.

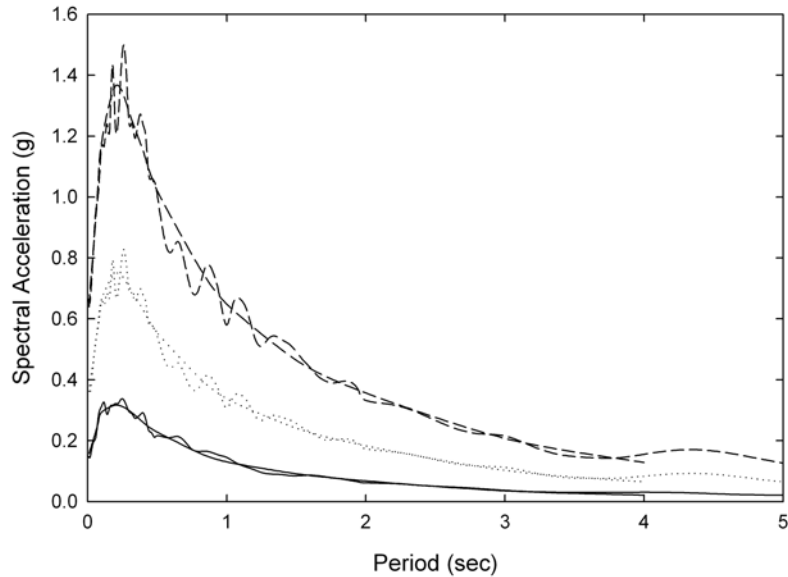


**Figure 3-22: Response Spectra and Target Spectra for Synthetic Rock Input Motions at 72-, 475-, and 2,475-Year Hazard Levels**

The rock input motions were used as input motions to a series of equivalent linear site response analyses. The site response analyses used the shear wave velocity data shown in Table 3-5, along with the Vucetic-Dobry soil model (with plasticity index, PI, of zero for all layers except the silt at depths of 10-21 ft, for which PI = 20). The response spectra for the resulting ground surface motions are shown in Figure 3-23.

The shapes of the ground surface spectra reflect the thick layer of soft soils that underlies the Spokane Street over-crossing. Soil deposits with these characteristics tend to reduce the short period components of a ground motion and amplify the longer period components, particularly when the input ground motion is strong. This effect can be seen by comparing the ground surface spectrum of Figure 3-23 with the rock spectrum of Figure 3-22 for each hazard level. For the relatively weak 72-year ground motion, the strains induced in the soil are relatively small, so the stiffness of the soil remains relatively high, and the ground surface spectrum has a shape similar to that of the rock spectrum. For the 475-year ground motion, however, larger strains are induced in the soil, so the stiffness of the soil decreases and the short period portion of the spectrum is reduced; at the same time, the longer period portion of the ground surface spectrum is

considerably greater than that of the rock spectrum. This type of behavior is seen to an even greater degree with the 2,475-year spectra.

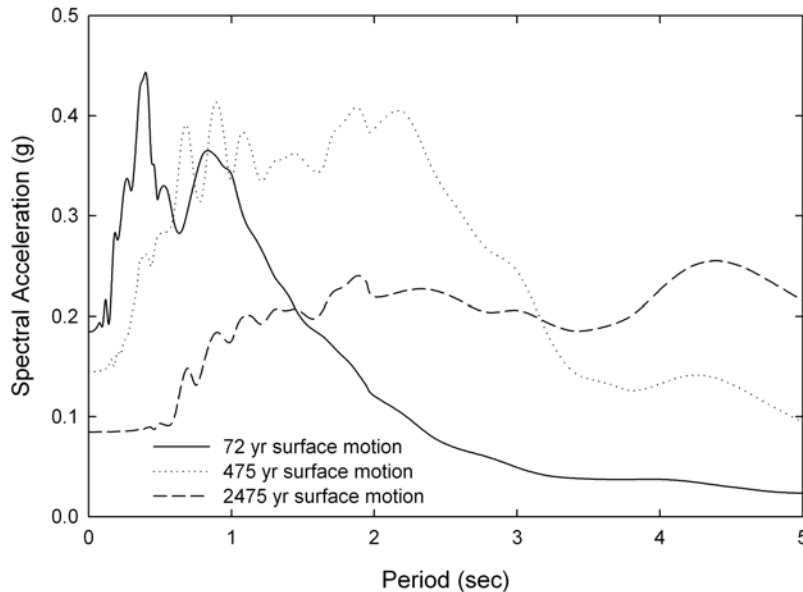


**Figure 3-23: Computed Ground Surface Response Spectra for 72-yr, 475-yr, and 2,475-yr Hazard Levels**

### 3.8 Model Verification Evaluation

The model was verified with three different methods, described in sections 3.8.1 – 3.8.3.

The modal analysis on the global model showed that, in most of the lower modes, the mode shape consisted of motion of a single frame and that response was dominated by motion in one direction (longitudinal, transverse or rotational). This behavior occurred because the modal analysis was conducted with the gap elements at the expansion joints open, in which case the frames do not interact with each other, except through the foundation elements and split columns. Therefore, for motions that would not cause contact at the expansion joints (small motions in any direction or any motion that was purely transverse and therefore parallel to the open expansion joints) the structural response should be predictable by using spectral analysis on a single frame. This fact formed the basis for two of the methods of verification.

### 3.8.1 Period Verification

In the first method of verification, the fundamental mode of an individual frame (Frame 1) in the global model in each translational direction was checked against a simple single degree of freedom (SDOF) representation. The periods corresponding to the fundamental modes of all individual frames were obtained by finding the global mode that provided the largest mass participation of the frame in the direction in question. They are reported in Table 3-7. For the SDOF representation of Frame 1, the columns were treated as the only deformable elements and their combined stiffness was assigned to the SDOF system. The period of the SDOF system matched reasonably well with the period obtained from the global model. While this verification did not guarantee the absence of minor errors in the global model, it suggested that the model was reproducing correctly the major trends in behavior.

**Table 3-7: Period of Fundamental Modes for Individual Frames**

Frame #	1	2	3	4	5	6	7
Longitudinal	0.57	0.57	0.81	0.87	0.87	0.91	1.11
Transverse	0.49	0.61	0.77	0.86	0.93	0.93	0.98

### 3.8.2 Spectral Verification

If the structural response depends primarily on the response of the frames acting separately (i.e., pounding does not occur), the result of response spectrum analyses on the individual frames can be used to confirm the response of the global model. The displacement produced by the FE analysis on the global model for an individual frame (Frame 1 – transverse direction) was verified through a separate calculation. The structural damping of 3 percent was combined with the effective soil damping of the frame (3.5 percent for Frame 1 in the transverse direction). Using this damping value, the fundamental period ( $T = 0.49$  sec from Table 3-7) and the appropriate earthquake input (475 year.), the spectral displacements were obtained from the appropriate displacement response spectrum curve, as shown in Figure 3-24. That figure indicates that, for a period of 0.49 seconds, the spectral displacement is approximately 0.057 feet. The maximum

displacement of Frame 1 from the time history analysis of the global model is 0.055 feet. This good agreement further confirmed that the global model was working correctly.

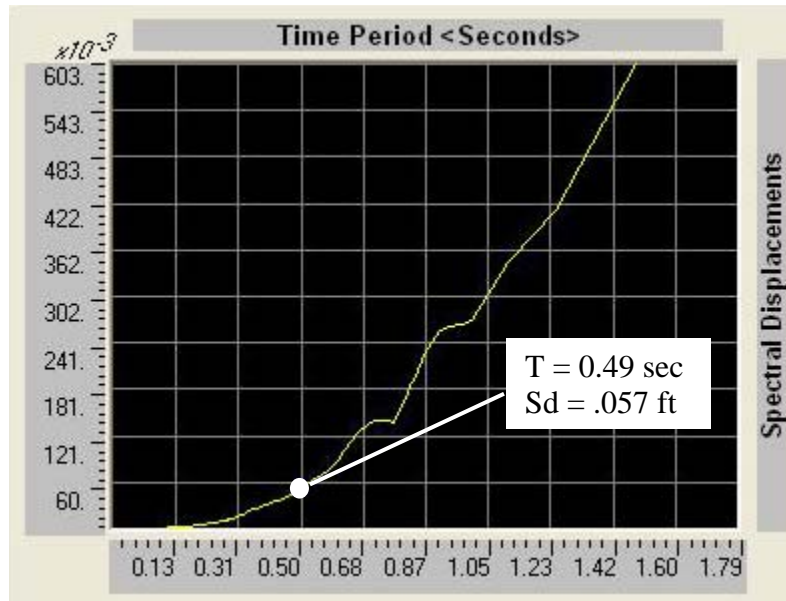


**Figure 3-24: Displacement Response Spectrum for 6.5 Percent Damping**

### 3.8.3 Field Verification

The bridge is approximately 50 years old, and during its lifetime it has experienced two moderate earthquakes (in 1965 and 2001). Its age suggests that it has been subjected to ground motion of approximately the same amplitude as the 72-year return period ground motion used in these analyses. In addition, the peak ground accelerations measured near the structure during the Nisqually earthquake of February 2001 lay in the range 0.15 - 0.20g. These are comparable to the 0.18g peak ground acceleration of the 72-year synthetic earthquake. Therefore, the locations of field expansion-joint damage, assumed to have been caused by pounding, were compared to the locations of gap closures predicted by the global model when subjected to the 72-year earthquake input motion. The analysis indicated that, of the six gaps between frames, the five southernmost closed. Figure 3-25 shows the predicted gap closures (indicated by solid lines). For comparison, pounding damage in the field is evident between Frames 3 and 4 and between Frames 5 and 6. An example is shown in Figure 2-12. The presence of the west off-ramp made

inspection difficult between frames 4 and 5 and between frames 5 and 6. The only clear discrepancy exists between Frames 2 and 3, where contact was predicted but was not evident in the field. This discrepancy was deemed acceptable, given the approximate nature of the check and the fact that the 50-year life of the over-crossing is slightly less than the 72-year return period of the ground motion used in the analysis.

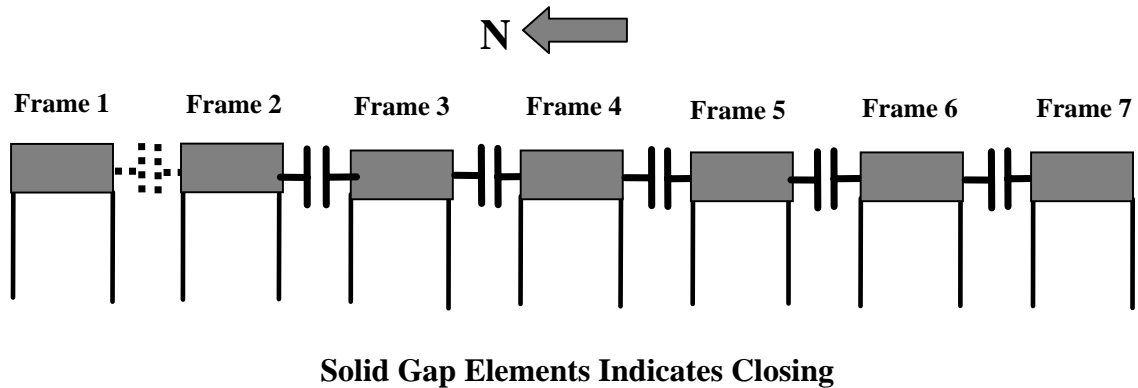


**Figure 3-25: Gap Closures in Model Due to 72-Year Earthquake**

### **3.8.4 Summary of Verifications**

The verification methods described above suggest that the global model was able to reproduce the major trends in behavior expected of the prototype. The longitudinal motion involves contacts between frames, so attempts to model it by considering the response of each frame individually were likely to provide correlations that were less close than those of the transverse direction. However, the good correlation between predicted and observed pounding provided additional confidence in the model's validity for longitudinal motion, even though some uncertainty existed over the equivalence between the field input motion and that used in the analyses.



## **4 ANALYSIS RESULTS AND EVALUATION OF AS-EXISTING STRUCTURE**

### **4.1 Introduction**

An evaluation of the expected seismic response of the SR 99–Spokane Street over-crossing structure was a primary component in the determination of the need for and development of a seismic retrofit measure. Therefore, an accurate evaluation of the seismic capacities, demands, and demand/capacity ratios in the various response mechanisms was needed. In this chapter, such an evaluation is presented. Because the outrigger bents are expected to be the most vulnerable elements, the goal of this analysis was to quantify the vulnerability of the outriggers through a demand/capacity evaluation of critical response mechanisms.

The potential response mechanisms for the SR 99–Spokane Street over-crossing outriggers include beam or column flexural yielding, joint shear stress, joint radial tension, bar anchorage, beam shear, and beam torsion. The tests at Washington State University, introduced in Section 2.2, indicated that joint shear, radial tension in the joint, bond stresses in the column and beam bars, and beam torsion caused significant damage to the test specimens in the form of cracking and spalling of the concrete and debonding of the reinforcing steel. In each response mechanism, the capacity of the test specimen was obtained from the measured data and was expressed in terms that were independent of scale (i.e., either dimensionless or in terms of stress). Because the test specimens were geometrically similar to their counterparts in the prototype structure, the scale-free capacities of the test specimens were assumed to represent the corresponding capacities of the prototype. They were then used to compute the required demand/capacity ratios.

The demands on the outrigger elements were determined by using the analytical model described in Chapter 3. The response of the bridge was considered for the three different site-specific seismic hazard levels defined in Chapter 3. The outrigger bents, including beams, joints and columns, were the main focus of this investigation because the majority

of the main-line columns were jacketed during the Phase I retrofit program, and damage to those elements was not expected. The demands were determined by subjecting the global model of the as-existing structure to the earthquake input motions described in Section 3.7. The motions were applied in two separate horizontal directions, in which the “longitudinal” direction represented earthquake motion in the north-south direction and the “transverse” direction represented motion in the east-west direction. These results were used to determine the global demands, such as displacements and drift ratios, in each outrigger bent. Local demands on the individual outrigger elements for each potential response mechanism were evaluated, and, with the previously computed capacities, were used to compute demand/capacity ratios. The demand/capacity ratios were used to identify critical elements within each of the outrigger bents. These results were then used to develop the retrofit measures presented in Chapter 5.

## **4.2 Capacity Assessment of Outrigger Bents**

The potential response mechanisms of the outriggers had to be identified and their capacities had to be quantified. These capacities could be determined by using either codified equations (e.g., ACI or AASHTO) or structure-specific (or related) experimental results. The latter approach was preferable. The capacities were quantified by using the results of the tests that were conducted at Washington State University (WSU) and sponsored by WSDOT (McLean and Shattarat 2004), when available, and by using code-based methods for the remainder. The scope of the test program prevented every outrigger in the as-existing structure from being tested at reduced scale. Two specimens were tested: the “short” specimen was a scaled representation of outrigger Bent 20 in the north structure, and the “long” specimen was a scaled representation of outrigger Bent 36 in the south structure. Therefore, it was possible in some cases to validate an analysis procedure against the available tests, and then to use that procedure to estimate the capacities of the as-existing outriggers.

Because loading in and out of the plane of the outrigger bent produces different mechanisms, the responses in the two directions were considered independently. For the

in-plane or transverse direction in the finite element (FE) model, the following response mechanisms can lead to damage to the outrigger:

- in-plane column yielding
- in-plane beam yielding
- joint shear
- joint radial tension
- bar anchorage stresses
- beam shear.

For the out-of-plane or longitudinal direction in the FE model, potentially damaging response mechanisms include the following:

- out-of-plane column yielding
- out-of-plane (weak axis) beam yielding
- bar anchorage stresses
- torsion combined with out-of-plane beam shear.

In addition, torsion in the beam induces shear stress in the joint and theoretically could cause joint damage. However, joint failure caused by such stresses has not been reported, and standard mechanisms for evaluating capacity in that mechanism do not exist, so it was assumed that this mechanism was not critical. In the following sections, each response mechanism is evaluated separately.

For an outrigger bent subjected to in-plane loading, the force demands may depend on the direction of loading, since beam or column positive or negative moment capacities may differ. For clarity, the terms “opening” and “closing” moments, as depicted in Figure 4-1, will be used instead of “positive” and “negative” moments. The figure reflects the experimental setup used in the WSU tests, which were performed upside-down relative to the outrigger bents in the as-existing bridge. For consistency with the discussion of the as-existing outrigger results, the terms “inside” and “outside” bars correspond to the placement of the bars in the actual bridge. Therefore, for the beams of the WSU test specimens, the “inside” bars were physically above the “outside” bars, as shown in Figure 4-1.

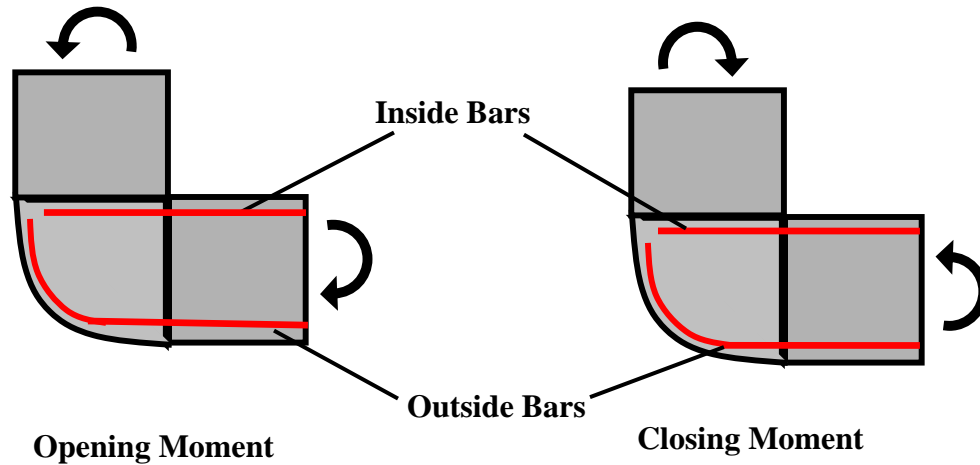


**Figure 4-1: Opening and Closing Moments on Test Specimens**

#### **4.2.1 Beam and Column Flexural Response**

The flexural response of the beams and columns merits analysis for two reasons. First, flexural failure of the element could theoretically occur under very large excitations, although the probability of such failure is low, as explained below. Second, and more important in practice, the forces induced in the bars by member flexure constitute the loads on the adjacent elements, such as the joints. The poor detailing of the joints makes them relatively vulnerable, so knowledge of the loads on them is important.

With proper detailing, a beam or column can sustain deformation demands that exceed the yield displacement without loss of load-carrying capacity. The full-height column jackets from the Phase 1 retrofit stiffened the columns significantly, so deformations, and hence column yielding, are concentrated in the gaps between the end of the jacket and the beam at the top of the column, or the foundation at the bottom of the column. This concentration of deformation induces bar strains (and stresses) that are higher than those that would exist in the absence of the jacket. However, the gap is small in comparison with the column diameter, so the concrete in it experiences considerable confinement from the jacket. At the ductility demands expected, flexural failure and consequent loss

of capacity is therefore improbable, provided that the bars have adequate tension strain capacity.

The force and stress demands on the adjacent elements can be determined from the moment demands on, or plastic flexural capacities of, the beams or columns. Therefore, the yield and maximum moments of the beams and columns were determined to provide bounds for these force demands. In addition, the beam and column yield moments were compared to determine which would occur first and control the force demand.

The response at the cross section level of each beam and column of each outrigger bent (both experimental and actual) was computed with a moment-curvature analysis. The analysis was conducted on a cross-section representative of the geometry and reinforcement of the unjacketed portion of the column or end of the beam that was adjacent to the joint. Appropriate values of the axial load were used. The cross-section was subdivided into fibers, and the moment-curvature response was determined by using the material properties appropriate for each fiber (i.e., those representative of unconfined concrete, confined concrete, and reinforcing steel). For a given curvature, a neutral axis location was assumed, and compatibility was used to establish the strain in each fiber (assumed to be a linear strain distribution across the cross section). Axial force equilibrium was used to determine the location of the neutral axis, and once it was satisfied, the moment corresponding to the selected curvature was determined. Figure 4-2 shows a typical response.

Three material models were used for these analyses. The Modified Burns and Siess model was used (Burns and Seiss 1962) to simulate the material properties of the reinforcing steel, while the material properties of the unconfined and confined concrete were modeled with the Mander et al. model (Mander, Priestley, Park 1988). For the beams, only the unconfined concrete model was used because the spacing of the transverse steel was deemed to provide insignificant confinement. For the columns, because yielding would initiate in the unjacketed regions, the properties of the confined concrete were based on the spacing and layout of the as-existing transverse

reinforcement. Although the steel jacket provides additional confinement over this region, neglecting this added confinement would not change the moment-curvature results significantly. In the analyses of the experimental specimens, the measured material strengths of the test specimen were used (see Section 2.2).

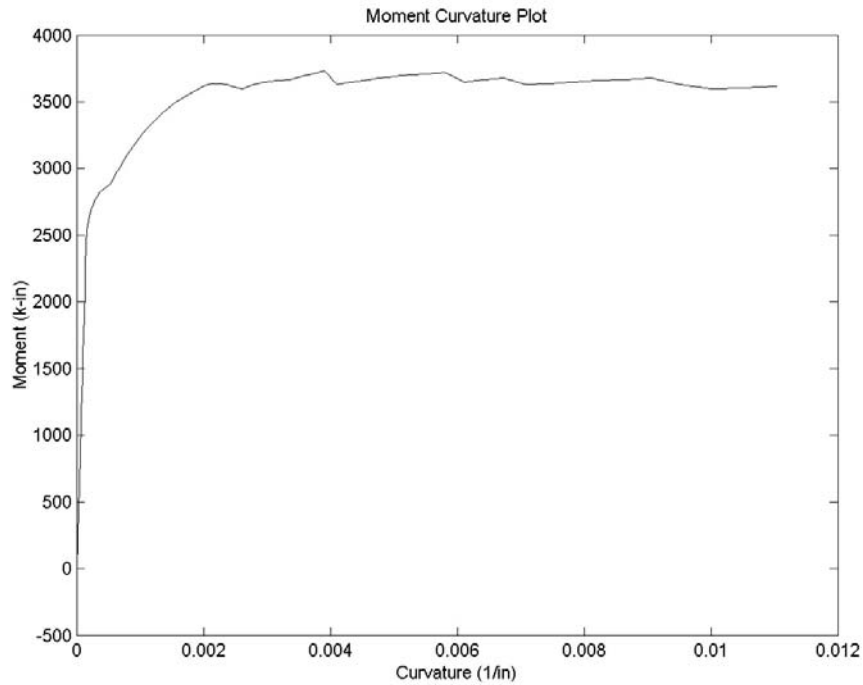


**Figure 4-2: Typical Theoretical Moment-Curvature Response (WSU Short Beam, Opening Moment)**

The reinforcing bars that extended to the back face of the joint were included in the analyses. (Figures 2-6 and 2-7 show details of the test specimens.) Although the anchorage lengths of some of the straight bars do not meet current ACI 318 requirements (ACI 2002), many of them are located in intermediate layers where the bar strains are relatively small and the bond demands are consequently low. Furthermore, bond failure of these bars was not observed in the tests. They were therefore treated as being fully bonded and were included in the analysis.

The theoretical opening and closing in-plane yield moments for each WSU test specimen are presented in Table 4-1. As described in Chapter 2, “short” and “long” refer to the specimen with a short outrigger beam and a long outrigger beam, respectively.

Equilibrium at the center of the joint shows that, in all cases, the column would yield before the beam for both opening and closing moments. The controlling yield moments are highlighted in bold in the table. In addition to the yield moments, the theoretical ultimate moments that correspond to the maximum moment on the moment-curvature plot are tabulated.

**Table 4-1: Critical In-Plane Moments of Test Beams and Columns**

		$M_{\max\text{-exp}}$ (k*ft) (measured)		$M_y$ (k*ft) (theoretical)		$M_u$ (k*ft) (theoretical)	
		Opening	Closing	Opening	Closing	Opening	Closing
Short Outrigger	Beam	168	226	211	290	313	382
	Column	125	235	<b>165</b>	<b>165</b>	264	264
Long Outrigger	Beam	113	121	126	94	180	150
	Column	88	124	<b>92</b>	<b>92</b>	161	161

The maximum experimental moments are also shown in Table 4-1. For the column, this moment was calculated by multiplying the maximum actuator load from the load-displacement graphs of the specimens by the height of the actuator to the face of the joint. The beam moment at the interface of the beam and the joint was calculated from equilibrium at the center of the joint. As presented in the following sections, the maximum experimental forces were used to determine lower bounds to some of the response mechanism capacities in the test specimens, which assumed that the specimen was at incipient failure in those mechanisms. The capacities for the specimens were used as a basis for determining capacities for the as-existing outriggers.

Because measured bar strains (and/or stresses) were not available, the results of the moment-curvature analysis were used to determine the bar stresses in the outermost bars of the column and beam of each test specimen. For example,  $f_{s,\max\text{-exp}}$  is the theoretical

magnitude of the bar stress that corresponds to the maximum measured moment. These calculations are also shown in Appendix B, and the results are displayed in Table 4-2. The ratios of  $f_{s,max\_exp}$  to the yield and ultimate stresses obtained from coupons of the reinforcing steel of the test specimens ( $f_{sy}$  and  $f_{su}$ ) are also presented. Recall from Section 2.2 that for No. 5 bars (short-specimen beam and column and long-specimen beam longitudinal reinforcement), the measured yield stress was 53.6 ksi, and the measured ultimate stress was 79.6 ksi, while for No. 4 bars (long-specimen column reinforcement), the measured yield stress was 53.4 ksi, and the measured ultimate stress was 87.5 ksi. As indicated by comparison of the moments tabulated in Table 4-1, under opening moments bar yielding did not occur. However, under closing moments, the yield stress was exceeded in the column of the short specimen and in the beam and column of the long specimen. In addition to indicating the state of stress in the reinforcement, the maximum bar stresses,  $f_{s,max\_exp}$ , were used to calculate bond stress capacities (Section 4.2.4), which were then compared to the respective demands on the as-existing outrigger bents.

**Table 4-2: Maximum Bar Stresses and Stress Ratios for In-Plane Specimens**

		$f_{s,max\_exp}$ (ksi)		$f_{s,max\_exp}/f_{sy}$		$f_{s,max\_exp}/f_{su}$	
		Opening	Closing	Opening	Closing	Opening	Closing
Short Outrigger	Beam	42.2	40.4	0.79	0.75	0.53	0.51
	Column	39.8	64	0.74	1.19	0.50	0.80
Long Outrigger	Beam	47.4	54.2	0.89	1.01	0.54	0.68
	Column	51.2	61.5	0.96	1.15	0.59	0.70

Displacement ductility provides an approximate global indicator of the severity of damage expected to an outrigger. Large displacement ductility demands may result in significant damage and eventual loss of lateral-load carrying capacity in an outrigger element. To quantify the displacement ductility capacities achieved by the WSU specimens corresponding to significant degradation of lateral-load carrying capacity, the displacement ductility for each specimen was calculated with Equation 4-1 and the load-displacement graphs provided by the WSU research team.

$$\mu_{\Delta\text{-exp}} = \frac{\Delta_{u\text{-exp}}}{\Delta_{y\text{-exp}}} \quad (4-1)$$

where:

$\mu_{\Delta\text{-exp}}$  = displacement ductility at loss of load carrying capacity

$\Delta_{u\text{-exp}}$  = measured displacement at loss of load carrying capacity

$\Delta_{y\text{-exp}}$  = measured yield displacement

Figures 4-3 and 4-4 show the in-plane load-displacement histories of the short and long specimen; the measured yield displacement and displacement at loss of load carrying capacity are indicated. The measured yield displacement,  $\Delta_{y\text{-exp}}$ , as determined by Shattarat (2004) is based on either strain gauge measurements on the beam or column bars (closing moments) or through a calculated procedure (opening moments). The measured ultimate displacement,  $\Delta_{u\text{-exp}}$ , is the displacement at which the force drops to 80 percent of its peak value (NZS:3101 1995), determined from the load-displacement histories.

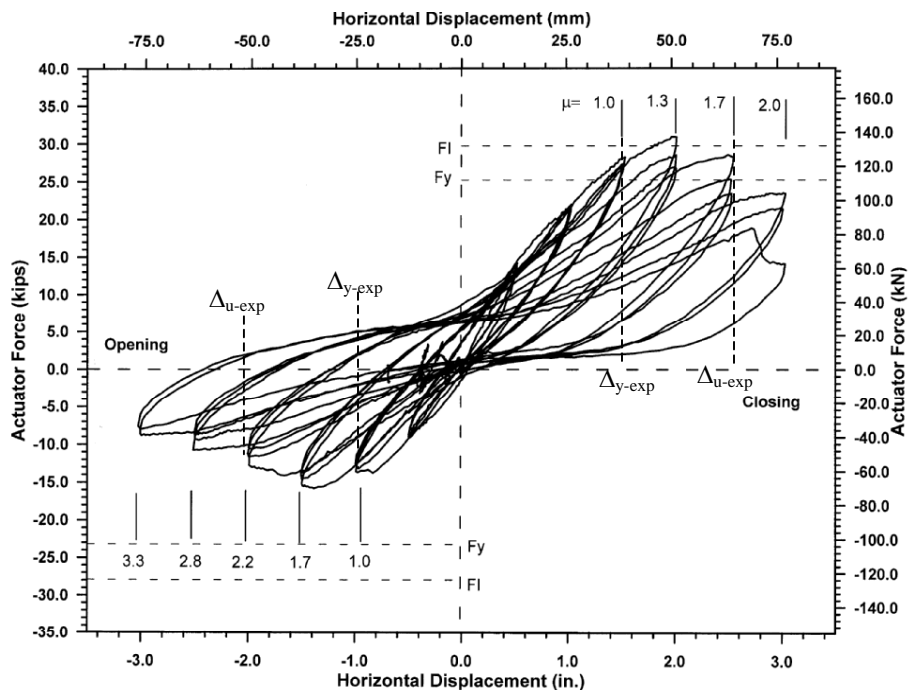


**Figure 4-3: Actuator Force-Horizontal Displacement History for the As-Built Short Specimen Subjected to In-Plane Loading (Courtesy of Washington State University)**

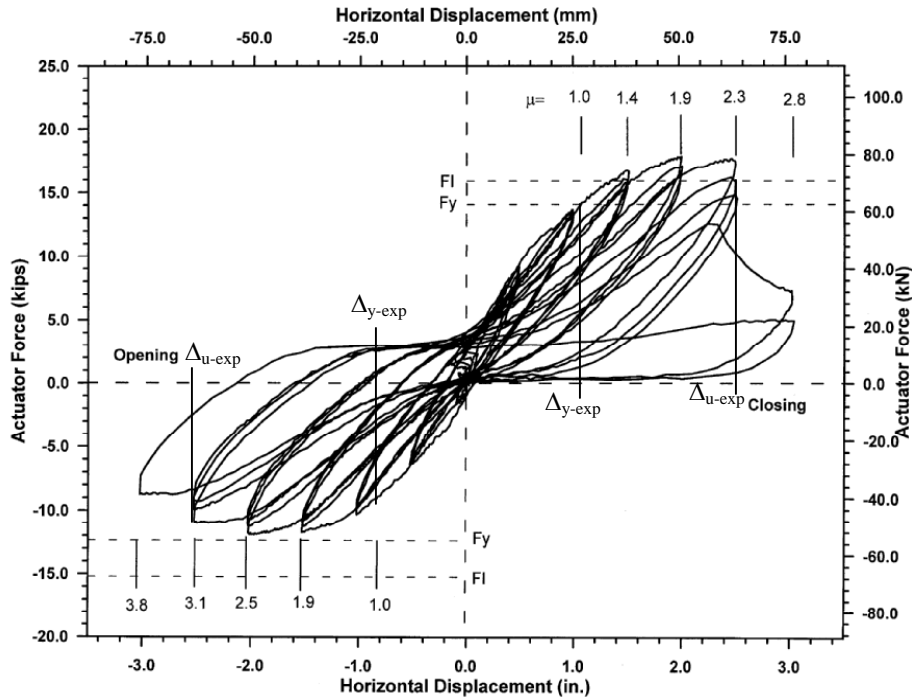


**Figure 4-4: Actuator Force-Horizontal Displacement History for the As-Built Long Specimen Subjected to In-Plane Loading (Courtesy of Washington State University)**

The ultimate displacement ductility values of the two test specimens was in the range of 2 to 3, indicating that the ductility capacity of the outrigger bents was low. Table 4-3 presents the calculated results for both opening and closing moments of the long and short specimen.

**Table 4-3: Maximum Displacement Ductilities Achieved in the In-Plane Experiments**

	Short	Long
Closing Moment	1.7	2.3
Opening Moment	2.2	3.1

#### 4.2.2 Joint Shear Under Transverse Loading

High joint shear stresses can result in joint damage and can contribute to strength loss under transverse loading due to both opening and closing moments. The WSU specimens sustained damage in the joint region, as shown in Figure 4-5. The diagonal crack pattern

suggested that the damage resulted from closing moment demands. The circumferential cracking could have been due to a splice failure under closing moment demands or radial tension stresses under opening moment demands.

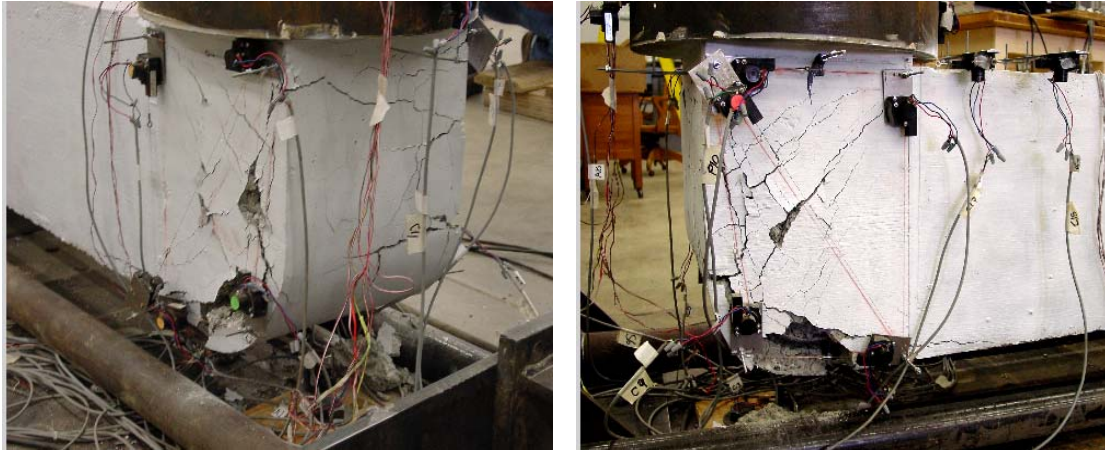


**Figure 4-5: Joint Shear Damage in WSU “Long Outrigger,” In-Plane Loading (Courtesy of Washington State University)**

To estimate the stress corresponding to joint shear failure, the average horizontal joint shear stress corresponding to the maximum experimental moment was calculated for both the long and short outrigger. (Note that although the horizontal and vertical shear stresses must always be equal at a point, this is not true for the average shear stresses, which are the only values that can be computed from the experimental data.) The average horizontal joint shear stress was used, since most codes and texts (for example, ACI 318 2002) use horizontal joint shear for demand and capacity comparisons. Figure 4-6 shows a free-body diagram of the joint region, including the components needed to calculate joint equilibrium and the corresponding average horizontal joint shear stress demand.

To calculate the horizontal joint shear stress, the beam moment must first be determined. If the beam moment strength controls the outrigger capacity, the beam flexural strength can be used and the determination is straightforward. However, if the column moment strength controls, as is the case in the diagram, the beam moment corresponding to the flexural strength of the column must be computed by using equilibrium.

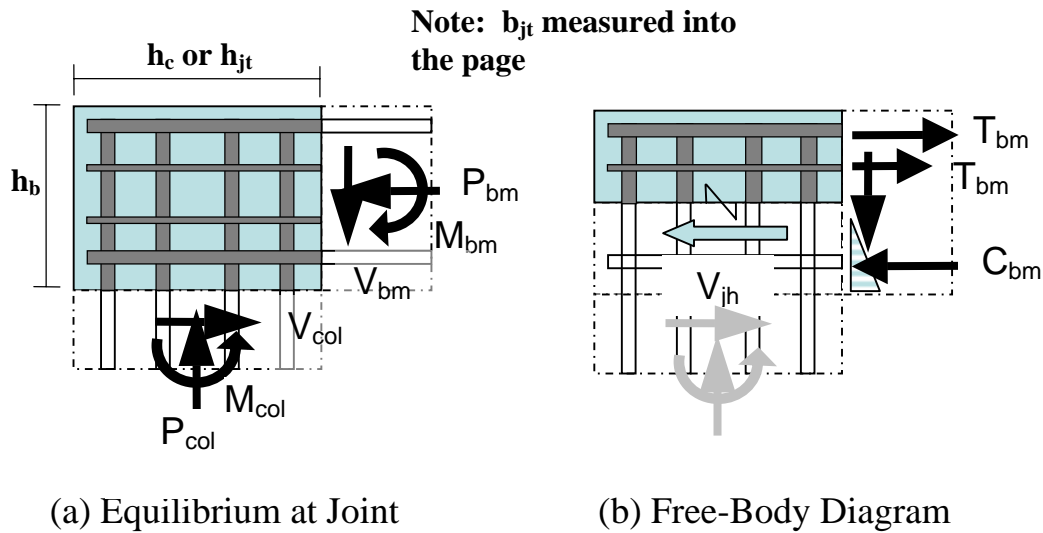


**Figure 4-6: Horizontal Joint Shear Stress Determination Under Closing Moment**

Under closing moments, it follows from Figure 4-6 that the beam moment corresponding to the flexural strength in the column can be calculated with Equation 4-2:

$$M_{bm} = M_{col} + V_{col} \frac{h_b}{2} - P_{col} \frac{h_c}{2} \quad (4-2)$$

Under opening moments, the column shear and moment in Figure 4-6 change direction while the axial load remains the same. Therefore, the beam moment is calculated as follows:

$$M_{bm} = M_{col} + V_{col} \frac{h_b}{2} + P_{col} \frac{h_c}{2} \quad (4-3)$$

The calculated beam moment is then used to determine tension forces in the beam bars. This is done by first performing the moment-curvature analysis described in Section 4.2.1. From the beam moment, the stresses can be obtained, and the force in the beam bars is then calculated by multiplying the bar stress by the corresponding area of steel. The joint shear force can then be calculated by summing the tension forces in the bars as follows:

$$V_{jh} = \sum T_{bm} \quad (4-4)$$

The average horizontal joint shear stress can then be determined from Equation 4-5.

$$v_{jh} = \frac{V_{jh}}{b_{jt} * h_{jt}} \quad (4-5)$$

The calculated results are shown in Table 4-4. Because the column yielded before the beam for both specimens under both opening and closing moments, the horizontal joint shear was based on the beam moment corresponding to the column flexural strength for all cases.

**Table 4-4: Normalized Horizontal Shear Stress on Test Specimens, ( $v_{jh} / \sqrt{f'_c}$  psi), at Peak Load**

Short – Closing	Short- Opening	Long – Closing	Long-Opening
8.9	7.2	9.4	6.7

As mentioned previously, damage due to both opening and closing moments in the long specimen was observed. For the short specimen, damage occurred because of opening moments; however, there was no indication of significant diagonal cracking due to closing moments (as seen in Figure 2-8). Nevertheless, the joint shear stress demand due to closing moments was similar to that of the long specimen, which experienced significant diagonal cracking. The results of the tests are confusing in this regard.

Quantifying the joint shear capacity for opening moments was complicated by the occurrence of radial cracking in both the short and long specimens. The cracking may have been caused by an anchorage or splice failure due to closing moments or radial tension stresses (a form of joint shear) due to opening moments. Because it was unclear whether lateral strength degradation was caused by joint shear in either specimen, a lower bound approximate value of  $7\sqrt{f'_c}$  psi was used as the joint shear stress capacity to represent an average of the opening moment joint shear stress. The actual capacity may

be higher if another response mechanism caused the loss of load carrying capacity, but due to the ambiguity in the specimens' behavior, the lower bound capacity is used.

### 4.2.3 Radial Tension

Damage in an outrigger joint subjected to in-plane loading can be caused by high radial tension stresses. Radial tension stresses are essentially the diagonal tension component of the joint shear stress in a knee-joint and are caused by an opening moment. Figure 4-7 diagrams a simplified force-transfer mechanism for the tensile forces that result from the force couple because of opening moment. When the tensile stress demand exceeds the tensile strength of the concrete, a crack forms and the load path changes. The horizontal and vertical forces imposed respectively by the beam and column force couples can no longer be equilibrated by the diagonal tension force across the joint. The only remaining load path is a curved one, around the outer face of the joint. Compressive force along this path induces bending and causes the arch of concrete to move away from the joint in the radial direction. The bars on the outer face of the joint bend outward, which results in widening of the circumferential cracks and spalling of the cover concrete. This form of joint damage was observed in the tests, as shown in Figure 4-8.

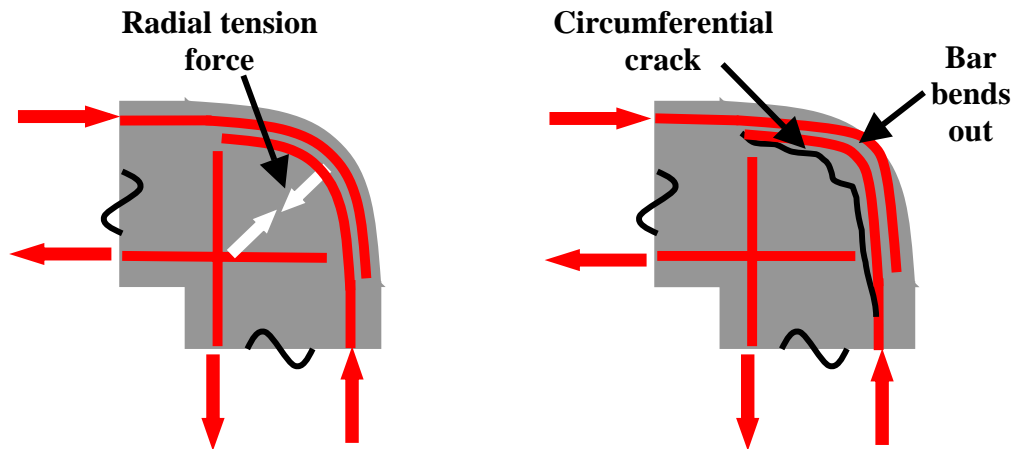
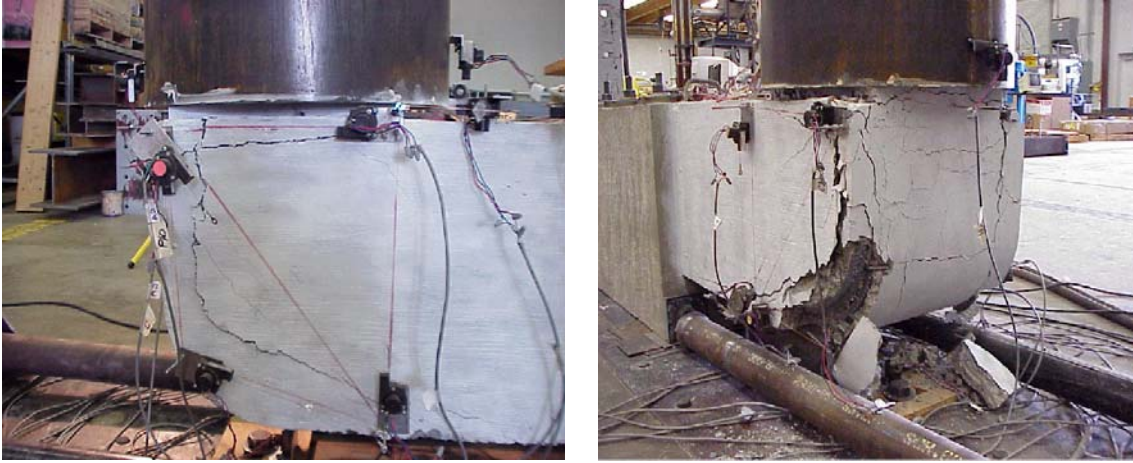
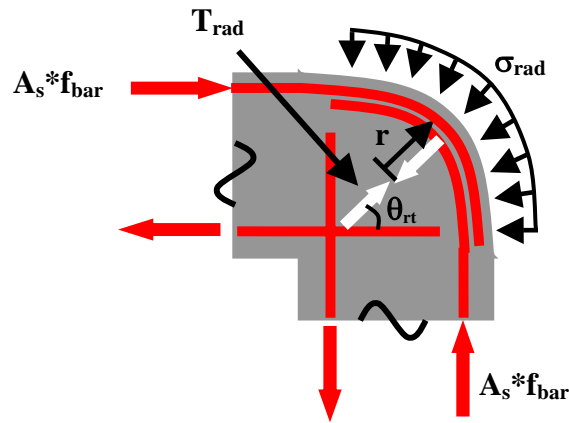


Figure 4-7: Radial Tension in Outrigger Joint: Forces on Bars



**Figure 4-8: Radial Tension Damage to WSU Short Outrigger, In-Plane Loading (Courtesy of Washington State University)**



**Note: Thickness of joint ( $b_{jt}$ ) measured perpendicular to page**

**Figure 4-9: Definition of Variables for Radial Tension**

The radial tension stress depends on the geometry of the joint and the radius of the hooked bars around the joint (see Figure 4-9). Assuming that the width of the joint is equal to the depth of the joint, and the bar force in the outside column bar is equal to the bar force of the outside beam bar, the force resultant of the radial tension is calculated as follows:

$$T_{rad} = \sqrt{2} * A_s * f_{bar} \quad (4-6)$$

The average stress is computed under the assumption that the force is uniformly distributed along the curved section of the reinforcing steel at the exterior of the knee joint. A relationship between the radial tension force and radial tension stress can then be determined as:

$$\begin{aligned}
 T_{rad} &= \int_{-45^{\circ}}^{45^{\circ}} b_{jt} * \sigma_{rad} * r \cos \theta_{rt} * d\theta_{rt} = b_{jt} * \sigma_{rad} * r \sin \theta_{rt} \Big|_{-\pi/4}^{\pi/4} \\
 &= \sqrt{2} * b_{jt} * \sigma_{rad} * r
 \end{aligned}
 \tag{4-7}$$

Therefore, the radial tension stress can be calculated as follows:

$$\sigma_{rad} = \frac{T_{rad}}{\sqrt{2} * r * b_{jt}} = \frac{A_s * f_{bar}}{r * b_{jt}}
 \tag{4-8}$$

where:

$\sigma_{rad}$  = radial tension stress

$T_{rad}$  = radial tension force resultant based on compression force in the beam bars

$A_s$  = area of curved beam or column bars

$f_{bar}$  = compression bar stress demand

$r$  = radius of curved bars

$\theta_{rt}$  = angle between radial tension force resultant and the horizontal

$b_{jt}$  = thickness of outrigger joint

To determine the compression bar stress on the test specimens, an approximation of the bar stress corresponding to the maximum experimental moment was needed. Because radial tension stresses result from opening moments, these moments were used for the calculations. Again, a moment-curvature analysis was performed, as described in Section 4.2.1, and the compression bar stress on the outside bars was determined from the associated moment.

Results for the test specimens are shown in Table 4-5. For both specimens, the columns yielded before the beams under opening moment; therefore, the stresses in the column bars exceeded those in the beam bars. As a result, the radial tension stress was based on the stress in the column bars. Significant radial tension damage was observed in the short

specimen, and circumferential cracking was also observed in the long specimen. Because both the long and short specimen stresses were similar, a radial tension stress of  $4\sqrt{f'_c}$  psi was used as the capacity for comparison with the as-existing outrigger demands.

**Table 4-5: Normalized Radial Tension Stresses on WSU Outrigger Joints**

$$(\sigma_{rad} / \sqrt{f'_c})$$

	“Short”	“Long”
Column Bars	4.2	3.9

#### 4.2.4 Bar Anchorage

Damage from loading in the transverse direction may also occur because of inadequate anchorage of the beam or column bars into the joint region. Research indicates that the bond capacity of a bar in well-confined concrete degrades with bar yielding and cycling (Eligehausen et al. 1983). More severe, and faster, degradation is expected for bars embedded in poorly confined concrete, which better reflects the conditions in the outrigger joints of the SR 99–Spokane Street over-crossing structure.

Circumferential cracking along the exterior of the joint may indicate anchorage damage due to high stresses along the spliced region under closing moments. In addition, as discussed previously, this damage pattern may be initiated by radial tension under opening moment. In either case, anchorage of the exterior bars is compromised by these cracks. Signs of this damage could be seen in the “outside” column bars for both test specimens at displacement ductility demands of between 1 and 3. Figure 4-10 shows this damage pattern for both specimens. In addition, horizontal splitting cracks developed at the location of the beam “inside” bars (upper bars in the figure) in the short specimen; this indicates high bond stresses. This damage also occurred at a displacement ductility demand of between 1 and 3 and propagated as the displacement ductility demands increased.

### Short Specimen



### Long Specimen



**Figure 4-10: Crack Pattern in WSU Short and Long Outrigger, In-Plane Loading (Courtesy of Washington State University)**

To evaluate the bond capacity associated with the anchorage conditions in the test specimens, the following approaches were used, resulting in two different average bond capacities. The theoretical average bond stress demands for the beams and columns of each specimen under both opening and closing moment were calculated to correspond to the maximum actuator force. The average of the experimental bond stress values was used as an approximate bond capacity for the demand/capacity evaluation of the as-existing outriggers. In addition, the theoretical stresses implied by the ACI-318 expressions for embedment or splice lengths (ACI 2002) were calculated. Table 4-6 presents the average bond stresses calculated by each method and a comparison of the two.

The anchorage details influence the likelihood of bar failure. In the specimens, three separate anchorage conditions were considered, to reflect the conditions in the actual bridge:

- spliced bars
- straight bars
- bars with 180-degree hooks.

**Table 4-6: Normalized Average Bond Stress,  $\tau_{bond} / \sqrt{f'_c}$  (psi) on Test Beam and Column Bars in Tension**

		Beam		Column	
		Opening	Closing	Opening	Closing
Short	Exp. Bond Stress	8.0	4.5	7.0	7.2
	ACI Bond Stress	2.9	3.2	4.1	3.2
	Exp./ACI	2.7	1.4	1.7	2.2
Long	Exp. Bond Stress	(180 hook)	6.4	6.3	5.9
	ACI Bond Stress	(180 hook)	3.2	4.2	3.2
	Exp./ACI	---	2.0	1.5	1.8
Average Exp. Bond Stress		8.0	5.5	6.7	6.6

The outside beam and column bars curve around the exterior face of the joint and are spliced at this location. Although the bars consist of 90-degree bends, the details do not meet the current ACI standard (ACI 318 2002), and therefore, an increase in capacity due to the bend was not considered. The average bond stress for this condition,  $\tau_{bond}$ , corresponds to the curved splice length and was calculated with Equation 4-9:

$$\tau_{bond} = \frac{A_{bar} * f_{s\_max-exp}}{\pi * d_b * l_{sp}} \quad (4-9)$$

where:

$A_{bar}$  = area of bar

$f_{s\_max-exp}$  = maximum experimental bar stress presented in Section 4.2.1

$d_b$  = diameter of bar

$l_{sp}$  = length of splice

The inside beam and column bars terminate with straight ends, and the calculation of bond stress for this condition was similar to that for the spliced bars. Equation 4-10 was used, and the only difference from Equation 4-9 was that the embedment length of the straight bar was used instead of the splice length.

$$\tau_{bond} = \frac{A_{bar} * f_{s\_max-exp}}{\pi * d_b * l_d} \quad (4-10)$$

All of the variables were defined previously except for the following:

$l_d$  = embedment length of bar

The last anchorage condition consists of bars terminating in a 180-degree hook, a configuration that the beam inside bars of the long specimen exhibit. This condition improves the anchorage significantly and reduces the likelihood of premature anchorage damage; therefore, these bars were assumed to be fully developed.

It is possible that bar anchorage failure could occur before yielding of the beams or columns of the outrigger bents. It is also possible that post-yield strain hardening could induce higher bond stresses and reduced bond capacity, which could then lead to anchorage failure (Raynor et al. 2002). Therefore, an accurate estimate of the bar stress is important. To obtain reasonable values, the procedure described in Section 4.2.1 and Appendix B was used to estimate the maximum experimental bar stress.

The calculated average bond stresses were normalized with respect to  $\sqrt{f'_c}$  psi and are presented in Table 4-6. The bond stresses were within the range of 4 to  $8\sqrt{f'_c}$  (psi). Previous experimental results have suggested that the average bond capacity of a yielded bar anchored in a well-confined region is between 6 and  $12\sqrt{f'_c}$  psi (Lehman et al., 2001). Therefore, anchorage damage could be expected because the confinement within the joint region is limited.

Further insight into the severity of the bond stresses was also possible by comparing the calculated experimental values with another method of evaluation. Here, the average bond stress implied by ACI 318 was used. To calculate the average bond stress, the required development lengths for each anchorage condition were substituted into equations 4-11. The basic development length equation for seismic loading, as provided in ACI Section 21.5.4.1, is for the development of hooked bars. The straight bar development length is given as the hook length multiplied by a factor of 3.5 for top cast

bars and by a 2.5 factor for all other bars. For the WSU specimens, the 3.5 factor was applied to the beam inside bars (i.e., the bars that were on top in the as-cast and as-tested orientation and that were in tension under opening moment), and the 2.5 factor was applied to all others. In addition, because the outrigger joints were not well confined, the development length was multiplied by 1.6 as required by Section 21.5.4.3. The resulting values of development lengths under opening moments were transformed into average bond stress values by the following formula:

$$\tau_{bond} = \frac{A_{bar} * f_y}{\pi * d_b * l_d} \quad (4-11)$$

This formula is the same as equations 4-9 and 4-10 except that the bar yield stress,  $f_y$ , is used instead of the maximum experimental bar stress, and the variable  $l_d$  corresponds to the ACI required development length of a bar.

For the specimen outside bars under closing moments, ACI Section 12.15.1 requires Class B lap splice lengths to be used. The required splice length was calculated as the previously determined development length multiplied by a 1.3 factor. The resulting values of splice lengths under closing moments were transformed into average bond stress values with Equation 4-11 and the required length of the lap splice in lieu of the development length.

The resulting average ACI bond stresses (normalized with respect to  $\sqrt{f'_c}$  psi) are presented in Table 4-6 for the beam and column bars stressed in tension. Also, the averages of the experimental bond stresses are tabulated for use as the bond stress capacities in the demand/capacity evaluation of the outrigger bents.

Under opening moment, the large experimental to ACI bond stress ratio in the short specimen beam bars validated the anchorage damage seen in the beam inside bars in Figure 4-10. The long specimen beam inside bars did not exhibit this type of damage because of the presence of the 180-degree hooks. Under closing moments, both the long and short specimen displayed circumferential cracking along the exterior bars of the joint, as seen in Figure 4-10. The relatively high bond stress ratios under closing moments for

both specimens also supported the observation. However, it is also possible that radial tension or joint shear initiated damage and reduced bond capacity, resulting in the observed cracking and eventual loss of lateral load carrying capacity.

#### 4.2.5 Beam Shear

Under in-plane loading, the outrigger beam may be susceptible to damage caused by beam shear. Beam shear can cause diagonal cracks to form in the vertical faces of the beam. These cracks usually start near the supports and propagate up the face of the beam. For beams without sufficient transverse reinforcement, the cracks may widen under repeated large load cycles and lead to beam failure.

In the experiments, the test setup was statically determinate, and the beam shear was equal to the applied axial load. As will be shown, this shear demand was less than the value based on the beam's plastic moment capacity, so larger shear stress demands are possible in the bridge. No beam shear damage was observed in the WSU test specimens.

To evaluate the likelihood of shear failure in a beam subjected to seismic loading, the maximum possible shear demand, which is associated with the development of plastic moments at both ends of the beam, can be compared with the theoretical shear capacity presented in ACI (ACI 318-02 2002). The maximum shear demand is given by:

$$V_{pl} = \text{Max} \left( \frac{(M_{p1}^+ + M_{p2}^-)}{L_{clear}}, \frac{(M_{p1}^- + M_{p2}^+)}{L_{clear}} \right) \quad (4-12)$$

Figure 4-11 shows a pictorial description of the shear calculation. In Equation 4-12, the variable  $L_{clear}$  represents the clear span length of the beam between the joint and deck. The plastic moment at the end of the beam adjacent to the deck is represented as  $M_{p1}$ , and the plastic moment at the end of the beam adjacent to the joint is represented as  $M_{p2}$ . ACI 318-02 requires that the value of  $M_{p1}$  be calculated as the nominal moment strength of the beam using a bar stress of  $1.25 f_y$ . Because the maximum possible moment at the joint end of the beam was known from the experiments, it was used for  $M_{p2}$ .  $M_{p1}$  was computed by following the ACI approach.

The calculated plastic shear demands, as well as the experimental shear demands for the specimens, are presented in Table 4-7.

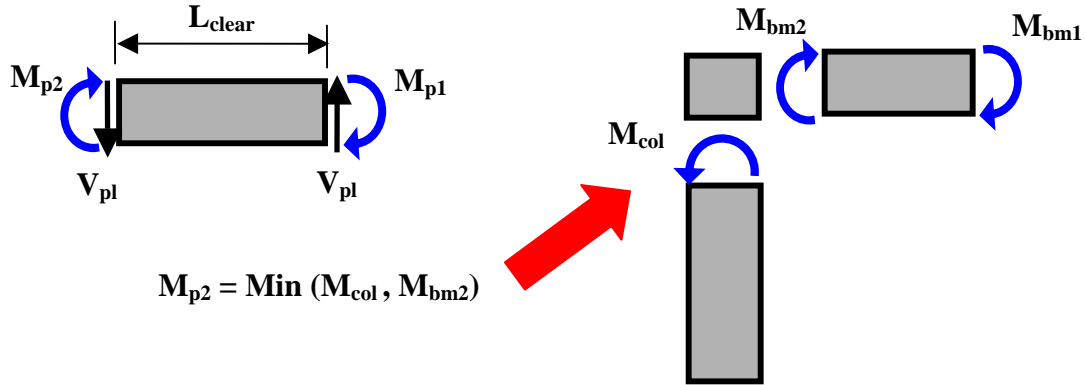


**Figure 4-11: Calculation of Plastic Seismic Shear Demand**

**Table 4-7: Beam Shear Demand on and Theoretical Capacity of Specimens (kips)**

	$V_{pl}$	$V_{exp}$	$V_s$	$V_c$	$V_n = V_s + V_c$	$V_{exp}/V_n$	$V_{pl}/V_n$
Short	260	50	187	41	228	0.2	1.1
Long	122	30	211	30	242	0.1	0.5

In calculating the theoretical shear capacity, ACI 318-02 Section 21.3.4.2 recommends neglecting shear strength attributed to the concrete,  $V_c$ , if significant cracking is expected during seismic loading or if the axial load is less than  $0.1f'_cA_g$  and the plastic shear demand ( $V_{pl}$ ) exceeds half of the total shear demand. The WSU short and long specimens met the latter criteria. However, because very little beam shear cracking was observed in the test specimen, both the shear capacity attributed to the concrete ( $V_c$ ) and steel ( $V_s$ ) are presented in Table 4-7. The shear strength attributed to the concrete was calculated with Equation 4-13:

$$V_c = 2 * \sqrt{f'_c} * b * d \quad (4-13)$$

where:

$V_c$  = shear strength attributed to the concrete

$f'_c$  = concrete compressive strength

b = width of beam

d = distance from extreme compression fiber to centroid of longitudinal tension reinforcement

The shear strength attributed to the steel included contributions from both the vertical and diagonal stirrups (see Figure 2-\_\_\_ for details of the test specimens). The contribution from the vertical stirrups was calculated with Equation 4-14:

$$V_s = \frac{A_v * f_y * d}{s} \quad (4-14)$$

The contribution from the diagonal stirrups was calculated with Equation 4-15:

$$V_s = \frac{A_v * f_y * (\sin(\alpha) + \cos(\alpha)) * d}{s} \quad (4-15)$$

where

$V_s$  = shear strength provided by reinforcing steel

$f_y$  = reinforcing steel yield strength

s = spacing of stirrups or closed hoops

d = distance from extreme compression fiber to centroid of longitudinal tension reinforcement

$\lambda$  = angle between inclined stirrups and longitudinal axis of member

The total capacity,  $V_n$ , is the sum of the two shear-strength components and is provided in Table 4-7. In addition, the experimental and plastic shear demand/capacity ratios are presented.

From the results, it can be seen that the shear demands on both specimens were much lower than the plastic shear demands that might have resulted if the entire bent had been tested, including the effects of the seismic shear component. Therefore, as tested, the shear strength of the specimen exceeded the experimental shear demand. This is evident by the lack of shear cracks in the beam for both test specimens.

If the vertical load in the tests had been equal to the plastic shear demand, the short specimen might have been susceptible to shear damage because the plastic shear demand,  $V_{pl}$ , was greater than the ACI shear strength,  $V_n$ . However, the conservatism of the ACI equation for shear strength due to concrete,  $V_c$ , must be taken into account. Research has indicated that, for a small shear span to depth ratio, the shear strength due to the concrete is significantly greater than  $2\sqrt{f'_c}bd$  (Rebeiz, Fente, Frabizzio 2001). The data used in these studies indicated that, for small reinforcement ratios and a span to depth ratio of approximately 1.0 (which were the properties of the WSU short specimen),  $V_c$  may be as high as  $6\sqrt{f'_c}bd$ . If the shear strength attributed to the concrete were to have this value, the shear strength,  $V_n$ , would exceed the plastic shear demand,  $V_{pl}$  (310 kips vs. 260 kips). Therefore, had the plastic moments been achieved, it is still possible that a shear failure would not have occurred in the short specimen.

#### **4.2.6 Beam Torsion and Out-of-Plane Shear**

The response mechanisms of beam torsion combined with out-of-plane shear are unique to out-of-plane loading. Torsion behavior resembles that of shear in that the torsional moment is resisted primarily by the concrete before cracking, but the concrete contribution to the resistance drops significantly after cracking. After cracking, the torsional resistance can be idealized as a space truss consisting of the longitudinal reinforcement, which represents the top and bottom chords of the truss; the transverse steel, which represents the horizontal elements; and diagonal concrete struts, which represent the diagonal elements. For the space truss to be effective, continuity at the joints is necessary, and therefore closed hoops are needed.

In the outrigger beams in this study, the total area of vertical ties is larger than that of the horizontal ties. It is therefore likely that the members' resistance to combined torsion and vertical shear may be greater than to torsion plus horizontal shear. Concrete cracking indicative of torsion was observed in the WSU experiments. Figure 4-12 shows this type of diagonal cracking in the "short" outrigger that was subjected to out-of-plane loading.



**Figure 4-12: Torsion Cracks in “Short” Outrigger, Out-of-Plane Loading (Courtesy of Washington State University)**

The torsion resulting from the maximum actuator force was compared with the theoretical ACI capacity for the test specimen. Torsional strengths corresponding to cracking and nominal capacities were calculated. Using ACI 318-02, the torque required to cause cracking was calculated by following recommendations from ACI Section 11.6.1, as provided in Equation 4-16. This equation does not include the effects of out-of-plane shear and therefore, the results represent an upper bound on the cracking torque.

$$T_{cr} = 4 * \sqrt{f'_c} \frac{A_{cp}^2}{p_{cp}} \quad (4-16)$$

where:

$T_{cr}$  = cracking torque

$f'_c$  = concrete compression strength

$A_{cp}$  = area enclosed by outside perimeter of concrete cross section

$p_{cp}$  = outside perimeter of concrete cross section

Similarly, the nominal torsion strength of the beam after cracking was calculated by following ACI 318-02 Section 11.6.3.6. The equation (Equation 4-17) is based on the assumptions that the concrete has no tension strength, that the hoops are closed, and that the hoops are the critical elements.

$$T_n = \frac{2 * A_o * A_t * f_{yv} * \cot(\theta)}{s} \quad (4-17)$$

where:

$T_n$  = nominal torsion strength at yield of transverse reinforcement

$A_o$  = gross area enclosed by shear flow path

$A_t$  = area of 1 leg of closed stirrup resisting torsion

$s$  = spacing of transverse torsion reinforcement

$f_{yv}$  = yield strength of transverse reinforcement

$\theta$  = angle of compression diagonals in truss analogy for torsion, equal to  $45^\circ$  for non-prestressed members

Because the horizontal shear reduces the nominal torsion resistance in the top and bottom legs of the transverse hoops, a method is needed to account for this reduction in torsion capacity. The torsion strength in Equation 4-18 is based on the strength of one leg of the closed stirrup resisting torsion. Reducing the strength of the stirrup by the shear demand acting on it gives the revised torsion capacity as follows:

$$T_n = \frac{2 * A_o * (A_t - \frac{A_{v-dem}}{2}) * f_{yv}}{s} * \cot(\theta) \quad (4-18)$$

where  $A_{v-dem}$  is derived from Equation 4-14 by substituting  $V_{dem}$  for  $V_s$  in the expression as shown in Equation 4-19.

$$A_{v-dem} = \frac{V_{dem} * s}{f_{yv} * d} \quad (4-19)$$

For the WSU test, the out-of-plane shear demand,  $V_{dem}$ , was equal to the applied actuator force at the nominal torsion capacity as follows:

$$V_{dem} = F_{act} = \frac{T_n}{H_{act}} \quad (4-20)$$

where:

$F_{act}$  = applied actuator force

$H_{act}$  = height of actuator

Combining equations 4-18 through 4-20 gives:

$$T_n = \frac{2 * A_o * A_t * f_{yv}}{s * (1 + \frac{A_o * \cot(\theta)}{d * H_{act}})} * \cot(\theta) \quad (4-21)$$

Although the WSU test specimen did not have closed hoops, for comparison purposes, the calculations were completed assuming that the transverse steel could develop maximum torsion capacity. Table 4-8 shows the ACI cracking torque and the nominal torsion capacity with the corresponding actuator force. The theoretical column yield moment (as presented in Table 4-8) and the maximum experimental torque are also tabulated for comparison with the nominal torque. The maximum experimental torque was calculated by using the maximum actuator force from the load-displacement curve (see Figure 4-13) multiplied by the height of the actuator. Finally, the maximum experimental to ACI torque ratio is tabulated for comparison with the as-existing outriggers.

**Table 4-8: Summary of Torsion Demands on WSU “Short” Outrigger Beam**

T <sub>cr</sub> (k*ft) ACI	T <sub>n</sub> (k*ft) ACI	Actuator Force at T <sub>n</sub> (k)	M <sub>ycol</sub> (k*ft)	T <sub>max-exp</sub> (k*ft)	Exp/ ACI
20	83	10.1	165	98	1.2

The results suggest that both the upper bound cracking and nominal torque resistance values were exceeded and the column yield moment was not. However, Shattarat (2004) states that yielding of the transverse steel was not observed. A review of the experimental results indicated that the actuator force at the nominal torsion capacity (10.1 kips shown in Table 4-8) was approximately equal to the load at which softening occurred in the specimen, as seen on the load-displacement curve shown in Figure 4-13. This observation as well as the hysteretic response suggests that yielding of the transverse steel occurred. The force-displacement curve shows that the displacement ductility was approximately 2.5 in the “pull” direction and 5.0 in the “push” direction, which indicates that despite the non-code conforming stirrup and tie details (the transverse reinforcement was detailed using 90-degree hooks), the transverse reinforcement of the test specimen provided some ductility. The different responses in the two directions are confusing because the specimen was symmetric and theoretically should have displayed the same

yield displacements and displacement ductility in the “push” and “pull” directions. Also, the experimental cracking torque,  $T_{cr}$ , (approximately 65.6 k\*ft corresponding to the actuator force shown on the load-displacement graph) was much higher than the ACI cracking torque based on Equation 4-16 and presented in Table 4-8.

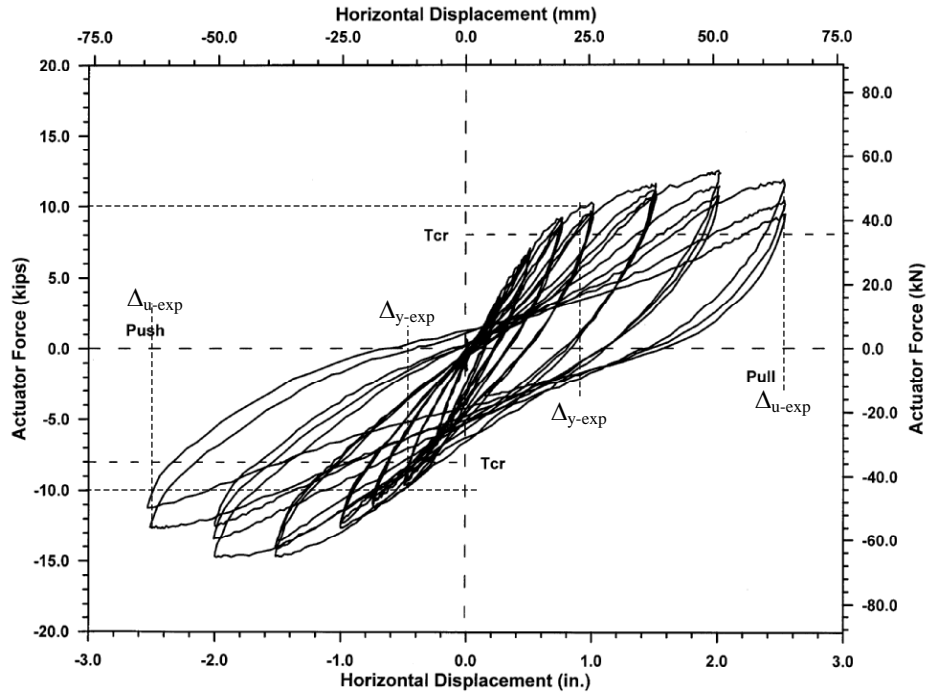


**Figure 4-13: Actuator Force-Horizontal Displacement History for the As-Built Short Specimen Subjected to Out-of-Plane Loading (Courtesy of Washington State University)**

### 4.3 Global Demands on Outrigger Bents

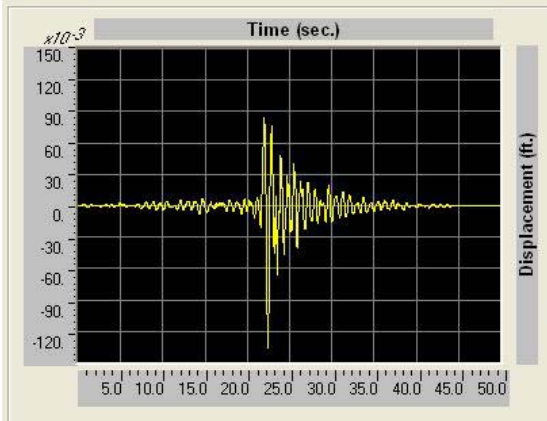
The demand analysis of the as-existing north concrete structure employed a finite element (FE) model of the structure as described in Chapter 3. The model was subjected to ground motions representative of three different seismic hazard levels in both the longitudinal and transverse directions. The demands for each response mechanism were based on the largest calculated response from all analyses. Both global and local demands were calculated. Global demands on the outriggers included displacements, drifts, and displacement ductility demand. Local demands included beam and column flexure, joint shear stress, radial tension stress, bar anchorage stress, beam shear and

beam torsion and are presented in Section 4.4. The demands were compared with the capacities discussed previously and used to determine the potential for failure due to the response mechanisms (e.g., joint shear, radial tension, etc.).

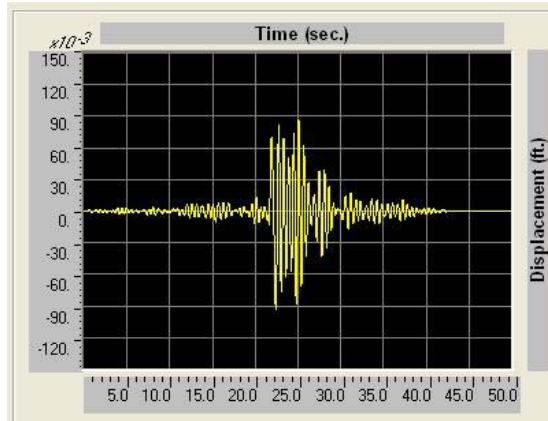
#### **4.3.1 Displacement and Drift Demands**

To compare the predicted global demands and the theoretical global capacities, displacements, drifts, and displacement ductility demands were calculated. The displacement demand on each of the outrigger bents was determined first. Figure 4-14 shows an example of the displacement histories of one of the critical outrigger bents, Bent 9 in Frame 3, for the three simulated ground motions in both the longitudinal and transverse directions. To facilitate comparison of the response histories, the results are shown using the same scale. Many characteristics of the displacement histories of Bent 9 also apply to other bents, and therefore, the bent-specific response can be generalized. For example, the frequency of the input motion to the structure dropped as the return period of the ground motion increased because of softening of the soils (see Section 3.7). In addition, the peak displacement amplitudes that resulted from the 72- and 475-year earthquakes were of similar magnitude, but those from the 2475-year earthquake were smaller. Also, the controlling hazard level was typically either the 72- or 475-year earthquake for each bent. For Bent 9, the 72- and 475-year earthquake controlled the displacements in the longitudinal direction and transverse direction, respectively.

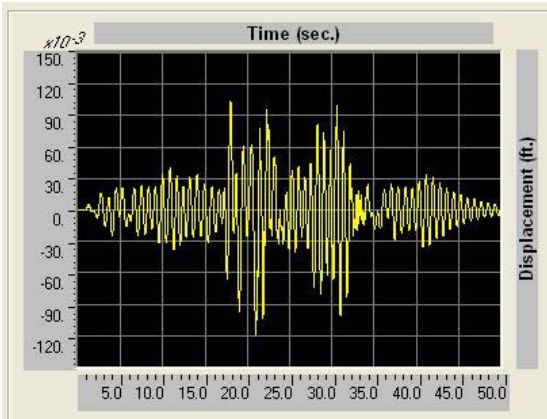
The peak displacements at the joint of each outrigger bent are presented in Table 4-9 for both the 72- and the 475-year earthquakes, as these were the controlling return periods for all the outrigger bents. The displacements shown in bold are the maximum displacements for each outrigger bent in each direction. In general, higher numbered bents were taller and sustained larger displacements. Furthermore, because of the height of the structure, the longer periods of frames 6 and 7 resulted in the longer period 475-year ground motion controlling the frames' and associated bents' maximum displacements.



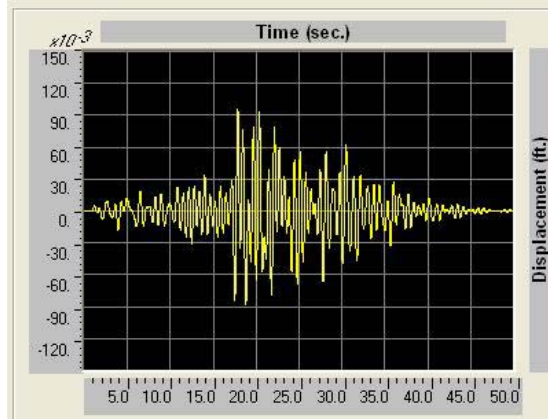
72 yr. Earthquake – Longitudinal



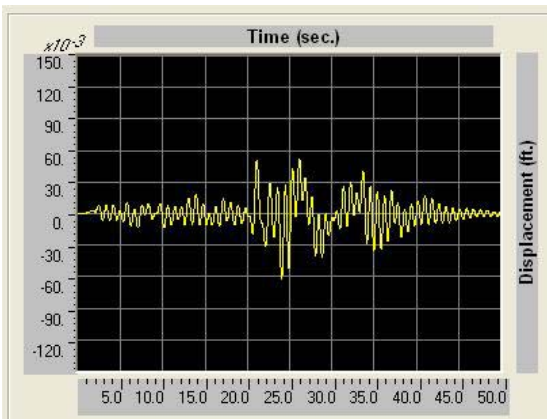
72 yr. Earthquake – Transverse



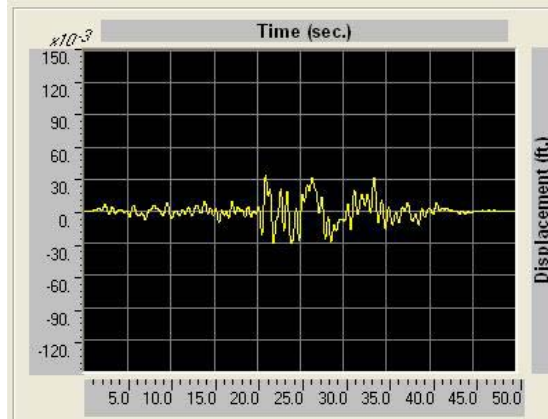
475 yr. Earthquake – Longitudinal



475 yr. Earthquake – Transverse



2475 yr. Earthquake – Longitudinal



2475 yr. Earthquake - Transverse

**Figure 4-14: Outrigger Bent 9 Displacement Histories (ft)**

**Table 4-9: Maximum Displacements (ft) at Outrigger Joints (72- and 475-Year Earthquakes)**

Frame	2	3				6		7
Bent	9N	9S	10	11	12	20	21	25
Long. – 72	0.064	<b>0.136</b>	<b>0.187</b>	<b>0.203</b>	<b>0.203</b>	0.266	0.268	0.338
Long. – 475	<b>0.071</b>	0.119	0.159	0.173	0.172	<b>0.280</b>	<b>0.280</b>	<b>0.343</b>
Trans. – 72	<b>0.145</b>	0.094	<b>0.123</b>	0.164	0.200	0.269	0.257	0.338
Trans. – 475	0.143	<b>0.096</b>	0.105	<b>0.165</b>	<b>0.227</b>	<b>0.342</b>	<b>0.336</b>	<b>0.381</b>

The drift ratios that corresponded to the maximum displacement at each outrigger joint were calculated by dividing each displacement by the height of the column and are tabulated in Table 4-10. As a result of the split columns, the beams and joints on either side of the expansion joint at Bent 9 had the same properties, and therefore in this table, as well as for the results in subsequent sections, only the larger of the two outrigger responses is presented.

**Table 4-10: Maximum Drift Ratios at Outrigger Bents (%)**

	Bent 9	Bent 10	Bent 11	Bent 12	Bent 20	Bent 21	Bent 25
Longitudinal	0.40	0.53	0.55	0.53	0.57	0.55	0.63
Transverse	0.42	0.35	0.44	0.59	0.70	0.67	0.70

The drift ratios calculated for each of the outrigger bents were well below 1 percent. Typically, such small drift ratios correspond to minimal structural damage. However, because the bridge columns were retrofitted, it is possible that the yield displacements, and therefore drift ratios at yield, were smaller than those associated with traditional reinforced concrete columns. This could result in displacement ductility demands that would cause damage in the adjacent outrigger elements. The displacement ductility demands and associated yield capacities are addressed in detail in the following sections.

### 4.3.2 Displacement Ductility Demands

The displacement ductility demands on the outrigger bents provide an indication of possible damage to the elements of the outriggers. Under transverse loading, either the beam or column of the outrigger bent can yield in flexure; therefore, the displacement ductility demand on both the beam and column must be considered. Under longitudinal loading, interpretation of the experimental results indicated that the beam transverse steel yielded in torsion before the column yielded in flexure. Therefore, only the beam was considered in the analyses of the longitudinal response. To determine the displacement ductility demand, the yield displacement for each of the outrigger beams and columns were determined.

A rigorous modeling procedure to determine an accurate representation of the outrigger columns with full-height steel jackets including all sources of deformation was presented in Section 3.3.5 and Appendix A. However, that analysis assumed fixity at both column ends. To appropriately model the boundary conditions and additional flexibility resulting from the adjacent elements, the results of the FE analysis were used. The yield displacement due to transverse loading was then obtained through direct scaling of the results as shown in Equation 4-22.

$$\Delta_y = M_y \frac{\Delta_{FE-trans}}{M_{FE-trans}} \quad (4-22)$$

The subscript FE in this and all subsequent equations refers to values obtained from the finite element analyses. Because yielding occurred in the shortunjacketed portion of the column, either at the top or bottom, the yield moment,  $M_y$ , was obtained for each unjacketed cross-section by following the moment-curvature analysis procedure described in Section 4.2.1. The moment and displacement demands determined from the FE analysis due to transverse loading,  $M_{FE-trans}$  and  $\Delta_{FE-trans}$  respectively, provided a representation of the column stiffness that included the flexibility of the adjacent elements. To use these results, it was essential that the effective column stiffness be represented accurately in the FE model, and this was achieved by following the procedure described in Section 3.3.5 and Appendix A. Although concrete cracking results in small nonlinearities, and yielding of one outrigger column affects the force distribution to other

columns, these effects do not significantly impact the yield displacement calculation because the global displacements of the structure are governed by the stiffness of the main-line columns.

Equation 4-22 can also be used to calculate the yield displacement of the beam under transverse loading. The moment and displacement from the FE analysis remains the same, but the yield moment of the beam was used for the variable  $M_y$ , instead of the yield moment of the column. Because the top and bottom reinforcement of the beam is different, the yield moments and the associated yield displacements due to opening and closing moments differ.

A similar scaling procedure was used to calculate the yield displacement of the beam under longitudinal loading as shown in Equation 4-23.

$$\Delta_y = T_y \frac{\Delta_{FE-long}}{M_{FE-long}} \quad (4-23)$$

The moment and displacements,  $M_{FE-long}$  and  $\Delta_{FE-long}$ , come from the FE analysis based on longitudinal loading, and the variable  $T_y$ , represents the yield torque on the beam.

Calculated yield displacements of the beam and column in both the longitudinal and transverse loading directions are presented in Table 4-11. Beam results are presented for both opening and closing moments under transverse loading. Note that a longitudinal result for Bent 25 was not appropriate because the deck rests on rollers and is not rigidly connected to the frame. Also, for Bent 11, because of the lack of torsion reinforcement, there is no theoretical yield torque and therefore, a longitudinal yield displacement is not applicable. Finally, for Bent 21, the outrigger joint frames directly into the deck and since no beam exists, a longitudinal value is not appropriate.

**Table 4-11: Yield Displacement (ft.) of the Outrigger Beams and Columns**

		Bent Number						
		9	10	11	12	20	21	25
Beam	Transverse Opening	0.06	0.15	0.25	0.28	0.20	0.17	0.42
	Transverse Closing	0.11	0.14	0.09	0.17	0.36	0.17	0.68
	Longitudinal	0.05	0.07	---	0.09	0.12	---	---
Column	Transverse	0.10	0.12	0.09	0.15	0.21	0.20	0.49

Using the equal-displacement rule proposed by Veletsos and Newmark (1960), wherein the displacement of a nonlinear single degree of freedom (SDOF) system is assumed to be equal to that of a linear SDOF system with the same initial stiffness and 5 percent viscous damping, the maximum displacement ductility of each column was calculated with Equation 4-24:

$$\mu_{\Delta} = \frac{\Delta_{FE}}{\Delta_y} \tag{4-24}$$

**Table 4-12: Maximum Displacement Ductility Demands on Outrigger Beams and Columns**

		Bent Number						
		9	10	11	12	20	21	25
Beam	Opening	<b>2.4</b>	0.8	0.7	0.8	<b>1.7</b>	<b>1.9</b>	<b>0.9</b>
	Closing	1.3	0.9	1.8	1.4	0.9	<b>2.0</b>	0.6
	Longitudinal	<b>2.8</b>	<b>2.9</b>	---	<b>2.2</b>	<b>2.4</b>	---	---
Column	Opening	1.5	<b>1.1</b>	<b>1.9</b>	<b>1.5</b>	<b>1.7</b>	1.6	0.8
	Closing	<b>1.5</b>	<b>1.1</b>	<b>1.9</b>	<b>1.5</b>	<b>1.7</b>	1.6	<b>0.8</b>

The maximum outrigger displacement ductility demands are shown in Table 4-12. A displacement ductility demand that exceeds 1.0 signifies column yielding. Under transverse loading, the ductility is highlighted in bold for the member with the larger

displacement ductility (also the member that yielded first). Notice that it is possible for the beam to control under opening moment while the column controls under closing moment, and vice versa. As mentioned previously, the displacement ductility demands in the longitudinal direction were based on yielding of the beam transverse steel in torsion.

The calculated displacement ductility demands can be compared to those of the tests to provide an initial evaluation of the critical outrigger bents and the potential for damage to them. The results of the WSU tests, presented in Section 4.2.1, indicated that significant deterioration of the lateral-load carrying capacity under transverse loading occurred at a displacement ductility of approximately 1.7 for the short specimen under closing moment, 2.2 for the short specimen under opening moment, 2.3 for the long specimen under closing moment, and 3.1 for the long specimen under closing moment (Table 4-3). For longitudinal loading, displacement ductilities of 2.5 and 5.0 were reached in the pull and push directions, respectively. Recall that significant deterioration in the lateral-load carrying capacity is defined at the displacement where the load reduces to 80 percent of its peak value (NZS:3101 1995).

In the transverse direction, the displacement ductility demands for beam opening moments at Bent 9, and for column opening moments at bents 11 and 20, exceeded the short specimen values. Bents 9 and 10 also exhibited high displacement ductility demands in the longitudinal direction. Additional attention must be given to the analysis of these four bents. The remaining as-existing displacement ductility demands were lower than the experimental values. However, damage in the tests was initiated at lower ductility demands, suggesting that potential response mechanisms for outrigger bents with displacement ductility demands of larger than 1.0 should be checked.

#### **4.4 Demand/Capacity Evaluation of Outrigger Bent Components**

The global demands on some of the outrigger bents suggested that they may be susceptible to damage due to one or more response mechanisms. To evaluate the potential damage modes, the local demands were evaluated and compared with the corresponding capacities. The procedure used for this evaluation was as follows. First,

the demands were calculated in the as-existing outriggers on the basis of the maximum moments or bar stresses previously determined to be due to transverse and longitudinal loading. Then the results of the demand analyses and the capacities from experimental results or ACI procedures were compared to evaluate the likelihood of occurrence of each response mechanism. The evaluation specifically addressed joint shear, radial tension and anchorage, beam shear, and beam torsion. Column shear was not included in the evaluation because, as observed from the experimental results, the column jackets, present as a result of a previous retrofit measure, are expected to prevent this response mechanism from occurring. In addition, the jackets provide ductility such that column flexural yielding will not directly result in loss of lateral load carrying capacity.

#### **4.4.1 Beam and Column Flexural Response**

As discussed in Section 4.2.1, the flexural response of the outrigger beams and columns are not critical. However, the local flexural demands form the basis of the demands for other response mechanisms. The stress state of the beam or column bars determines, in part, the magnitude of the shear transferred to the joint, the bond demand within the joint region, the beam shear demand under transverse loading, and the torsion transferred to the beam under longitudinal loading. Therefore, it is important not only to determine whether the member yields in flexure, but to determine the bar stress under maximum seismic demands and the resulting demands on the adjacent elements. The moment or bar stress demand in the column or beam (depending on which controls initial yielding) can be used to determine the demands on the adjacent elements through equilibrium. To do this, relations were developed to link the predicted displacement demand with the moment.

The determination of demand moments depended on whether yielding occurred and which element controlled the yielded response. If the column controlled, the column demand moment was determined. First a relationship between the theoretical curvature demand and the maximum FE displacement was established. The moment-curvature relationship, from the procedure outlined in Section 4.2.1, was then used to determine the demand moment corresponding to the theoretical curvature demand. Details of this

calculation procedure are presented in Appendix B. After the column demand moment was determined, the beam moment was computed by using the equilibrium equations presented in Section 4.2.2 (equations 4-2 and 4-3).

Note that for the as-existing outriggers, the column forces shown in Figure 4-6 were determined through the FE analysis, and only the axial load resulting from gravity loading was considered. When the analysis was conducted, it was understood from the WSU researchers that their tests did not include any seismic component in the axial load on the column. It was later determined that this understanding was incorrect and that the column load in the tests contained a constant component that was intended to simulate seismic effects. Details of its magnitude, how it was calculated, or the way in which a constant load was intended to represent the varying load to be expected during an earthquake remain unclear.

A similar approach was used if the beam yielding controlled the onset of inelastic action. The beam demand moment was first calculated from the displacement-curvature and moment-curvature relationships presented in Appendix B. From the beam moment, the column demand moment was then determined with equilibrium equations. If neither the beam nor the column yielded, the elastic beam and column moments determined from the FE analysis were used. This condition occurred at Bent 25.

Determination of the demand moments for Bent 21 required special attention. For this outrigger, the beam was predicted to yield before the column. However, because the column frames directly into the deck, the procedure in Appendix B becomes complicated to implement. Therefore, the yield moment was used as a lower bound estimate of the demand moment. A displacement ductility demand of approximately 2 from Table 4-12 implies that the demand moment could be significantly larger than the yield moment.

The outrigger moment demand values ( $M_{dem}$ ) are presented in Table 4-13. Yield and maximum moments of the members from moment-curvature analyses are also presented

for comparison with the calculated moment demand. The yield moment corresponding to the member that yielded first is highlighted in bold for each bent.

**Table 4-13: In-Plane Yield, Maximum, and Demand Moments of As-Existing Outrigger Beams and Columns**

		$M_y$ (k*ft)		$M_{max}$ (k*ft)		$M_{dem}$ (k*ft)	
		Opening	Closing	Opening	Closing	Opening	Closing
Bent 9	Beam	<b>813</b>	1500	1607	2430	999	1868
	Column	1312	<b>1312</b>	2351	2351	864	1619
Bent 10	Beam	2619	2501	4392	4251	2714	2014
	Column	<b>2043</b>	<b>2043</b>	3338	3338	2128	2128
Bent 11	Beam	3201	1209	4861	2314	1840	1395
	Column	<b>1141</b>	<b>1141</b>	1913	1913	1359	1359
Bent 12	Beam	4589	2761	6580	4688	4181	2766
	Column	<b>2529</b>	<b>2529</b>	3761	3761	3046	3046
Bent 20	Beam	<b>3773</b>	6857	7266	9252	6071	4815
	Column	3943	<b>3943</b>	6150	6150	5959	4919
Bent 21	Beam	<b>3469</b>	<b>3350</b>	5848	5206	3469	3350
	Column	4021	4021	6147	6147	3352	4389
Bent 25	Beam	<b>1989</b>	3200	3938	5527	1804	1804
	Column	2304	<b>2304</b>	3571	3571	1804	1804

The moment-curvature results were then used to determine the bar stresses in the outer most bars of the column or beam ( $f_{s_{dem}}$ ). These calculations are also presented in Appendix B, and the results are displayed in Table 4-14. As discussed in Section 3.3.2, the yield stress of the as-existing bars was 44 ksi, and the ultimate stress was 77 ksi.

**Table 4-14: As-Existing Outrigger Beam and Column Reinforcing Steel Stress Demand**

		f <sub>s</sub> dem (ksi)	
		Opening	Closing
Bent 9	Beam	44	<b>48.2</b>
	Column	27.3	44
Bent 10	Beam	25.9	34.4
	Column	44	44
Bent 11	Beam	40.0	44
	Column	44	44
Bent 12	Beam	36.2	44
	Column	44	44
Bent 20	Beam	44	29.6
	Column	<b>66.9</b>	44
Bent 21	Beam	44	44
	Column	34.9	33.0
Bent 25	Beam	39.5	23.8
	Column	33.0	33.0

Table 4-14 shows that yielding occurred in six of the seven outriggers. However, only on two (bents 9 and 20, with stresses highlighted in bold in the table) did the bar strain reach into the strain hardening region, causing bar stresses higher than  $f_y$ . Those two bents, therefore, required particular attention in evaluating the damage susceptibility of the outriggers. For the other cases in which the beam or column yielded, the curvatures may exceed the yield curvature (inducing larger strains and stresses in the interior bar layers), so the moment may be higher than the yield moment, even though strain hardening in the outer most bars has not yet occurred. To evaluate the potential for damage in the outrigger bents, the demand moments and bar stresses calculated from the FE results and

the capacity values discussed previously were used in the demand/capacity evaluation of each bent and are discussed in the following sections.

#### 4.4.2 Joint Shear Under Transverse Loading

Joint damage due to opening and/or closing moments was observed in the WSU experiments. To evaluate the potential for occurrence of this response mechanism, the joint shear values determined from the experiments were compared with the demands on the as-existing outriggers. The horizontal joint shear stress demands were determined by following the same procedure used to calculate the capacities of the WSU test specimens (see Section 4.2.2) and the demand moments listed in Table 4-13.

The calculated joint shear stress demands were normalized with respect to the square root of the concrete strength ( $\sqrt{f'_c}$  psi) and are presented in Table 4-15. Values are tabulated for opening and closing moments on the basis of the controlling moment demands from Table 4-13. Also presented in Table 4-15 are the demand/capacity ratios based on the lower bound joint shear capacity of  $7\sqrt{f'_c}$  determined in Section 4.2.2.

**Table 4-15: Normalized Shear Stress Demands on Outrigger Joints Under Opening and Closing Moments ( $v_{jh} / \sqrt{f'_c}$ )**

	Bent Number						
	9	10	11	12	20	21	25
Opening	3.8	6.2	5.4	9.0	7.1	7.4	4.6
Closing	5.4	4.0	3.8	5.2	6.8	5.6	4.0
D/C Opening	0.5	0.9	0.8	1.3	1.0	1.1	0.7
D/C Closing	0.8	0.6	0.5	0.7	1.0	0.8	0.6

The demand/capacity ratios for closing moments were all less than 1.0 except for Bent 20. This suggests that for these bents, while joint shear damage may occur, loss of load carrying capacity due to this response mechanism is less likely to occur, especially since the capacity used is a lower bound estimate. Under opening moments, the demand/capacity ratios were 1.0 or larger for the knee joints in outrigger bents 12, 20,

and 21, suggesting that they may sustain damage. Recall that Bent 21 is based on a lower bound value of the demand moment, and therefore, the joint shear stress and resulting demand/capacity ratio could be even higher.

#### **4.4.3 Radial Tension**

As seen in the WSU tests (Section 4.2.3), the radial tension demands resulting from the joint geometry and longitudinal bar detailing can be a source of significant damage. By loosening the concrete near the hooked bars at the exterior face, they can cause splitting damage, resulting in bond degradation under cyclic loading.

The radial tension demands on the as-existing outriggers were calculated with Equation 4-8, which was also used to calculate the capacity. To calculate the demands, however, the curvature corresponding to the demand moments presented in Table 4-13 was used instead of the curvature corresponding to the maximum experimental moment. From this curvature, the compression strain in the curved exterior bars was found by using the results from the appropriate moment-curvature analysis; from the strain, the bar stress was obtained from the stress-strain curve of the reinforcing steel.

The resulting radial tension stress demands were normalized with respect to the square root of the concrete strength ( $\sqrt{f'_c}$  psi) and are presented in Table 4-16. The results are based on column bar stress and beam bar stress and are separated in the table. Although the moment in the beam and column are associated through equilibrium, it is possible for the bar stresses to be significantly different because of the geometry and reinforcement of the sections. Therefore, as seen in the table, the calculated radial tension stresses may vary significantly for a given bent. The maximum radial tension stress was used to calculate the demand/capacity ratios for each bent, which are also tabulated. The radial tension stress capacity of  $4\sqrt{f'_c}$ , determined in Section 4.2.3, was used in all cases.

In the experiments, radial tension demands may have caused deterioration in the lateral load carrying capacity. Bent 20, after which the “short” specimen was modeled, has a very large radial tension stress demand (as indicated by the demand/capacity ratio of 3.0)

and is susceptible to the same type of damage seen in the tests. Bents 12 and 21 also have demand/capacity ratios larger than 1.0 and, therefore, are also considered to be vulnerable to significant radial tension damage. Again, since Bent 21 is based on a lower bound demand moment, the radial tension stress could be significantly higher. Bents 9, 10, 11, and 25 also have high radial tension stresses that may not cause deterioration in the lateral load carrying capacity but could result in damage to the joint.

**Table 4-16: Normalized Radial Tension Stress Demands on Outrigger Joints Based on Beam and Column Bar Stresses ( $\sigma_{rad} / \sqrt{f'_c}$ )**

	Bent 9	Bent 10	Bent 11	Bent 12	Bent 20	Bent 21	Bent 25
Beam	0.0	2.2	0.5	3.2	4.1	2.7	1.3
Column	3.7	3.8	2.3	7.8	12.1	4.6	4.2
Max D/C	0.9	1.0	0.6	1.9	3.0	1.2	1.0

#### 4.4.4 Bar Anchorage

Splitting cracks, indicative of anchorage damage, were observed in the WSU tests and may have resulted in deterioration in the lateral-load carrying capacity of the specimens under closing moments. The experimental capacity was determined by following the procedure outlined in Section 4.2.4. This procedure was also used to determine the bond stress demands. For the outside bars hooked around the perimeter of the joint, the bond stress demand was calculated using Equation 4-9, however, the bar stress demands from Table 4-14 replaced the experimental bar stress demands in the equation. Consistent with the capacity calculation, an increase in capacity resulting from the presence of 90-degree hooks was neglected because the bar details and confinement did not satisfy current ACI requirements (ACI 318-02 2002). For the straight bars, the bond stress demand was calculated using Equation 4-10. Again, the bar stress demands from Table 4-14 replaced the experimental bar stress demands in the equation. Tables 4-17 and 4-18 present the results of the calculations for the beam and column bars, respectively, as well as the bar sizes in each of the outrigger members. Although the beams have different sized bars

developed into the joint, only the information for the largest bar size is listed in the tables because larger bars correspond to larger bond stress demands for a given length.

**Table 4-17: Evaluation of Beam Bar Anchorage in Outrigger Joints**

Bent #	9	10	11	12	20	21	25
<b><u>Opening Moment</u></b>							
Bar Size	---	---	---	---	14	14	18
Bond Stress Demand ( $\tau_{bond} / \sqrt{f'_c}$ )	---	---	---	---	6.0	6.0	8.4
ACI Bond Stress ( $\tau_{bond} / \sqrt{f'_c}$ )	---	---	---	---	4.1	4.1	4.1
Demand/ACI	---	---	---	---	1.5	1.5	2.1
D/C	---	---	---	---	0.8	0.8	1.1
<b><u>Closing Moment</u></b>							
Bar Size	11	11	9	11	18	---	14
Bond Stress Demand ( $\tau_{bond} / \sqrt{f'_c}$ )	3.7	2.6	2.7	3.3	3.5	---	2.2
ACI Bond Stress ( $\tau_{bond} / \sqrt{f'_c}$ )	2.2	2.2	2.2	2.2	2.2	---	2.2
Demand/ACI	1.6	1.2	1.2	1.5	1.6	---	1.0
D/C	0.7	0.5	0.5	0.6	0.4	---	0.5

A few bents are not expected to experience anchorage damage for particular loading directions. Bents 9, 10, 11, and 12 have beam bottom bars with 180-degree hooks embedded into the joint. Because these hooks significantly improve anchorage capacity, for opening moments, these bents were not included in the demand/capacity evaluation. In addition, Bent 21 consists of beam top bars that curve around the exterior of the joint and become the column exterior bars. Because of the continuity, anchorage is not expected to be a critical issue, and an evaluation of closing moment anchorage for this bent was not performed.

**Table 4-18: Evaluation of Column Bar Anchorage in Outrigger Joints**

Bent #	9	10	11	12	20	21	25
<b><u>Opening Moment</u></b>							
Bar Size	11	11	11	14	14	14	14
Bond Stress Demand ( $\tau_{bond} / \sqrt{f'_c}$ )	2.9	4.4	4.4	5.3	8.0	4.2	4.0
ACI Bond Stress ( $\tau_{bond} / \sqrt{f'_c}$ )	4.1	4.1	4.1	4.1	4.1	4.1	4.1
Demand/ACI Ratio	0.7	1.1	1.1	1.3	2.0	1.0	1.0
D/C	0.4	0.7	0.7	0.8	1.2	0.6	0.6
<b><u>Closing Moment</u></b>							
Bar Size	11	11	11	14	14	---	14
Bond Stress Demand ( $\tau_{bond} / \sqrt{f'_c}$ )	2.1	3.3	3.3	4.0	5.9	---	3.0
ACI Bond Stress ( $\tau_{bond} / \sqrt{f'_c}$ )	3.1	3.1	3.1	3.1	3.1	---	3.1
Demand/ACI Ratio	0.7	1.1	1.1	1.3	1.9	---	1.0
D/C	0.3	0.5	0.5	0.6	0.9	---	0.5

The bond stress capacity calculations based on ACI requirements are also presented in tables 4-17 and 4-18 for comparison purposes. As with the calculations of the WSU tests, the required splice length for the hooked exterior bars and the development length for straight bars were calculated on the basis of ACI Section 12.15.1 and 21.5.4, respectively. Although no recommendations are made for number 14 or 18 bars in Section 21.5.4 because of insufficient experimental data, the same procedure was used to determine their required embedment lengths. From these splice lengths and embedment lengths, the bond stress was calculated using the same procedure discussed in Section 4.2.4. Once the ACI bond stresses were obtained, the bond stress demand/ACI ratio was calculated. The results are shown in tables 4-17 and 4-18. Finally, the demand/capacity ratio was determined by dividing the bond stress demand by the average experiment bond stress from the WSU tests. Recall that the average experiment bond stress values were

8.0 for beam opening moments, 5.5 for beam closing moments, 6.7 for column opening moments, and 6.6 for column closing moments as reported in Table 4-6.

Tables 4-17 and 4-18 show that almost all of the demand/ACI ratios were above 1.0, confirming that the splice and embedment lengths of the reinforcing steel in the beams and columns do not meet ACI requirements. However, most of the demand/capacity ratios for both the column bars and the beam bars were below 1.0. Only the Bent 25 beam bars under opening moments and the Bent 20 column bars under opening moments had D/C ratios equal to or greater than 1.0. The possibility of damage to these bents or even loss of lateral load carrying capacity due to loss of anchorage is strong. Also, because the demands on the Bent 21 bars were based on a lower bound demand moment, there is a possibility that significant anchorage damage could occur at this location.

Although the other bents had lower demand/capacity ratios, there is still a possibility for anchorage damage for a number of reasons. First, radial tension damage under opening moments could weaken the bond of the outside bars and result in anchorage damage or splice failure under much lower bond stress demands due to closing moments. Second, the bond stress calculations were based on the assumption of stress uniformly distributed over the entire embedment length. This may be reasonable for a well confined system. However, for a poorly confined system such as the as-existing outrigger joints, the bond stress is much larger at the face of the joint. This could lead to splitting at this interface, in which case additional embedment length would provide very little benefit. This is a source of uncertainty in the predicted response of the as-existing outriggers, and therefore, anchorage damage is still possible regardless of the demand/capacity ratios.

#### **4.4.5 Beam Shear**

Transverse ground motion induces in-plane shear in the beam, to which must be added the shear force due to gravity load, as illustrated in Figure 4-15. Other forces may arise because of longitudinal motion, but here the transverse response is isolated.

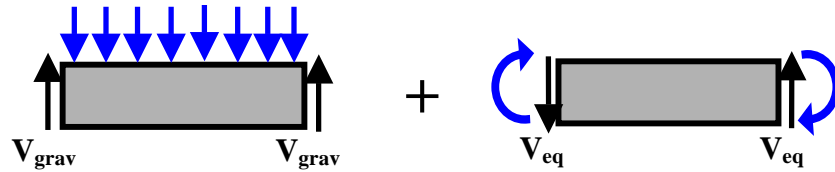


**Figure 4-15: Beam Shear Demand**

The seismic shear was determined by two procedures. The first method consisted of determining the maximum shear demands from the linear FE lateral analyses, and the resulting demand is referred to as  $V_{FE}$ . The second method was to determine the shear corresponding to the plastic moment demands (or maximum moment demands), similar to the procedure described for the WSU test specimen in Section 4.2.5. Equation 4-12 was used to calculate the plastic shear demand ( $V_{pl}$ ), with the moment demands from Table 4-13 used to determine  $M_{p2}$ . The plastic moment adjacent to the deck,  $M_{p1}$ , was determined by following the procedure used for the test specimens. The total shear demand was the sum of the plastic and gravity shear demands. Note that this procedure differed from the plastic shear calculated for the test specimens because in the experiments, gravity and an approximation of seismic loads were applied through the column and transferred to the beam.

Seismic shear demands on the outrigger beams were calculated using both methods and are tabulated in Table 4-19. The shear demands due to gravity loads alone are also tabulated. As expected, the demands from the FE analyses were much smaller than the plastic shear demands. Yet it can be argued on the basis of the smaller response to the 2475-year earthquake that the design (475-year) earthquake may produce the largest possible demands on the SR 99–Spokane Street outrigger beams. If this is the case, the plastic shear values may be conservative; however, an accurate measure of the plastic shear can be determined only from an inelastic analysis.

Because the seismic shear demand on the WSU test specimens did not correspond to the shear demand on the as-existing outrigger beams, an experimental capacity was not

available. Therefore, the beam shear capacities were based on ACI 318-02 and were calculated with equations 4-13 through 4-15 from Section 4.2.5. As discussed, ACI 318-02 Section 21.3.4.2 recommends that  $V_c$  be ignored when the shear capacity is calculated if axial loads are small or if the plastic shear demand ( $V_{pl}$ ) exceeds one-half of the total shear demand. These criteria were met for all of the as-existing outrigger beams, and therefore, the shear capacity from the concrete and steel are presented separately in Table 4-19.

On both issues (use of capacity design shear demands and neglect of  $V_c$ ), the conditions in the SR 99–Spokane Street over-crossing are such that ACI requires the more conservative assumptions. However, the results of the FE analysis indicate that the expected shear demands on the outrigger beams are lower than the concrete component of the shear capacity. This is also confirmed by the minimal amount of diagonal cracking in the existing beams, despite the fact that the viaduct has been through two earthquakes, the second of which was approximately equivalent to a 72-year event. It may thus be argued that the combination of two conservative assumptions leads to excessive conservatism. FEMA 356 suggests a less conservative approach in which the concrete component of the shear capacity is included when the plastic shear demand is used. Table 4-19 presents demand/capacity ratios calculated on several different bases. An outrigger beam does not exist at Bent 21, and therefore, beam shear calculations at this bent are not applicable.

The following is a list of variables used in Table 4-19:

$V_c$  = concrete contribution to shear capacity

$V_s$  = steel contribution to shear capacity

$V_{FE}$  = shear demand from FE analysis

$V_{pl}$  = plastic shear demand from ACI capacity design

$V_{grav}$  = shear demand from gravity load

**Table 4-19: Outrigger Beam Shear (kips) and Demand/Capacity Ratios**

	Bent 9	Bent 10	Bent 11	Bent 12	Bent 20	Bent 21	Bent 25
$V_c$	216	269	281	269	394	---	197
$V_s$	56	1358	542	1393	1431	---	107
$V_{FE}$	77	80	162	149	268	---	93
Max $V_{pl}$	159	718	1102	1750	2261	---	129
$V_{grav}$	23	134	127	313	363	---	91
$(V_{FE}+V_{grav})/(V_s+V_c)$	0.4	0.1	0.4	0.3	0.3	---	0.6
$(V_{pl}+V_{grav})/(V_s+V_c)$	0.7	0.5	1.5	1.2	1.4	---	0.7
$(V_{FE}+V_{grav})/V_s$	1.8	0.2	0.5	0.3	0.4	---	1.7
$(V_{pl}+V_{grav})/V_s$	3.3	0.6	2.3	1.5	1.8	---	2.1

From the results, a firm conclusion can be drawn only for Bent 10, which had a demand/capacity ratio of less than 1.0 for all three cases and is therefore not shear critical. In all the others, use of the most conservative but code-mandated assumption (accepting the demand as  $V_{pl}$  and ignoring  $V_c$ ) suggests that the beams are susceptible to shear damage. On the other hand, the least conservative assumption (use of the computed shear demand,  $V_{FE}$ , and inclusion of the concrete shear strength,  $V_c$ ), suggests that the beams are adequate. Furthermore, bents 11, 12, and 20 fail under the FEMA 356 procedure, whereas bents 9 and 25 have D/C ratios above 1.0 for the other intermediate procedure (use of the computed shear demand,  $V_{FE}$ , and ignoring the concrete shear strength,  $V_c$ ). Therefore, all of the outrigger bents except Bent 10 are considered to be vulnerable to beam shear damage.

#### 4.4.6 Beam Torsion and Out-of-Plane Shear

The outrigger beams experience both torsion and horizontal shear due to seismic loading in the longitudinal direction and vertical shear due to gravity loading. As seen in the WSU experiments, torsion causes significant cracking in the concrete and yielding of the reinforcement in the beams.

Evaluation of the outrigger beam's response to torsional loading was complicated by the fact that the element stiffnesses change when the concrete cracks. Bending moments in the elements are generally large enough to cause cracking under seismic loading, so the members can be assigned cracked properties at the start, and iteration with different stiffnesses to reflect the extent of cracking is seldom necessary. However, this is not necessarily true of torsion, for which iteration is likely to be needed if the stiffness values used are to be consistent with the level of induced forces. This is particularly true when cracking in one degree-of-freedom, such as torsion, affects stiffness and strength in another, such as out-of-plane bending. Such an analysis can be achieved with a full 3-D nonlinear finite element model, but at a considerable computational cost. Here the behavior was approximated by manually changing the selected element stiffnesses in the elastic model and then subsequent re-analysis. This procedure adopted for the longitudinal direction was different than the transverse direction analysis, in which cracked section stiffness values were used initially. This is because few torsion cracks were observed in the structure, whereas significant bending cracks are present. Also, very little information is available on cracked elastic torsional stiffness, and therefore, the iterative procedure was necessary.

Torsion occurs because the structural displacements induce bending moments in the columns, which are equilibrated by torsion moments in the beams. For an outrigger joint, the torsion moment in the beam must be equal to the bending moment in the top of the column. Therefore, if the column yields at the top, the beam torque will be determined by the column yield moment rather than by the moment demand from analysis based on elastic behavior (see Figure 4-16). Thus, the true beam torsion demand ( $T_{dem}$ ) is the smaller of the torque found through the elastic FE analysis ( $T_{FE-el}$ ) and the column yield moment ( $M_{ycol}$ ). In this analysis, the column yield moment corresponded to first yield of the reinforcement and was obtained by using the previously described moment-curvature analysis.

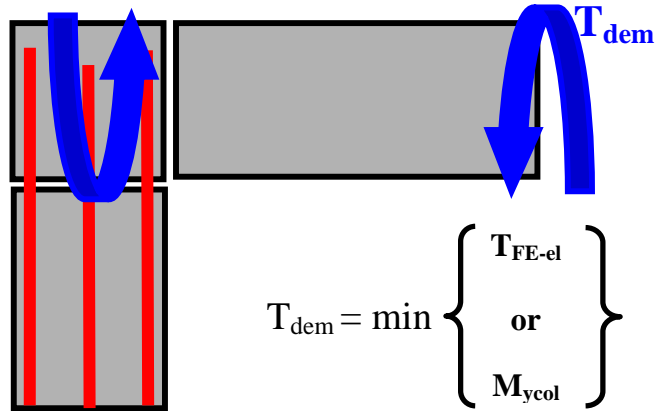


**Figure 4-16: Beam Torsion**

A summary of the torsion evaluation of the as-existing outrigger beams is presented in Table 4-20. The first two rows show the cracking torque,  $T_{cr}$ , determined by Equation 4-16 in Section 4.2.6, and the torsion demand from the elastic FE model,  $T_{FE-el}$ .

**Table 4-20: Outrigger Beam Torsion Evaluation**

Frame	2		3		6		7	
Bent	9N	9S	10	11	12	20	21	25
$T_{cr}$ (k*ft)	164	164	373	262	451	533	---	---
$T_{FE-el}$ (k*ft)	172	321	2066	1846	3318	4390	---	---
$\Delta_{FE}$ 72 yr (ft)	0.064	0.136	0.187	0.203	0.203	0.266	0.268	0.338
$\Delta_{FE}$ 475 yr (ft.)	0.071	0.119	0.159	0.173	0.172	0.280	0.280	0.343
$\Delta_{pl}$ 72 yr (ft)	0.060	0.097	0.190	0.213	0.214	0.271	0.274	0.335
$\Delta_{pl}$ 475 yr (ft.)	0.070	0.108	0.184	0.206	0.208	0.259	0.262	0.361
$k_{t-cr}/k_{(t-el)SR-99}$	0.36	0.20	0.22	0.11	0.23	0.22	---	---
$T_{FE-pl} = T_{dem}$ (k*ft)	76	67	685	316	1712	2059	---	---
$M_{ycol}$ (k*ft)	1116	1116	2211	1141	2951	3937	---	---
$T_n$ (k*ft)	59	34	401	---	1043	1170	---	---
$T_{dem}/T_n$	1.3	2.0	1.7	---	1.6	1.8	---	---
D/C	1.1	1.7	1.4	---	1.3	1.5	---	---

Because the torsion demand was larger than the cracking torque, a cracked secant torsional stiffness had to be assigned to the beam. An iterative procedure was adopted to determine the appropriate stiffness. The procedure assumed that the global displacements remained essentially unchanged by a change in element stiffness. First, a relationship between torque and twist angle was determined on the basis of the experimental study of reinforced concrete rectangular beams subject to torsion by Rahal and Collins (2003). From an approximated average curve, the elastic and plastic stiffnesses were estimated (see Figure 4-17).

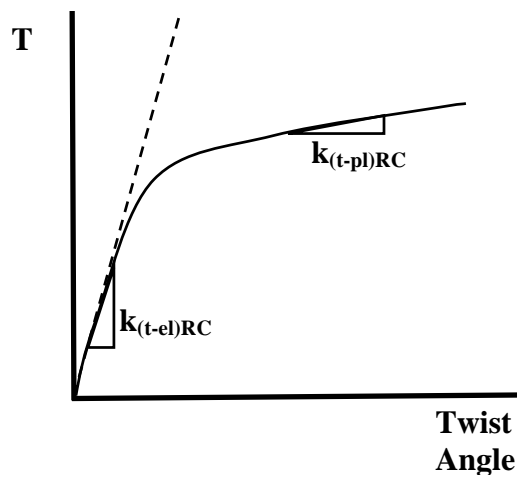


**Figure 4-17: Representation of Torque-Twist Angle Curve from Rahal-Collins**

The stiffnesses from the approximated Rahal and Collins curve ( $k_{(t-el)RC}$  and  $k_{(t-pl)RC}$ ) were used to generate a bi-linear approximation of the torque-twist angle curve for each of the as-existing beams (see Figure 4-18). First, the elastic stiffness of the curve was determined by obtaining the torque and twist angle from the elastic FE analysis as follows:

$$k_{(t-el)SR-99} = \frac{T_{FE-el}}{\varphi_{FE-el}} \quad (4-25)$$

where:

$k_{(t-el)SR-99}$  = elastic torsional stiffness of SR 99 outrigger beam

$T_{FE-el}$  = torque demand on outrigger beam from FE analysis

$\varphi_{FE-el}$  = twist angle of outrigger beam from FE analysis

Then the nominal torque,  $T_n$  was determined by using Equation 4-17. The twist angle at yield was then calculated as follows:

$$\varphi_y = \frac{T_n}{k_{(t-el)SR-99}} \quad (4-26)$$

where:  $\varphi_y$  = twist angle of outrigger beam at yield

Finally, to complete the curve, the plastic torsional stiffness was calculated as follows:

$$k_{(t-pl)SR-99} = k_{(t-el)SR-99} \frac{k_{(t-pl)RC}}{k_{(t-el)RC}} \quad (4-27)$$

where:

$k_{(t-pl)SR-99}$  = plastic torsional stiffness of SR 99 outrigger beam

$k_{(t-el)RC}$  = elastic torsional stiffness from approximated Rahal-Collins curve

$k_{(t-pl)RC}$  = plastic torsional stiffness from approximated Rahal-Collins curve

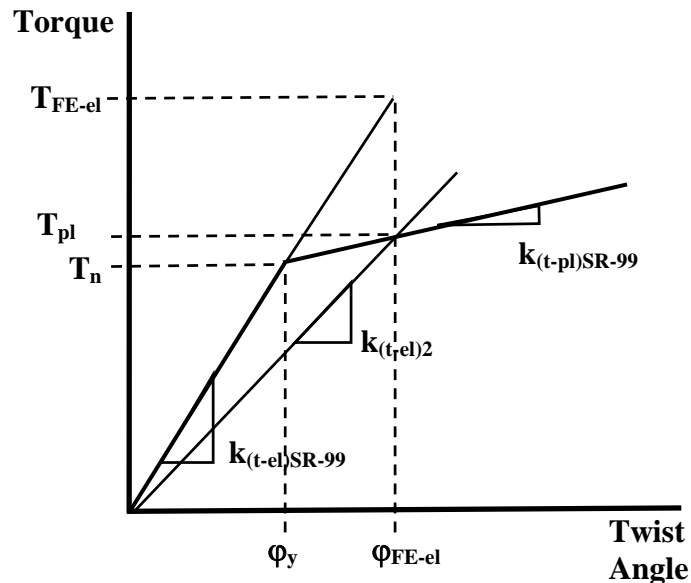


**Figure 4-18: Representation of Torque-Twist Angle Curve for an As-Existing Outrigger Beam**

The new secant stiffness was determined from the curve. Under the equal-displacement rule (Velesos, Newmark 1960), the plastic torque,  $T_{pl}$ , corresponded to torque on the plastic curve at the twist angle determined from the elastic analysis ( $\phi_{FE-el}$ ). The secant stiffness was then:

$$k_{(t-el)2} = \frac{T_{pl}}{\phi_{FE-el}} \quad (4-28)$$

The new secant stiffness was compared with the original elastic stiffness, and the ratio of the two was determined. Then, this ratio was used as a scale factor that was applied to both the torsion constant and the weak axis moment of inertia in the FE model, since cracking of the beam reduces the out-of-plane bending stiffness as well. The FE analysis was re-run, and the procedure was repeated until the secant stiffness converged. This procedure was similar to those typically used in non-linear FE programs. For the as-existing outrigger beams, the ratio of the final required cracked secant stiffness to the elastic stiffness ( $k_{t-cr}/k_{(t-el)SR-99}$ ) is presented in Table 4-20. The next two rows in the table show the torque in the beam computed from the FE analysis and the yield moment of the column. The smaller of those two values (which turns out to be the torque in the beam for all of the outrigger bents) defines the torsion demand,  $T_{dem}$ .

The longitudinal displacements of the outrigger joints using the elastic FE model ( $\Delta_{FE}$ ) and the reduced stiffness models ( $\Delta_{pl}$ ) for the 72-year and 475-year earthquake are also shown in Table 4-20. In general, the displacements of the reduced stiffness model are similar to those determined with the full elastic stiffness of the beam, so the assumption of approximate equality is valid.

The nominal torque,  $T_n$ , for each outrigger is also presented in the table. Notice that for Bent 9, the nominal torque value is lower than the cracking torque,  $T_{cr}$ . This is because the calculation for nominal torque is based only on the reinforcing steel assuming that the concrete has cracked. If the concrete was uncracked, then the actual torsion capacity becomes the cracking torque. However, for all of the as-existing outriggers, the elastic torque on the beam ( $T_{FE-el}$ ) exceeds the cracking torque, suggesting cracked conditions.

The ratio of torsion demand to nominal torque, and the demand/capacity ratio are also shown in Table 4-20. The demand/capacity ratio was calculated by dividing the torsion demand to nominal torque ratio ( $T_{dem}/T_n$ ) by the experimental version of this ratio. The experimental version (experiment/ACI ratio) was based on the WSU test as described in Section 4.2.6. The value is presented in Table 4-8 and was approximately 1.2.

Torsion values are not listed for bents 11, 21, and 25 for a variety of reasons. The outrigger beam at Bent 11 utilizes open U-shaped stirrups for shear resistance, but the lack of closed hoops results in zero nominal torsion strength after cracking. The outrigger at Bent 21 consists of a column that partially frames into the deck, and therefore no outrigger beam exists. At Bent 25, the deck rests on rocker bearings connected to the beam, so no torsion can be induced in the beam.

All of the outrigger beams had demand/capacity values that were above 1.0, suggesting that anticipated damage to the bents would be similar to or worse than the damage observed in the WSU tests. Although open stirrups and capping bars were used instead of closed hoops for all of the beams, this detail developed the full nominal torsion capacity,  $T_n$ , of the beam in the WSU test specimen. The evidence on torsion capacity with open stirrups is thus conflicting: the procedures of ACI 318 led to a computed torsional strength of zero, whereas the test showed that, in this case, the detail was effective. Therefore, the potential for premature loss of torsion resistance due to opening of the 90-degree hooks remains.

As mentioned previously, the elastic torque demand ( $T_{FE-el}$ ) exceeds the cracking torque ( $T_{cr}$ ) for all of the outrigger beams. Many of the tabulated elastic torque demands are based on the 72-year earthquake (see Section 4.3.1 for the discussion on the controlling ground motions for each bent). Yet, the 2001 Nisqually earthquake, which had an intensity similar to the 72-year earthquake, did not produce any visible diagonal cracks in the outrigger beams. This suggests that either the structure did not experience ground motions of the intensity of those used in the analysis, or the structure has some beneficial characteristics that were not captured by the as-existing model. One possible explanation

is that the longitudinal motion, which is the only one to induce a torsional response, was relatively small in the Nisqually earthquake. However, this supposition conflicts with the evidence of pounding damage at the transverse expansion joints. (Recall that the analytical model predicted pounding in most of the places where it was observed in the field.) Another possibility is that the shear stress demand of  $4\sqrt{f'_c}$  (psi) implied by ACI 318-02 (ACI 2002) for torsional cracking is too low. A third possibility, relating to the shorter span beams, is that the torsion strength increases with shorter span to depth ratios, similar to the effects observed for beam shear. Regardless, it is surprising that the torsion damage in the Bent 11 beam is minimal, even with the lack of torsion reinforcement.

#### 4.5 Summary of Results

Table 4-21 summarizes the outrigger bents that are vulnerable to loss of load carrying capacity in a seismic event. The response mechanisms are those described previously. For each response mechanism, the bents shaded in dark gray are those with a high likelihood of damage. The bents shaded in light gray have an uncertain probability of damage based on interpretation of results and assumptions. The bents with no shading have a low likelihood of damage resulting from the given mechanism. Retrofit schemes to mitigate these hazards are presented in Chapter 5.

**Table 4-21: Potential Response Mechanisms for Outrigger Bents Subjected to Opening Moments**

	Bent 9	Bent 10	Bent 11	Bent 12	Bent 20	Bent 21	Bent 25
Joint Shear							
Radial Tension							
Anchorage							
Beam Shear						N/A	
Beam Torsion						N/A	N/A

**Table 4-22: Potential Response Mechanisms for Outrigger Bents Subjected to Closing Moments**

	Bent 9	Bent 10	Bent 11	Bent 12	Bent 20	Bent 21	Bent 25
Joint Shear							
Anchorage						N/A	
Beam Shear						N/A	
Beam Torsion						N/A	N/A



## **5 RETROFIT OPTIONS**

### **5.1 Introduction**

In Chapter 4, the seismic demands on the as-existing elements of the Spokane Street over-crossing were evaluated analytically. The corresponding capacities were also estimated based on the WSU tests (McLean and Shattarat 2004). By comparing demands and capacities, the analysis showed that the outrigger joints and beams were the most vulnerable components in the structure. Nearly all of the columns are jacketed and, therefore, have ample ductility capacity. The only unjacketed column in the north concrete structure is the outrigger at Bent 25, and because it is tall and flexible, its behavior is essentially elastic.

In this chapter, retrofit measures are discussed. In Section 5.2, retrofit measures for individual components are addressed. In some cases, these measures would benefit an element other than the one being retrofitted; for example, column modifications to reduce the column stiffness would benefit the joints by decreasing the demand on them. In Section 5.3, system retrofit measures are discussed. These represent possible choices from which a policy-maker can select a retrofit scheme. They consist of either combinations of element modifications or alterations to the system, rather than any single component. As an example of the latter, cutting the columns and introducing isolating bearings would reduce the demand on several elements, including the joint, and thereby reduce the vulnerability of the overall structure.

Each component retrofit measure is presented in a common format:

- description of the vulnerabilities addressed by the modification
- concept for suggested retrofit measure
- summary of the seismic evaluation results for the vulnerable elements
- applicability to the structure
- potential for application in other structures.

## 5.2 Outrigger Component Retrofit Options

### 5.2.1 Column Retrofit

#### Vulnerabilities Addressed by the Retrofit

The as-existing columns are fitted with full height steel jackets. While these jackets benefit the columns themselves by increasing their ductility capacity, they may have a negative effect on the adjacent components by increasing the demands on them. This is particularly true of the joints. Therefore, when column modifications are considered, the major vulnerability to be investigated is that of the joint.

A steel jacket stiffens the column against lateral load. However, because the jacket is discontinuous at the column ends, it does not affect the yield moment of the column. An increase in column stiffness coupled with no change in strength results in a lower yield displacement and the potential for increased ductility demand. This in turn leads to higher bar strains and stresses at the ends of the column and, therefore, larger forces on the adjacent elements for a given column displacement. The most critical demands are likely to be the joint shear stresses, the radial tension stresses, and the anchorage stresses. The mainline columns are connected to the pile-cap at the bottom and the joint in the box girder at the top, both of which have adequate capacity to resist the joint shear stresses, either because of their size (e.g., the foundation) or because of their confinement (the box girder joints have transverse beams in one direction and the box girder webs in the other). By contrast, the outrigger columns are connected at the top to the outrigger joint, which is poorly confined and is vulnerable to joint shear stress demands.

#### Retrofit Concept

The concept of the column retrofit considered here is to reduce the shear demand on the joint by reducing the column ductility demand. This can be done by keeping the full height jackets on the main line columns but reducing the jackets on the outrigger columns so that they cover only a small length at each end of the column, as shown in Figure 5-1. Experimental results have indicated that a partial-jacket retrofit measure in which only the critical regions are retrofitted will achieve the objective (Chai et al. 1991). The global

displacements of the structure are dominated by the stiffness of the main line columns and would be changed only slightly by modifying the outrigger column jackets. On the other hand, the yield displacement of the outrigger columns could be increased significantly by removing the central part of the jacket. At the same time, the outrigger columns would be still confined at their ends, at the location of the potential plastic hinges. The use on the outrigger columns of a full-height fiber jacket, in which all the fibers ran circumferentially and added no longitudinal stiffness, might also achieve the objectives. However, it was not considered here because the steel jackets are already in place.

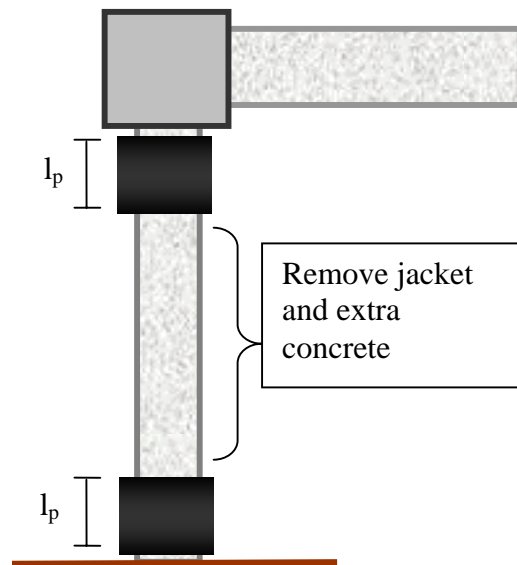


**Figure 5-1: Column Modification**

In the Spokane Street over-crossing, the modification would require the removal of part of the existing jacket on the outrigger columns. In a structure that had not already been retrofitted by jacketing all the columns, the retrofit would consist of placing a full-height jacket on each of the main line columns and a partial height jacket at the top and bottom of each outrigger column.

### Seismic Evaluation

The seismic analyses of Chapter 4, together with the evaluation in Chapter 3 of the column modeling technique, showed that a full-height jacket would stiffen the column by

a factor of 2 to 7, depending on the dimensions of jacketed sections. Table 4-12 shows that the ductility demands in the outrigger columns are on the order of 1.0 to 2.0. These values suggest that removal of the entire column jacket would bring the ductility demand down below 1.0, and the column could theoretically remain elastic. However, removing the entire jacket is unacceptable because it would leave the column vulnerable in the event of an unexpectedly large earthquake. Therefore, the partial jacket scheme is proposed. As indicated in tables 4-21 and 4-22, all of the outriggers have at least one potentially critical response mechanism that could result in loss of lateral load carrying capacity. Therefore, this column modification scheme applies to all outrigger bents of the as-existing system.

#### *Applicability to the Structure*

The column jacket modification is a structurally viable approach for the outrigger bents in which the ductility demand could be reduced to 1.0 or below, since the column would then behave elastically. The beam would also need to be checked to ensure that the torsion and shear demands were acceptable. Other features of the retrofit should also be considered. These include constructability, economics, and aesthetic considerations. To implement the process, the jacket would have to be cut off and the excess concrete removed. Potential problems include flame-cutting the steel jacket while it remains in direct contact with the concrete behind it, and removal of the excess concrete in such a way that it leaves a clean, visually acceptable surface. The quality of the final surface might not be a critical issue if other aspects of the surrounding structure were deemed to have a similar aesthetic value.

#### *Potential for Application to Other Structures*

The concept has applicability to other structures with outrigger bents. Constructability may be the greatest difficulty faced in the Spokane Street over-crossing; application to a structure that had not previously been retrofitted by jacketing would be simpler because it would require installing only a partial height jacket at each end, and this would pose no special problems. On each project, a structure-specific analysis, accounting as accurately

as possible for the true column stiffnesses, would be necessary. The modeling methods described above are recommended.

## **5.2.2 Joint**

### *Vulnerabilities Addressed by the Retrofit*

Joint performance is critical to the structure's ability to carry gravity load. The laboratory tests performed by McLean and Shattarat (2004) showed that the joint is vulnerable to damage. Joint damage is usually identified as being caused by either joint shear stresses or bar anchorage failure, but in these experiments the distinction was hard to draw. Three primary types of cracking were observed in the tests:

- circumferential cracking near the outer edge of the joint
- in-plane splitting at the two planes of reinforcement parallel to the plane of the bent
- radial cracking.

The circumferential cracking was the most severe and is attributed to wedging stresses in the splice of the outside bars under closing moments and to radial tension in the joint under opening moments. The radial tension was similar to the through-thickness tension found during "opening" bending of any curved beam, or it may be viewed as the diagonal tension component of a joint shear stress. Thus the circumferential cracking may have originated from either splice effects or joint shear effects, but the primary cause remains unknown. The distinction may not be important because the retrofit measures required for both are similar and consist of confining the joint.

The in-plane splitting is believed to have been caused by wedging stresses in the concrete induced by development of the straight beam and column bars in the faces of the joint. The radial cracking is attributed to the diagonal tension component of the joint shear stress under closing moments

### *Retrofit Concepts*

The joint retrofit must enable the outrigger to go through the expected earthquake motions without loss of gravity capacity. Lateral strength of the outrigger bent is less

important than its deformability because the mainline columns are expected to perform well and to retain enough lateral capacity to prevent collapse of the structure through P- $\Delta$  effects.

Two philosophies are possible for the joint retrofit. The first is to make the joint strong enough that inelastic deformations occur in some other component, such as the beam, where ductile response can be ensured. The second is to increase the deformation capacity of the joint so that deformations can occur there without risk of losing the gravity capacity of the system. The first, “strong,” philosophy is discussed here. A version of the second one, in which the joint is made more deformable by inserting an isolation bearing directly beneath it, is discussed in Section 5.3.5 as a system retrofit.

Three methods of strengthening the joint are considered, and they all increase the confinement of the joint (see Figure 5-2). The first consists of a concrete jacket prestressed in all three directions. The prestressing steel should be placed around the edges to avoid cutting the existing reinforcement in the joint or debonding it by local cracking. Steel plates may be required on the faces of the joint both to provide local bearing for the prestressing bars and to distribute the compression stresses more evenly. Compression is needed across the north and south joint faces to prevent the in-plane splitting caused by the development of the beam and column bars.

Ingham et al. (1997) tested a similar retrofit scheme, discussed in Section 2.1, which involved external prestressing of the joint as well as the beam. Their tests showed that a significant strength loss occurred as a result of opening moments when the specimen reached a displacement ductility demand of approximately 2. The prestressing was successful at increasing the strength of the specimen as well as preventing splice failure of the outside beam and column bars. Although this retrofit concept shows promise, some questions remain about the details:

- How much prestress, if any, is needed?
- Can prestress be applied reliably over such a short bar length without serious losses due to anchorage slip back, creep, etc?

- Can the prestressing forces be spread effectively over the joint faces?
- Can the anchorages be adequately protected against corrosion?

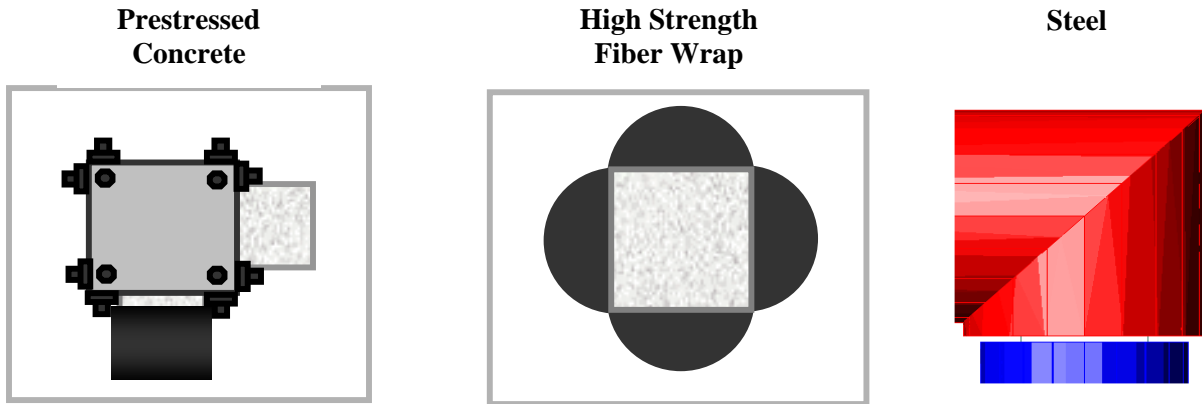


**Figure 5-2: Joint Retrofit Options**

The second method of strengthening the joint consists of applying dome-shaped precast panels on each side of the joint and securing the panels with a high strength fiber composite wrap. The purpose of the domes is to change the shape of the joint so that the fiber wrap is curved and provides confinement stresses that are distributed across the faces of the as-existing joint.

Pantelides et al. (1999) studied the use of a fiber wrap to retrofit cap beam to column joints in a bridge. Their experiments showed that the fiber wrap significantly increased the displacement ductility and joint shear strength of the bent. Although the tests were performed on interior joints, the results show promise for the proposed retrofit scheme. This scheme has conceptual advantages over the prestressing bar system in that the confinement stresses would be better distributed and the corrosion problem would be avoided, but it also presents some challenges. Some of the primary ones are as follows:

- The presence of the beam and column limit the directions in which the fiber can be wrapped completely around the joint.
- Prestressing the fiber wrap is desirable from the point of view of the joint performance but is difficult to achieve in practice. If it is attempted, it is necessary to choose a type of fiber that is not susceptible to creep rupture.

- Use of a dome, rather than a developable surface such as a cylinder, for the concrete panels means that flat sheets of fiber cannot be used for the jacket.

The third method consists of enclosing the joint within a steel jacket and filling the void between the jacket and the existing joint with grout or concrete. The goal is to make the joint stiff and strong, thereby forcing the inelastic deformations to occur in adjacent components. If the joint jacket is combined with beam and column jackets, it is advisable to select the locations where the inelastic deformations are to occur and there create zones of low strength but high ductility. If, for example, a single continuous jacket were used for all three components, the inelastic deformations would occur at an unspecified location and might cause unexpected and adverse effects.

Washington State University tested such a joint jacket in combination with separate beam and column jackets (McLean and Shattarat 2004). Small gaps were left between the end of one jacket and the start of the next, and the deformations of the system were concentrated there. Results from the tests suggested that this system would provide a significant increase in the strength of the joint and in the displacement ductility capacity of the system.

#### Seismic Evaluation

Analysis indicated that the demand/capacity ratios for joint shear stress in the as-existing outriggers range from 0.5 to 1.3. The demand/capacity ratios resulting from radial tension are between 0.6 and 3.0, and the demand/capacity ratios for bar anchorage are between 0.3 and 1.2. The largest of these demands are in bents 12, 20, 21, and 25, and retrofit of the joints in these bents is critical.

#### Applicability to the Structure

It is extremely important to retrofit the critical outrigger joints. The retrofit schemes presented would be relatively simple to implement for the standard outrigger bent. However, a few constructability issues would have to be addressed, and they include the following:

- When the retrofit was designed, it would be necessary to consider the interaction between the joint retrofit measure and any others (e.g., column jacket) that might be used.
- Locations where the joint is adjacent to the deck and no outrigger beam exists (namely Bent 21) present particular challenges because the potential for the occurrence of a damaging response mechanism is as high as in the other bents, yet application of the joint retrofit schemes would be more difficult.
- At the location of the split columns (bents 9 and 25), should the joints be retrofitted together or separately? For the steel jacket concept, the WSU experiments consisted of split column joints retrofitted together with successful results. However, the need to accommodate ongoing thermal and shrinkage deformations in the bridge would have to be evaluated.

#### *Potential for Application to Other Structures*

It is likely that other structures built before the mid 1970s contain joint details with vulnerabilities similar to those of the Spokane Street over-crossing. For them, a joint jacket would be a viable method of retrofit. Selection of the most appropriate detail would depend on the configuration of, and access to, the joint being retrofitted.

### **5.2.3 Beam**

#### *Vulnerabilities Addressed by the Retrofit*

Transverse seismic ground motions induce in-plane shear forces in the beams, which add directly to those caused by gravity. Longitudinal motions cause torsion and out-of-plane shear in the beams. The stresses caused by these forces are additive, but two possible combinations of shear stress must be considered in determining the most severe case. In the side faces of the beam, the total shear stress is the sum of those caused by seismic torsion and gravity shear, while in the top and bottom faces the total shear stress is the sum of those caused by torsion and out-of-plane seismic shear force.

Most of the outrigger beams contain only light transverse reinforcement, and it is poorly detailed, consisting in some cases of open stirrups alone (Bent 11) and in others of open

stirrups and closure bars with 90-degree hooks. Thus the shear and torsion capacity of the beams after cracking is limited and uncertain.

### Retrofit Concept

To improve the shear and torsion performance of the existing outrigger beams, the proposed retrofit measures consist of providing additional transverse reinforcement. Three different methods of beam retrofit are proposed, and they are analogous to the three joint retrofit methods described in Section 5.2.2 (see Figure 5-3). It is important to note that these beam retrofit measures would increase the beam's torsional stiffness and strength, in which case they would increase the forces exerted in the joint. Therefore, a beam retrofit measure should be applied only in combination with a joint retrofit.

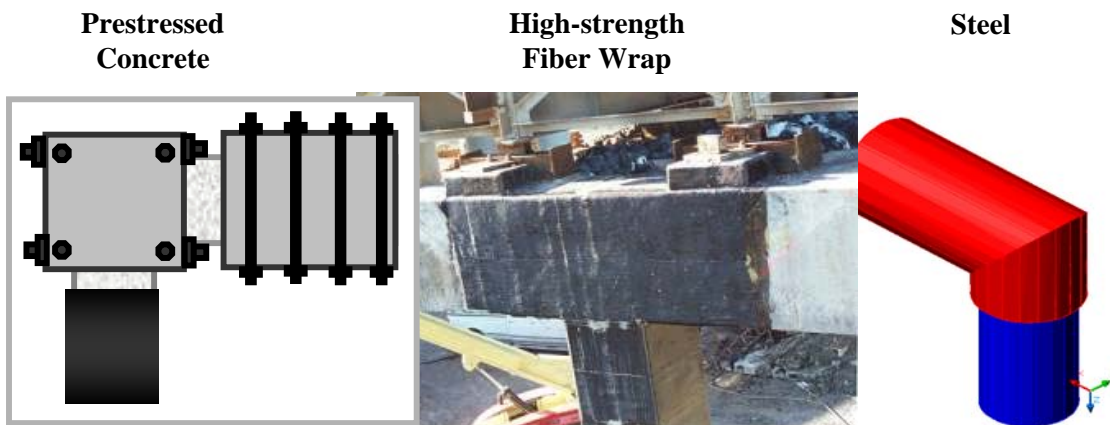


**Figure 5-3: Beam Retrofit Options**

The first beam retrofit method consists of placing prestressed concrete jackets around the beam. The prestressing bars are placed on the outside of the cross-section to avoid interference with the existing reinforcement. Steel plates may be required at the corners for bearing and confinement. A study of the exterior prestressing concept by Ingham et al. (1997), as introduced in the previous section, showed that the beam remained elastic when subjected to cyclic loading. Therefore, this measure shows even more promise for the beam than the joint. However, as with the joint retrofit, prestress loss in the bars and corrosion protection at the anchorage may pose problems.

The second method consists of a high-strength fiber composite wrap around the beam. It has been studied by Pantelides et al. (1999) at cap beam-column joints with success for interior joints as discussed in the previous section. Application to a beam poses fewer constructability problems than exist with a joint.

The third method is to use a grout-filled steel jacket around the beam. In Figure 5-3, the steel tube around the beam is shown as continuous with the tube around the joint. Test results from WSU (McLean and Shattarat 2004) showed that the steel beam jacket provides a significant improvement in the beam's gravity and lateral load carrying capacity under both longitudinal and transverse loading.

### Seismic Evaluation

Analysis of the shear demands due to transverse loading indicates that, depending on the evaluation method, all bents other than Bent 10 have demand/capacity ratios of above 1.0, as seen in Table 4-19. Therefore, a strength increase of these beams is needed for gravity plus lateral shear under transverse loading. Beam torsion and out-of-plane shear results from analyses indicated demand/capacity ratios ranging from 1.1 to 1.7, as seen in Table 4-20. Again, beam retrofit measures are suggested, in this case to increase the displacement capacity for horizontal shear plus torsion.

The retrofit measures presented above would increase strength by adding reinforcement or increasing the member size. They would also increase deformation capacity by adding confinement.

### Applicability to the Structure

The beam retrofit schemes are similar to the joint retrofit schemes, but additional constructability issues would have to be addressed, many of them arising from the beam connectivity to the deck. They include the following:

- Because of the slab overhand at the edge of the deck, care would have to be taken when the beam retrofit scheme was implemented in this area.

- The problems of retrofitting the outrigger beams at the split column locations, as described in the joint section above, would also apply here.

Some of the outrigger beams (such as Bent 20) have a span to depth ratio of less than 1.0. Use of a strut-and-tie model of the beam showed that the concrete struts can be oriented at an angle that is steep enough to carry the shear and torsion loading without the need for any ties. Therefore, in these cases, the capacity of the as-existing beam may be adequate.

### *Potential for Application to Other Structures*

As with the joint retrofit, the beam retrofit may also be applicable to similar structures built before the mid 1970s, depending on the beam details and the results of a bridge-specific analysis. Selection of the most appropriate retrofit scheme would depend on the configuration of the outrigger beams and connection to adjacent elements. Additional research on outrigger beams in torsion would be beneficial, since only a small amount of research has been conducted in this area to date.

## **5.3 System Retrofit Schemes**

### **5.3.1 Introduction**

The system retrofit schemes considered fall into two categories. The first consists of combinations of one or more component retrofit schemes, each of which is intended to increase the strength and/or deformation capacity of a particular component. The second category consists of using isolation devices, such as elastomeric or sliding bearings, that are intended to reduce the demand on critical elements. Thus, both approaches would reduce the demand/capacity ratio, but they would do so by opposite approaches. The effectiveness of each system retrofit scheme would need to be evaluated in terms of constructability, aesthetic appeal and cost. Such a detailed evaluation was not conducted here, since it lay outside the scope of the project, but important issues to be considered in it were identified.

Four component-based retrofit measures were considered:

- Scheme C. Retrofit of the Column alone

- Scheme J. Retrofit of the **J**oint alone
- Scheme J+C. Retrofit of the **J**oint and **C**olumn
- Scheme J+B. Retrofit of the **J**oint and **B**eam.

Two isolation schemes were considered:

- Scheme I-joint: An **I**solation bearing is installed directly below the joint. The moment there is reduced to zero.
- Scheme I-base: An **I**solation bearing is installed at the bottom of the column. The moment there is reduced to zero.

Each of the measures was evaluated as follows. First, the analytical model of the bridge was modified to account for differences in the outrigger bents, based on the specifics of the retrofit scheme. Then, the ground motions corresponding to the three different hazard levels were used to determine the response. Last, the responses of the outrigger bents were compared with expected capacities.

The evaluations are presented using a common format:

- description of system retrofit measure
- modifications made to the analytical model
- results of analyses
- design and construction implications and evaluation of effectiveness.

### **5.3.2 Column Modification Retrofit (Option C)**

To evaluate the effects of the proposed retrofit, the global analytical model was modified by changing the outrigger columns but keeping all other elements the same. The column modification consists of removing the central part of the grout filled column jacket, as discussed in Section 5.2.1, for each critical outrigger bent. A representation of the column with a partial jacket at each end was constructed to evaluate the lateral stiffness. The assignment of the partial jacket length was important for the modeling assumptions. In tests performed by Chai et al. (1991), the retrofit column jacket was required for

additional moment strength as well as confinement and, therefore, was extended to the point where the moment demand was 75 percent of the maximum end moments. For the SR 99–Spokane Street over-crossing columns, the sole purpose of the jacket would be confinement, since the goal of the retrofit scheme is to reduce demands to elastic levels. Therefore, a jacket length equal to the plastic hinge length was determined to be adequate for confinement purposes (recall that the confinement is a redundant feature, needed only in case of an unexpectedly large seismic event). The plastic hinge lengths for the columns were determined with Equation B-10 (see Appendix B). The lengths were typically one-half of the final column diameter or less.

Because the length of the jackets would be short relative to the length of the columns, the increase in the overall column stiffness would be minimal. Therefore, column representation was based on the unjacketed column stiffness over its full length, and the column was modeled with the five-part representation described in Appendix A and shown in Figure 5-4. The presence of the jackets might reduce the cracked section length assumed for the five-part column. However, a reduction in stiffness due to strain penetration into the jacket could balance the increase caused by the shorter cracked section length. Therefore, the 20 percent cracked section length used in Appendix A was used for the retrofitted columns as well.

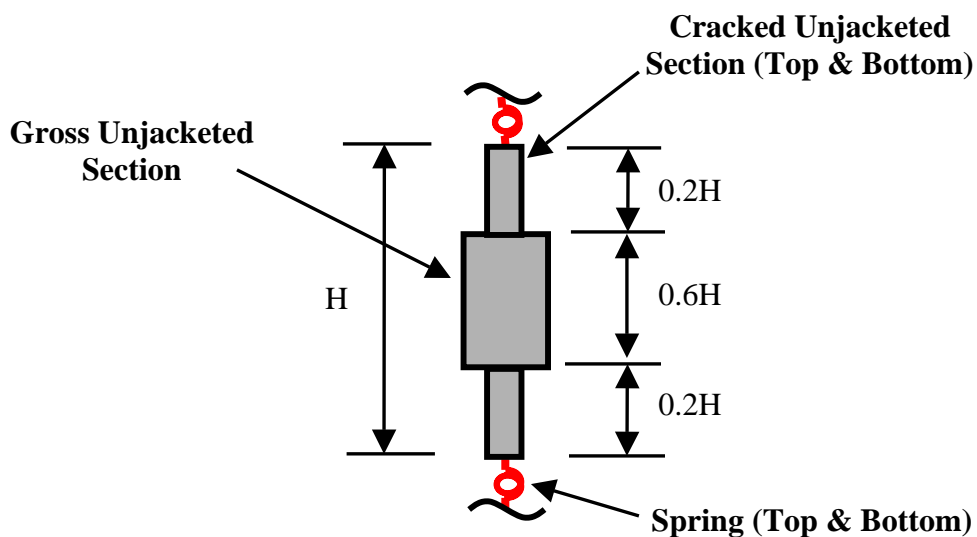


**Figure 5-4: Five-Part Column Representation**

An FE analysis was performed with the five-part columns in place at each outrigger. The displacement ductility demands are given in tables 5-1 and 5-2. They were significantly lower than those obtained with the as-existing model, largely because of an increase in the yield displacements of the outrigger columns. However, in a few locations, namely bents 9 and 11 in the transverse direction and Bent 11 in the longitudinal direction, the ductility demand was still equal to 1.0, implying the possibility of damage to the outrigger joint. In addition, although a demand/capacity ratio of less than 1.0 alleviates joint damage, there is still potential for beam shear and torsion damage. Therefore, this column retrofit scheme alone may not be adequate for all outriggers.

**Table 5-1: Maximum Displacement Ductility Demands for Element Strengthening Schemes, Longitudinal Direction**

Retrofit Scheme	Bent 9	Bent 10	Bent 11	Bent 12	Bent 20	Bent 21	Bent 25
As-Existing	0.3	0.9	1.6	1.1	1.1	1.4	---
C	0.3	0.8	1.0	0.9	0.8	0.9	---
J	0.3	0.9	1.6	1.1	1.1	1.4	---
J+C	0.3	0.8	1.0	0.8	0.7	0.7	---
J+B	0.6	1.5	2.0	1.4	1.3	1.3	---

**Table 5-2: Maximum Displacement Ductility Demands for Element Strengthening Schemes, Transverse Direction**

Retrofit Scheme	Bent 9	Bent 10	Bent 11	Bent 12	Bent 20	Bent 21	Bent 25
As-Existing	1.5	1.1	1.9	1.5	1.7	1.7	0.8
C	1.0	0.7	1.0	0.9	0.8	0.9	0.8
J	1.5	1.1	1.8	1.5	1.7	1.7	0.8
J+C	1.0	0.7	1.1	0.9	0.9	0.9	0.8
J+B	1.5	1.3	2.0	1.7	1.9	1.8	0.9

The column retrofit scheme would reduce the deformation demand on the columns, and thus the joint shear stress demand on the joints, so that in most cases the elements remain elastic. If beam shear and torsion demands were also low, this result for the joint implies

that the desired level of mitigation would have been achieved in those cases. The constructability and economy of the scheme are difficult to establish for the Spokane Street over-crossing because they depend on the ease with which the jacket could be cut cleanly and the surplus concrete removed. In a structure in which the columns had not been jacketed, the retrofit would consist of applying a partial length jacket at each end. This would be a relatively simple operation, and if it obviated the need for a joint jacket, it would likely be an economical solution.

### **5.3.3 Joint Retrofit with Optional Column Modification (Options J and J+C)**

Joint response is critical to the lateral and gravity load carrying capacity of the outrigger. In this scheme, the joints would be retrofitted with one of the proposed measures described in Section 5.2.2. The outrigger joint is the most critical element for retrofit, and the column modification alone may not be sufficient to protect it. Therefore, column modification should be viewed as an enhancement to the joint retrofit because it would reduce the displacement ductility demands on the column.

The joint retrofit scheme was analyzed with and without column modification. The expansion joint at Bent 9 was left open, assuming that the joints were not wrapped together (the steel jacket retrofit scheme tested by WSU consisted of split column outriggers wrapped separately). Regardless of the joint retrofit system chosen, the stiffness of the joint would increase. Therefore, in the analytical model of the retrofitted structure, the joint flexibility springs for all of the outriggers were increased by a scale factor representing the stiffness change caused by jacketing. Analyses were performed on the retrofit models, and displacement ductility demands were tabulated (see tables 5-1 and 5-2).

As expected, if the joints were retrofitted without column modification (Scheme J), the displacement ductility demands would not change from those predicted for the as-existing system. Also, if column modification was included (Scheme J+C), the displacement ductility demands would not change from those predicted for the stand-alone column modification scheme (Scheme C). The results suggest that the same joints

that required retrofit in the as-existing model would also require joint retrofit if the column was not modified. However, if the column were modified, it is possible that joint retrofit might not be required because the displacement ductility demands would be much smaller. Results from the WSU tests on specimens retrofitted with steel jackets showed that displacement ductility demands between 4.6 and 6.3 can be achieved without degradation. The computed displacement ductility demands were much smaller. In addition, research (e.g., Pantiledes et al. 1999, Shattarat and McLean 2004) has indicated that the retrofitted joints are capable of sustaining larger joint shear stress demands, thereby minimizing joint damage. Therefore, this retrofit scheme seems to be a viable option.

#### **5.3.4 Joint and Beam Retrofit (Option J+B)**

Previous analyses showed that many of the outrigger beams and columns yield. For flexural yielding to occur in the longitudinal direction, large torsion forces must be transferred through the outrigger beams. These forces combined with gravity or seismic shear may crack the beam and may require beam retrofitting in addition to the joint retrofit. In addition, large in-plane shear demands under transverse loading may require strengthening of the beams for shear purposes. For this retrofit scheme, the beams would be jacketed using one of the measures discussed in Section 5.2.3.

Performing a beam retrofit on the middle bents of the frame would be relatively straightforward. However, retrofitting the split bents so that the elements remained separate might be difficult, depending on the retrofit method chosen. Therefore, the possibility of wrapping both elements together should be considered. Preliminary analyses suggested that if, for example, the beams and columns of Bent 9 were encased in a single jacket, but those at bents 6 and 12 were not, the thermal forces induced in frames 2 and 3 would be acceptable. Eliminating the expansion joint at Bent 9 therefore appears feasible. However, the beam retrofit proposed by WSU has the beams jacketed separately, and therefore, the analysis reflected these conditions.

The joint and beam retrofit model was based on the joint-only retrofit scheme model (Scheme J) with a few modifications. The effective bending stiffness of the outrigger beams was increased by a scale factor representing the stiffness of the beams retrofitted with steel jackets divided by the stiffness of the unjacketed beams. This was accomplished by increasing the modulus of elasticity of the beams by the appropriate scale factor in the strong and weak axis directions. Also, the effective torsional stiffness of the beams was increased with a similar procedure. The analyses were run and the resulting outrigger displacement ductility demands are shown in tables 5-1 and 5-2.

The effect of adding a beam jacket would not change the global displacements significantly in comparison to those of the as-existing structure or the joint-only retrofit scheme. However, the member stiffnesses, especially in the longitudinal direction, would increase, and therefore their yield displacements would decrease, resulting in larger displacement ductility demands. This is evident when retrofit scheme J+B is compared to retrofit scheme J and the as-existing structure in Table 5-1. However, the resulting displacement ductility demands would still be smaller than the displacement ductility capacities (lower bound of 4.6) achieved in the WSU tests. In addition, a jacketed beam would have significantly higher shear and torsion strength. Therefore, the proposed retrofit scheme is a feasible option.

### **5.3.5 Isolation of Column (Option I)**

Instead of increasing the capacities of the critical outrigger elements through strength retrofitting, the demands on them can be reduced by isolation. The global displacements of the structure are dominated by the properties of the mainline columns, so they will change only slightly even if the properties of the outrigger columns are altered radically. However, changes in the outrigger column properties can be used to reduce the demands and thereby provide an overall benefit. The column can be isolated by inserting a bearing at any vertical location. Here, only two locations were considered: the top and bottom of the column, as shown in Figure 5-5.

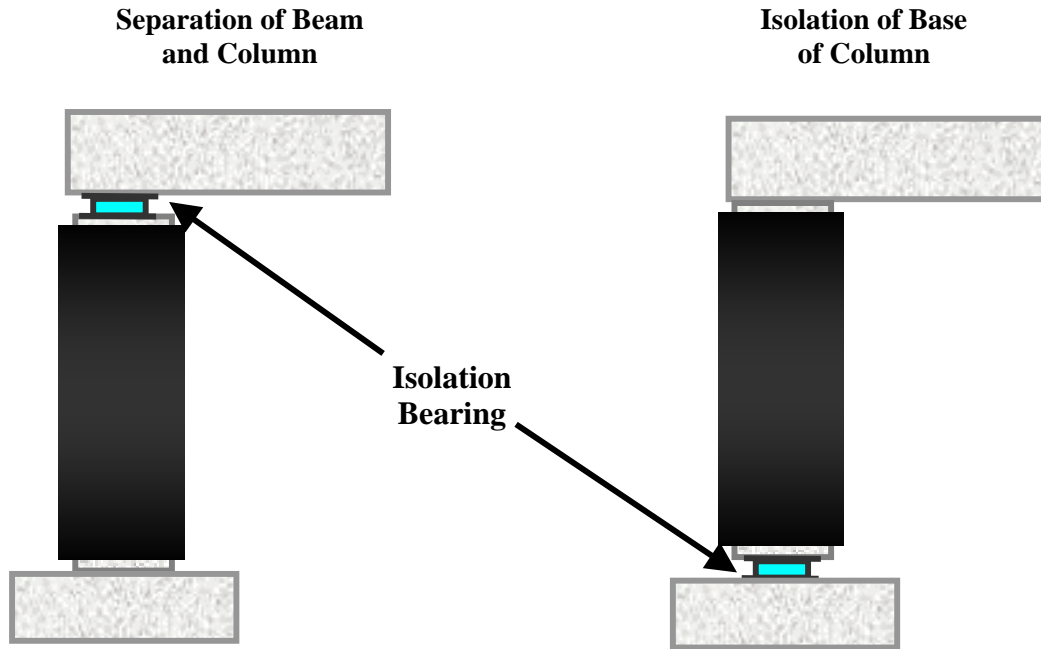


**Figure 5-5: Column Isolation Retrofit Schemes**

In both cases the column would have to be cut and the bearing installed. From a construction point of view, isolation at the base is likely to be simpler because the work could be conducted from the ground. However, isolation at the top is likely to provide greater structural benefits because it would eliminate the bond and shear demands on the joint and the torsion demand on the beam. Some flexural ductility demand would remain at the base of the column, but the confinement there would be likely to provide adequate ductility capacity.

A bearing type would have to be selected. The main choice is between a deformable (elastomeric) system and a sliding system, and either could be made to work in this case.

Analyses were conducted with isolators in each location. For isolation at the top, the as-existing model was revised as follows. All outrigger columns were detached from the beams, and the bearing was given zero horizontal resistance. This implied an elastomeric bearing with zero shear stiffness or a frictionless sliding bearing. The analysis was performed, and the absolute displacements at the outrigger joint are tabulated in Table 5-3. These displacements may be considered upper bounds because the bearing resistance

would not, in practice, be zero. Column base moments induced by sliding bearings were estimated on the basis of the axial load on the column and a friction coefficient of 0.06. These are also presented in Table 5-3. The forces induced in an elastomeric isolator would depend on the properties of the isolator and might be either higher or lower than those in the sliding system. The yield moments at the base of the column determined from moment-curvature analyses are also tabulated, as well as the moment demand to yield moment (D/C) ratios.

**Table 5-3: Maximum Isolator Displacement (ft.) and Column Base Moments (k-ft.) for Top Isolation**

		Bent #						
		9	10	11	12	20	21	25
Transverse	$\Delta_{iso}$ (ft.)	0.22	0.22	0.23	0.32	0.30	0.32	0.42
	$M_{y-base}$ (k*ft)	1312	1494	1141	1388	2331	2212	1910
	$M_{dem-base}$ (k*ft)	31	320	303	712	1036	1330	270
	D/C	0.0	0.2	0.3	0.5	0.4	0.6	0.1
Longitudinal	$\Delta_{iso}$ (ft.)	0.28	0.25	0.25	0.25	0.33	0.33	0.45
	$M_{y-base}$ (k*ft)	1116	1515	1141	1610	2331	2212	3097
	$M_{dem-base}$ (k*ft)	31	320	303	712	1036	1330	270
	D/C	0.0	0.2	0.3	0.4	0.4	0.6	0.1

For an isolator at the top of the column, the maximum displacements from the analyses were relatively small, and it would be possible to design either an elastomeric or a sliding isolator for the largest displacement. In addition, the column moments at the base were below the corresponding yield moments, as seen by the demand/capacity ratios of less than 1.0. Therefore, the top isolation scheme appears feasible.

For an isolator at the base of the column, an iterative analysis based on a revised as-existing model was used. First, displacements from the top isolation system and the estimated friction force from the sliding bearing were used to calculate an initial secant stiffness of the isolator. The isolator was modeled as an elastic spring. An analysis was run to obtain a new set of displacements at the bearing locations, and the stiffness was recalculated. This process was repeated until the stiffness converged. The final moments at the top of the outrigger columns are tabulated in Table 5-4. For comparison purposes, the moments at the top of the outrigger columns from the analysis of the as-existing structure are also tabulated.

**Table 5-4: Outrigger Column Moments (k\*ft) for Column Isolation Retrofit Scheme**

		Bent #							
		9N	9S	10	11	12	20	21	25
Retrofit S (Base)	M <sub>col</sub> transverse	1233	908	990	643	793	981	736	5449
	M <sub>col</sub> longitudinal	1371	2078	2245	1632	1444	4521	5581	1103
As- Existing	M <sub>col</sub> transverse	1943	1229	2189	2127	3795	6508	6692	1804
	M <sub>col</sub> longitudinal	169	315	2042	1829	3292	4359	5501	293

The moments in the transverse direction were significantly smaller with the isolators. This would reduce the potential for response mechanisms such as joint shear, radial tension, anchorage, and beam shear failure. However, in the longitudinal direction, the moments for most of the outrigger bents equaled or exceeded those in the as-existing structure. By placing the isolators at the base, the inflection point of the column would move to the base instead of being near the center, as it would be in the absence of isolators. Thus, although the shear demands would be smaller because of the reduction in stiffness from the isolator, the lever arm would be nearly doubled and, for the longitudinal direction, the resulting moments would be almost the same. Because the

longitudinal moments would be similar to those in the as-existing structure, the same potential for damage due to out-of-plane response mechanisms (i.e., beam torsion) would be present. Therefore, placing the isolators at the base of the column would provide little, if any, benefit.

## 6 SUMMARY AND CONCLUSIONS

### 6.1 Summary

The SR 99–Spokane Street over-crossing contains a number of outrigger bents. The outrigger bents were constructed to accommodate the railroad that passes under the bridge at an oblique angle. The outrigger bents constitute significant irregularities in the structure and could induce undesirable response mechanisms in the event of an earthquake, particularly because the structure is made of reinforced concrete that contains non-ductile details. To mitigate the potential seismic hazard, the WSDOT completed a Phase I retrofit, which consisted of steel-jacketing almost all of the columns. However, vulnerabilities in the outrigger bents exist, as the beams and joints have not been retrofitted, and therefore the WSDOT is interested in evaluating the seismic behavior of the structure in its existing state. This report describes the seismic demand and capacity evaluation of the as-existing structure.

The structure runs north-south and is divided by the Spokane Street Viaduct. The north half was analyzed dynamically with a detailed, three-dimensional finite element model, in order to evaluate the demands on the components. Results from experiments conducted at Washington State University were used to establish component capacities.

The research objective was to evaluate the structure in its as-existing condition and, in combination with the WSU experimental study, to evaluate the vulnerability of the system. The research approach was as follows:

- Review previous studies to determine potential response mechanisms and retrofit measures.
- Perform a geotechnical evaluation, including developing site-specific ground motions and soil stiffness and damping values.
- Develop a reliable, detailed analytical model of the entire northern structure. Incorporate representative models for each of the important components of the

bridge (e.g., deck, columns, outrigger elements, expansion joints, soil-structure-foundation interaction elements). Verify the model using simpler models of individual parts of the structure and field observations.

- Subject the analytical model of the bridge to site-specific ground motions representative of different seismic hazard levels to determine local and global demands.
- Determine the capacities of the components of the outrigger bents using the test results from WSU and codified methodologies from ACI 318 and FEMA 356.
- Identify the most vulnerable outrigger elements and bents by comparing the demands to the capacities.
- Develop retrofit options based on the demand/capacity evaluation.

To determine the demand at the seismic hazard levels considered, a detailed FE model was developed. The analytical model included the following:

- a 3-D representation of the structure
- wide use of elastic elements. Nonlinear elements were used only in locations where nonlinear behavior was expected to influence the structural response
- soil–foundation-structure interaction, including stiffness and damping.
- in the substructure, single-segment columns that implicitly accounted for the stiffnesses of both the original and the jacketed sections, multi-element columns in the outrigger bents, bending and torsional stiffness representation in the outrigger beams, and in-plane flexibility of the beam-column joints
- in the superstructure, an explicit representation of the deck with horizontal and vertical plate elements, and explicit representation of expansion joints using contact elements
- simplified models of adjacent structures, such as off-ramps and steel over-crossing spans that are contiguous with main structure.

The ground motions developed through geotechnical evaluation included the following:

- three seismic hazard levels: 2, 10, and 50 percent in 50 years
- site-specific ground motions

- synthetic ground motions based on the propagation of bedrock motion up through the soil mass.

The seismic demand/capacity evaluation was based on the following:

- global displacement demands obtained from the dynamic analysis
- local deformations and forces on the outrigger components, which were derived from the global displacements
- component capacities determined largely from experimental research results but also from standard evaluation methods where test results were not available
- a demand/capacity evaluation to determine which bents were most vulnerable.

The results of the seismic evaluation and previous research results were used to develop the proposed retrofit measures. The measures

- were based on findings from the response evaluation
- included several different approaches; some relied on reducing the local demands and others increased the component capacities
- included the scheme tested by the WSU researchers.

## **6.2 Conclusions**

The study provides insight into the response and retrofit needs of the SR 99–Spokane Street over-crossing, as well as general findings regarding the seismic evaluation of reinforced concrete bridges. The following conclusions were drawn from the study.

### **6.2.1 Required Components of the Analytical Model**

- The dynamic response of the individual frames, especially in the longitudinal direction, depended on the way in which the deck was modeled. Models that did not simulate the distribution of the deck mass and stiffness resulted in a poor representation of the dynamic response.
- Interactions between adjacent frames occurred when the expansion joints between them closed. This behavior was most prevalent in the frames with the tallest columns because they are the most flexible and sustain the largest displacements.

- In the analytical model, compression-only gap elements were used to simulate this behavior. The commonly used alternative is to use conduct two analyses with models that respectively treat the frames as completely separate and as permanently connected, with the objective of bracketing the true solution. However, this procedure does not guarantee that the objective will be achieved.
- In the transverse direction, the interactions between frames were minimal, except at the split column locations where either part of the column or the footing was shared.
  - The stiffness of a jacketed column, and therefore its yield displacement and predicted ductility demand, are quite different from those of a conventional reinforced concrete column. The response of a jacketed column includes the strain penetration of the longitudinal reinforcement into the joint above and the footing below, and the flexural deformations of the jacketed section and the short unjacketed sections at the top and bottom of the column. All of these must be modeled to obtain realistic response values.
  - The flexibility of the soil affected the response, but the radiation damping had little influence.

### **6.2.2 Response Prediction**

- The response in all critical mechanisms is dominated by the 72- and 475-year return period earthquakes. The large soil strains that would be induced by the 2475-year earthquake would make the ground relatively flexible and reduce the accelerations delivered to the structure.
- The non-ductile details caused considerable uncertainty about the component capacities. This is illustrated by the fact that the 2001 Nisqually earthquake had approximately the same intensity as the 72-year earthquake, which was predicted to cause damage, yet the Nisqually earthquake caused almost no damage to the joints.
- The individual frames displayed a wide range of periods, determined largely by their column heights. The different periods of adjacent frames lead to structural

motions that are inevitably out of phase at some time. Pounding is thus unavoidable if the displacements are large enough.

- The displacement response of the structure is dominated by the main line columns, which are jacketed. This occurs because there are fewer outrigger columns than main line columns and because the outrigger columns are more flexible than the main line ones by virtue of being connected to the deck through relatively flexible beams. Changing the properties of the outrigger columns therefore made little difference to the predicted global displacements but did influence the displacement ductility demands on the outriggers and the forces induced in them.
- The presence of jackets on the columns of the outrigger bents exacerbates the demands on the joints because it causes the column deformations to be concentrated at the ends. Therefore, the predicted demands on the outrigger joints, e.g., the joint shear and bar anchorage stresses, were larger than they would have been in an outrigger bent with a traditional reinforced concrete column.
- The estimated displacement ductility demands in the outrigger bents were on the order of 2. While this is much less than the ductility capacity of a modern reinforced concrete structure, the local strain concentrations and the poor joint details in the SR 99 structure mean that that this level of displacement ductility demand could still cause significant damage. This was demonstrated by the companion experimental research.
- The joints were found to be the most vulnerable component of the outriggers. In the experiments, degradation of the bents due to transverse loading was largely attributable to joint damage.
- Evaluation of the experimental results indicated that the outrigger joints are vulnerable to joint shear damage, circumferential splitting around the curved outer edge, and loss of anchorage of the curved exterior bars. The capacities of the response mechanisms of the joint were largely determined through the experimental research results. Those results indicated that, under transverse loading, the circumferential splitting response is the most critical and cannot be properly evaluated with traditional methods of analyzing joint shear behavior but

is better treated as a radial tension phenomenon. An alternative equation was developed for this radial tension effect, which resulted in consistent predictions of the capacities of the two specimens that were loaded in-plane.

- Longitudinal (out-of-plane) loading of the bent causes significant torsion in the outrigger beam and predicted yielding of the transverse reinforcement. In many cases, the transverse reinforcement consists of either hoops with 90-degree bends or of U-stirrups with closure bars. Both of these are likely to open at the corners rather than yielding in a controlled manner, leading to non-ductile torsional failure of the beam. Considerable uncertainty accompanies this behavior.

### **6.2.3 Retrofit Options and Design Implications**

- A range of possible retrofits was examined, including the following:
  - Remove the central part of the column jacket in the outrigger bent columns. This would serve to make the column more flexible and increase the yield displacement, thereby reducing the demands on the adjacent elements such as the joints.
  - In a structure that has not already been retrofitted, consider confining with jackets only the top and bottom of the column and the joint.
  - Jacket the joint only. Preferably, also remove the column jacket over the central part to reduce the demand on the joint.
  - Jacket all components of the outrigger bents, including the beam, column, and joint.
  - Cut the column and introduce an isolation bearing. This could be done at any location in the column, but placing it at the top would provide the greatest benefit.
- The choice of retrofit method should take into account a number of criteria, such as cost, schedule, structural efficiency, and visual appearance.
- Jacketing only the joint and removing the central part of the column jacket are likely to be the two least intrusive options. They would also provide the least benefit. For the Spokane Street over-crossing, adopting both of them is predicted

to be just sufficient to protect the structure against the expected ground motions at all three hazard levels.

- Introducing an isolation bearing at the top of the column would provide the desired protection. It also would not encroach on the railroad right-of-way because the outer dimensions of the structure would not increase. Before adopting this approach, it would be necessary to develop a detailed plan for cutting the column and installing the bearing.
- Jacketing the entire beam, joint and column would increase the ductility capacity of the system and provide additional resistance to gravity-induced shear forces. The jacket could be designed to provide a very large ductility capacity, which would be beneficial in counteracting any uncertainty in modeling the ground motion or the structural response. However, such a jacket might encroach on the railroad right-of-way or other obstacles. Scheduling the construction to not clash with train passages and the cost of construction would both need to be considered. In the Spokane Street over-crossing, the column jackets are already in place, which would reduce the incremental cost.

## **6.3 Recommendations for Implementation**

### **6.3.1 Recommendations for This Structure**

The WSDOT should evaluate the costs and benefits of the following three options:

- Jacket the joint, remove most of the column jacket.
- Keep the column jackets. Add joint and beam jackets. (This is the system tested at WSU.)
- Introduce an isolation bearing below the joint at the top of the column.

### **6.3.2 Modeling Recommendations for Other Structures**

These recommendations pertain to structures whose columns have not yet been jacketed:

- The column model should include all the possible sources of deformation, including uncracked regions, cracked regions, and strain penetration. This is important because the deck is typically stiff, and most of the transverse displacement arises from the column deformations.

- The deck should be modeled with its mass and stiffness distributed transversely in such a way as to represent the true distribution of system properties. Use of a single spine girder is inadequate because the outrigger beam in the model is then much longer than the real one. Consideration should be given to using multiple spine girders, an equivalent plate, or an explicit representation of the (box girder) deck. The choice should take into account the computational resources available.
- The soil flexibility should be taken into account.
- Analyses should be conducted that consider a range of possible cracking conditions in the outrigger components.
- Evaluation of the joints should pay close attention to the circumferential splitting. This may be caused by either tension splice effects of the curved outer bars under closing moments or joint shear stresses (manifested as radial tension) under opening moments.

#### **6.4 Recommendations for Further Research**

- The response of joints should be studied in greater depth because that is where the greatest uncertainties lie. The outer curved bars are particularly vulnerable. Both experimental and analytical methods should be used. A range of details present in existing joints should first be established to guide the work. The calculated strain concentrations at the jacket ends should be confirmed experimentally.
- Evaluation of the torsional strength and stiffness of older beams that contain non-ductile detailing should be performed. A similar evaluation for the combined effects of shear and torsion should also be conducted.
- Member stiffness values used for different seismic hazard levels should be established.
- Practical modeling techniques, including deck, column, joint, and particularly soil-foundation-structure interaction models, should be developed that are useful over a wide range of existing bridge structures and that adequately capture the dynamic response of the system.

## 7 REFERENCES

- ACI Committee 318, "Building Code Requirements for Structural Concrete (ACI 318-02) and Commentary (ACI 318R-02): An ACI Standard," American Concrete Institute, Farmington Hills, MI.
- Allen, Tony M., letter report to M.M. Lwin, September 1, 1995.
- American Society of Civil Engineers, "FEMA 356: Prestandard and Commentary for the Seismic Rehabilitation of Buildings," Federal Emergency Management Agency, Washington D.C., November 2000.
- ATC (1983). "Seismic Retrofitting Guidelines for Highway Bridges". Report No. ATC 6-2, Applied Technology Council, Redwood City, CA., 220 pp.
- California Department of Transportation, "Bridge Design Aids", Sacramento, CA 1988, 5-1.
- Burns, N.H., and Seiss, C.P., "Load-Deformation Characteristics of Beam-Column Connections in Reinforced Concrete," Civil Engineering Studies, Structural Research Series No. 234, University of Illinois, January 1962, 261 pp.
- Chai, Y. H., Priestley, M. J. N., Seible, F., "Seismic Retrofit of Circular Bridge Columns for Enhanced Flexural Performance," ACI Structural Journal. Vol. 88, No. 5, Sept.-Oct. 1991, pp. 572-584.
- Chopra, A.K., "Dynamics of Structures: Theory and Applications to Earthquake Engineering," Prentice-Hall, New Jersey, Version 2, 2001, 844 pp.
- Collins, M.P., and Mitchell, D., "Prestressed Concrete Structures," Prentice-Hall, New Jersey, 1991.
- Computers & Structures, Inc., SAP2000 version 8, Berkeley, CA, 2002.
- Eligehausen, R., Bertero V., Popov E., "Local Bond Stress-Slip Relationships of Deformed Bars Under Generalized Excitations," Earthquake Engineering Research Center, Report no. 83-23, University of California, Berkeley, 1983.
- Griezic, A., Cook, W.D., and Mitchell, D., "Seismic Behavior and Retrofit of Outrigger Beam-Column Frames," Journal of Bridge Engineering, September/October 2001, pp.340-348.
- Housner, G.W., "Competing Against Time: Report to Governor George Deukmejian," The Governor's Board of Inquiry on the 1989 Loma Prieta Earthquake, May 1990, 264 pp.

- Ingham, J.M., Priestley, M.J.N., and Seible, F., "Seismic Response of Bridge Knee Joints Having Columns with Interlocking Spirals," *Bulletin of the New Zealand Society for Earthquake Engineering*, Vol. 30, No. 2, June 1997, pp. 114-132.
- Lehman, D.E., Gookin, S.E., Nacamull, A.M., and Moehle, J.P., "Repair of Earthquake-Damaged Bridge Columns," *ACI Structural Journal*, Vol. 98, No.2, March/April 2001, pp. 233-242.
- Lehman, D.E. and Moehle, J.P., "Seismic performance of well-confined concrete bridge columns." PEER-1998/01, Berkeley: Pacific Earthquake Engineering Research Center, University of California, 1998, 316 pp.
- Mander, J.B., Priestley, M.J.N., and Park, R., "Theoretical Stress-Strain Model for Confined Concrete," *Journal of the Structural Division, ASCE*, Vol. 114, No. 8, August, 1988, pp. 1804-1826.
- McLean, D.I., and Shattarat, N.K., "Seismic Behavior and Retrofit of Bridge Knee Joint Systems," Washington State Transportation Center, Washington State University, September 2004, 74 pp.
- Novak et al. 1993. "DYNA4 – A computer program for foundation response to dynamic loads," *User's Manual*, Geotechnical Research Centre, University of Western Ontario.
- NZS:3101:Part 1, "Concrete Structures Standard: Part 1 – The Design of Concrete Structures," Standards New Zealand, 1995.
- Pantiledes, C.P., Gergely, J., Reaveley, L.D., and Volnyy, V.A., "Retrofit of RC Bridge Pier with CFRP Advanced Composites," *Journal of Structural Engineering*, Vol. 124, No. 10, October 1999, pp. 1094-1099.
- Priestley, M.J.N., Seible, F., and Calvi, G.M., "Seismic Design and Retrofit of Bridges," John Wiley and Sons, Inc., New York, 1996, 686 pp.
- Priestley, M.J.N., Seible, F., Xiao, Y., and Verma, R., "Steel Jacket Retrofitting of Reinforced Concrete Bridge Columns for Enhance Shear Strength – Part 1: Theoretical Considerations and Test Design", *ACI Structural Journal*, Vol. 91, No. 4, July/August 1994a, pp. 394-405.
- Priestley, M.J.N., Seible, F., Xiao, Y., and Verma, R., "Steel Jacket Retrofitting of Reinforced Concrete Bridge Columns for Enhance Shear Strength – Part 2: Test results and Comparison with Theory", *ACI Structural Journal*, Vol. 91, No. 5, September/October 1994b, pp. 537-551.
- Raynor, D.R., Lehman, D.E., and Stanton, J.F., Bond-Slip Response of Reinforcing Bars Grouted in Ducts, *ACI Structural Journal*, September/October 2002, Vol. 99, No.5, pp. 568-576.

- Rahal, K.N., and Collins, M.P., "Combined Torsion and Bending in Reinforced and Prestressed Concrete Beams," *ACI Structural Journal*, Vol. 100, No. 2, March/April 2003, pp. 157-165.
- Rebeiz K.S., Fente, J., and Frabizzio M.A., "Effect of Variables on Shear Strength of Concrete Beams," *Journal of Materials in Civil Engineering*, Vol. 13, No. 6, November/December 2001, pp. 467-470.
- Shattarat, N.K., "Seismic Behavior and Retrofit of Outrigger Knee Joints," Ph.D. Dissertation, Department of Civil and Environmental Engineering, Washington State University, August 2004, 240 pp.
- Thewalt, C.R., and Stojadinovic, B., "Behavior of Bridge Outrigger Knee Joint Systems", *Earthquake Spectra*, Vol. 11, No. 3, August 1995, pp. 477-509.
- Veletsos, A.S., and Newmark, N.M., "Effect of Inelastic Behavior on the Response of Simple Systems to Earthquake Motions," *Proceedings of the Second World Conference on Earthquake Engineering*, Vol. 2, 1960, pp. 895-912.
- Zhang, H., Knaebel, P.J., Coffman, H.L., VanLund, J.A., Kimmerling, R.E., and Cuthbertson, J.G., " Seismic Vulnerability Study of the SR 99 Spokane Street Over-crossing," Washington State Department of Transportation, Jan. 1996.



# APPENDIX A

## A.1 Introduction

Deformations of the columns dominate the lateral displacements of the structure, so the columns should be modeled in a way that best captures their true behavior. The most common modeling problem that arises is allowing for the fact that part of the column is cracked, and part is not. This behavior is often simulated by using an effective stiffness,  $EI_{\text{eff}}$ , that is a fraction of the gross value. Nuncio-Cantera and Priestley (1991), for example, gave values for the fraction in terms of the longitudinal reinforcement ratio and the axial load. Simpler approximations (e.g., Park and Paulay 1975) have also been reported.

In the Spokane Street over-crossing the situation is complicated by the existence of jackets around most of the columns. The jackets stiffen the central region of the column both by virtue of geometry (the size of the concrete section increases over theunjacketed value) and by the addition of steel at the perimeter, where its presence increases the moment of inertia. The result is that three effects contribute to the column deformations. They are illustrated in Figure A-1 and are listed below in approximate increasing order of magnitude:

- curvature of the jacketed segment in the central region of the column
- curvature of the unjacketed segment at the end
- strain penetration along the bars into the jacketed section and into the joint beyond the unjacketed segment.

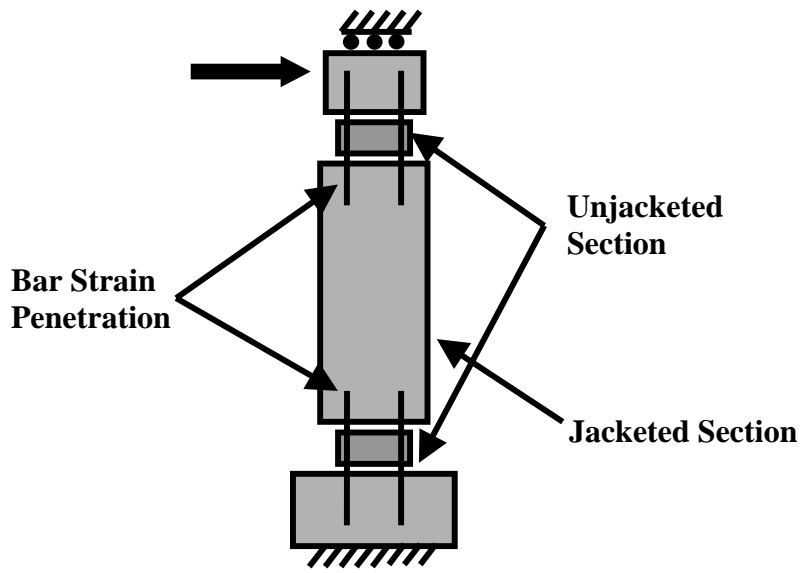


**Figure A-1: Sources of Deformation**

The strain penetration refers to the fact that, in the region adjacent to the short unjacketed segment, the strains in the bars are higher than those in the surrounding concrete. Therefore, the bars elongate more than would be calculated with a moment curvature analysis in which plane sections were assumed to remain plane. The additional bar elongation leads to additional rotation in the column.

The curvatures of the jacketed and unjacketed sections (excluding strain penetration) can be modeled by use of frame elements with suitable EI values. Modeling of the strain penetration, which is often the largest component of the total deformation, requires additional effort. The methods used here are described in Section A.2.

To model the columns including all sources of deformation required at least three elements (one unjacketed section at each of the top and bottom, and a jacketed central region). Because of the need to limit the run times to a reasonable value by limiting the number of degrees of freedom in the model, procedures to condense the column stiffness matrix without compromising accuracy were investigated. These methods are described in Section A.3. It was found that where the joints at the top and bottom of the column

were much stiffer than the column itself, or were approximately equal to each other, the column could be represented by a single element. These conditions were met in the main line columns, so a single-element representation that included the three sources of deformation was used there. In the outriggers, the presence of the beam introduces significant flexibility at one end of the column, so the conditions were not satisfied, and the column was therefore represented by three separate elements. Split columns were modeled in a similar way but presented additional difficulties that are addressed in Section A.4.

A different representation was needed for theunjacketed column at Bent 25. The column cracks over a greater length because no jacket is there to stiffen and strengthen it. Therefore, a representation that included the cracked sections was required and is described in Section A.5. The same procedure was used for the partially jacketed columns in retrofit Option C, described in Section 5.3.1, in which a small length of steel jacket was present at the top and bottom of the column but the central region remained unjacketed..

## **A.2 Modeling of Strain Penetration**

Figure A-2 illustrates the end region of a typical column in which the moment has just reached the yield value. There,  $L$  is the total length of the column and  $\alpha L$  is the length of the unjacketed section, where  $\alpha \ll 1.0$ . The bar strains are assumed to penetrate into the surrounding concrete over a length of  $\gamma l_d$ , where  $l_d$  is the development length prescribed by ACI 318-2002. A value of  $\gamma$  less than 1.0 indicates a bond capacity that is better than that assumed in the ACI equations. The value of  $\gamma$  is not known a priori but must be obtained by comparing the results of the model with experimental data.

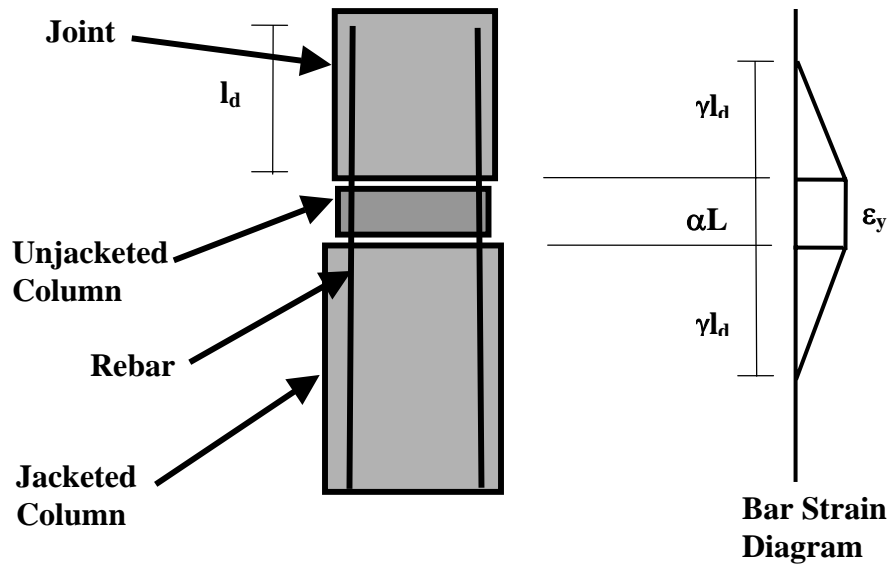


**Figure A-2: Strain Penetration at Column to Joint Connection**

Figure A-2 shows a constant strain in the column segment that is  $\alpha L$  long. The fact that the strain is modeled as constant in the segment, even though the column is elastic, is an approximation based on the assumption that the unjacketed section of the column is much shorter than the jacketed section, or that  $\alpha \ll 1.0$ . While theoretically this is a limitation of the model, in practice it has a negligible effect in comparison with other uncertainties, such as the value of  $E_c$ .

In this case, the bar is elastic, and the strain gradient along it in the penetration region is assumed to be linear, because the bond stress in the region is assumed to be constant. This model is the simplest one possible. Even for an elastic bar, more sophisticated representations of the bond (such as those considered by Raynor et al. 2002) are possible, but the data available for calibration lacked the detail necessary to justify their use. If the bar yields, the bond stress distribution tends to change significantly, which adds further complications, so yielding was not considered here.

The total elongation of the bar attributable to the length  $\alpha L$  of the element is therefore the area under the strain curve, or

$$\delta_s = \varepsilon_y (\alpha L + \gamma d) \quad (\text{A-1})$$

This elongation could be represented by a steel element of the same length,  $\alpha L$ , as the column element, but with a reduced modulus,  $E_{s,eff}$ , of

$$E_{s,eff} = E_s / \left( 1 + \frac{\gamma d}{\alpha L} \right) \quad (\text{A-2})$$

One possible way of obtaining for the short unjacketed column segment the appropriate  $EI_{eff}$  that accounts for both cracking and strain penetration is therefore to conduct a moment curvature analysis in which  $E_s$  is replaced by  $E_{s,eff}$ . Because bond for bars in compression is typically better than for bars in tension, individual bars will have different depths of strain penetration,  $\gamma d$ . Thus, different  $\gamma$  values should really be used for each bar.

An alternative approach is to ignore any strain penetration effects in compression and to evaluate the additional rotation of the cross-section directly from the bar strains and the distance from the bar to the neutral axis. This was the approach adopted here.

The total displacement of the bar, including strain penetration, is then

$$\delta_{tot} = \int \varepsilon * dl = \alpha * L * \varepsilon_y + 2 * \left( \frac{1}{2} * \gamma d * \varepsilon_y \right) = \varepsilon_y (\alpha L + \gamma d) \quad (\text{A-3})$$

The total curvature is then:

$$\phi_{tot} = \frac{\varepsilon_{avg}}{\xi d} = \frac{\delta_{tot} / \alpha L}{\xi d} = \frac{\varepsilon_y (\alpha L + \gamma d)}{\alpha L * \xi d} \quad (\text{A-4})$$

where  $\xi d$  is the distance from the extreme tension bar to the neutral axis. The flexural rigidity of the unjacketed section is then given by:

$$(EI_{eff})_{unj} = \frac{M_y}{\phi_{tot}} = \frac{M_y * \alpha L * \xi d}{\varepsilon_y (\alpha L + \gamma d)} = \frac{M_y * \alpha L}{\phi_y (\alpha L + \gamma d)} = \frac{EI_{cr}}{\left( 1 + \frac{\gamma d}{\alpha L} \right)} \quad (\text{A-5})$$

where  $EI_{cr}$ , the cracked flexural rigidity, was determined from a moment-curvature analysis on theunjacketed section. Because  $\alpha$  was known from the column geometry and  $E_{cr}$  could be computed from the cross-section properties, only  $\gamma$  needed to be evaluated from experimental data. The calibration of the coefficient  $\gamma$  is described in Section A.3.

### **A.3 Condensation of the Column Model**

Condensing out some of the internal degrees of freedom in the column model has the benefit of reducing the number of degrees of freedom in the global model, but it imposes the penalty that internal data, such as the local bar strains at the end of theunjacketed section, are lost. In the case of the main line columns, this was not important because the joints were not considered to be in danger of joint shear failure, so evaluation of the joint shear demands, through use of the local bar stresses, was unnecessary. Therefore, the three segments of the main line columns were condensed down to one.

At each end of the column, the curvature of theunjacketed segment and the strain penetration effects were combined into a single rotational spring of stiffness  $k_{\theta 1}$  (top) and  $k_{\theta 2}$  (bottom). These stiffnesses were then combined with that of the main, jacketed part of the column to obtain a translational stiffness of the column. The EI value for a single prismatic column was then found so that it gave the same translational stiffness as the real column.

In general, condensation of the system of one jacketed column and two rotational springs results in a stiffness matrix that cannot be represented by the 4 x 4 stiffness matrix of a single prismatic column because the ratios of the various elements in the matrix do not correspond to those in the matrix of a single column. While theoretically the individual terms of the matrix could be input into the finite element analysis program, or a non-prismatic column could be developed with the appropriate properties, the effort required to do so would counteract any savings in run time. Therefore, the assumption was made that the joints at each end of the column were infinitely rigid in rotation, in which case the model was feasible. The dimensions of the pile caps and the rigidity of the box girder were sufficient that the assumption of rotational fixity at top and bottom proved to be

acceptable. For such a system, the 2 x 2 flexibility matrix of the end rotations relative to the chord is

$$\begin{Bmatrix} \theta_1 \\ \theta_2 \end{Bmatrix} = \begin{bmatrix} \frac{L}{3EI} + \frac{1}{k_{\theta 1}} & -\frac{L}{6EI} \\ -\frac{L}{6EI} & \frac{L}{3EI} + \frac{1}{k_{\theta 2}} \end{bmatrix} * \begin{Bmatrix} M_1 \\ M_2 \end{Bmatrix} \quad (\text{A-6})$$

or

$$\begin{Bmatrix} \theta_1 \\ \theta_2 \end{Bmatrix} = \frac{L}{3EI} \begin{bmatrix} 1+c_1 & -\frac{1}{2} \\ -\frac{1}{2} & 1+c_2 \end{bmatrix} * \begin{Bmatrix} M_1 \\ M_2 \end{Bmatrix} \quad (\text{A-7})$$

where  $c_1 = \frac{1}{k_{\theta 1}} * \frac{3EI}{L}$  (A-8)

and  $c_2 = \frac{1}{k_{\theta 2}} * \frac{3EI}{L}$  (A-9)

Inverting the matrix leads to the stiffness equations

$$\begin{Bmatrix} M_1 \\ M_2 \end{Bmatrix} = \frac{3EI}{Lc_3} \begin{bmatrix} 1+c_2 & \frac{1}{2} \\ \frac{1}{2} & 1+c_1 \end{bmatrix} * \begin{Bmatrix} \theta_1 \\ \theta_2 \end{Bmatrix} \quad (\text{A-10})$$

where  $c_3 = (1+c_1)(1+c_2) - \frac{1}{4}$  (A-11)

But if the adjoining members do not rotate (i.e., the ends of the combined column element are fixed against rotation),

$$\theta_1 = \theta_2 = \frac{\Delta}{L} \quad (\text{A-12})$$

where  $\Delta$  is the lateral translation of the top of the column relative to the bottom. Also, equilibrium requires that

$$V = \frac{M_1 + M_2}{L} \quad (\text{A-13})$$

Equations A-10, A-12 and A-13 can be combined to give

$$k_{lat} = \frac{V}{\Delta} = \frac{M_1 + M_2}{\Delta L} = \frac{3EI}{L^3} \frac{(3 + c_1 + c_2)}{c_3} \quad (\text{A-14})$$

Equation A-14 may be verified for the special case in which the rotational stiffnesses of the end springs become very small in comparison with the stiffness of the main segment of column. Then  $c_1$  and  $c_2$  become  $\gg 1.0$  and

$$k_{lat} \approx \frac{3EI}{L^3} \frac{(c_1 + c_2)}{c_1 c_2} = \frac{k_{\theta 1} + k_{\theta 2}}{L^2} \quad (\text{A-15})$$

as it should. The lateral stiffness of a prismatic column is

$$k_{lat,prism} = \frac{12EI_{prism}}{L^3} \quad (\text{A-16})$$

so the moment of inertia of the required equivalent prismatic column is

$$I_{prism} = I \frac{(3 + c_1 + c_2)}{4c_3} \quad (\text{A-17})$$

For a given value of  $\gamma$ , the assumed strain penetration length coefficient, the values of  $k_{\theta 1}$  and  $k_{\theta 2}$  could be obtained from Equation A-5 and  $\alpha L$ , the column segment length. The values of  $c_1$ ,  $c_2$  and  $k_{lat}$  could then be computed with equations A-8, A-9, and A-14.

To calibrate the coefficients in the model, these equations were used to predict the lateral stiffness of jacketed columns tested by Priestley, Seible, Xiao and Verma (1994a and 1994b). Among those tested, columns R2R, R4R, and R6R were rectangular and were retrofitted with elliptical steel jackets. They were fixed against rotation at both ends, and a lateral load was applied to the top. Priestley, Seible, Xiao, and Verma reported the secant column stiffness ( $K_y$ ) at yield and the associated shear ( $V_y$ ). The experimental yield displacements were then calculated as:

$$\Delta_y = \frac{V_y}{K_y} \quad (\text{A-18})$$

In the column model, the unjacketed segment length,  $\alpha L$ , was assumed to be 2 in. Varying  $\alpha L$  was found to make little difference, which implies that the effects of strain penetration were much more important than the curvature in the short unjacketed section.

The coefficient  $\gamma$  was then varied until the best match with the measured data was achieved. This occurred at  $\gamma = 0.65$ . The final predicted and measured yield displacements for the test columns are shown in Table A-1.

**Table A-1: Experimental and Theoretical Yield Displacement (in.)**

Column #	R2R	R4R	R6R	Avg.
Measured	0.23	0.32	0.28	(-)
Predicted	0.18	0.35	0.27	(-)
Theo/Exp	0.78	1.09	0.96	0.94

The stiffnesses,  $EI_{\text{prism}}$ , for the equivalent prismatic columns were computed in all cases using a value of  $\gamma = 0.65$  for the strain penetration length coefficient.

#### **A.4 Modeling of Split Columns**

The jacketed, split columns between frames presented special problems. For the bents where the split columns joined at the foundation level, each of the split main-line columns was modeled as a single condensed frame element with the same procedure as that used for the normal mainline columns. However, for the cases in which the split columns joined into a single column above the foundation level, the condensation became difficult, so separate frame elements were used to model the jacketed and unjacketed sections, as was done in the outrigger columns. The top of the split column segment and bottom of the single column segment were modeled by using unjacketed properties, but the region where the two split segments joined to form a single unit was treated as jacketed.

#### **A.5 Modeling of Unjacketed and Retrofitted Columns**

A five-part column was used to represent the unjacketed outrigger column at Bent 25, as well as the modified outrigger columns in retrofit option C, as show in Figure A-3.

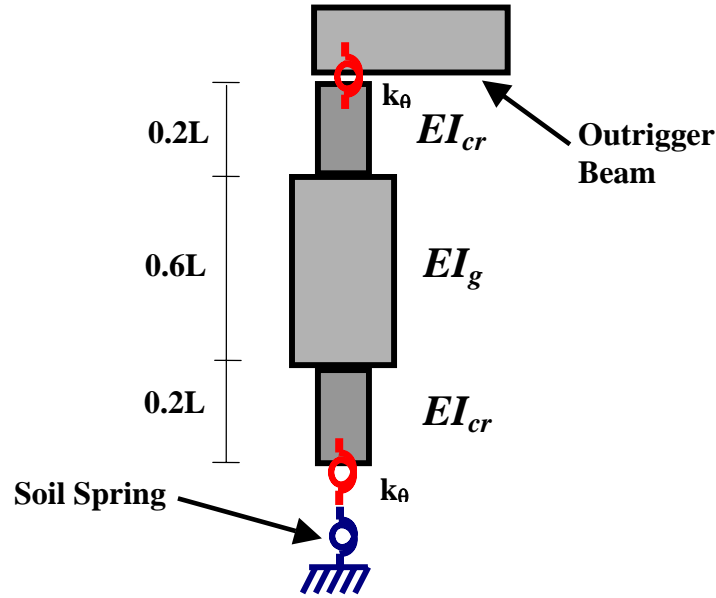


**Figure A-3: Representation of Unjacketed Column at Bent 25 and Retrofitted Columns**

A zero-length spring was used to model the strain penetration of the reinforcing bars at the top and bottom of the column. Unlike in the jacketed column representation, only the strain penetration into the joint at the top or into the footing at the bottom was included in the spring stiffness because no jacket around the column exists to prevent its cracking and to stiffen it. Therefore, the bar elongation due to strain penetration was one-half of the component calculated in Equation A-3. The rotational stiffness of the spring was calculated as:

$$k_{\theta} = \frac{M_y}{\theta_y} = \frac{M_y * \xi d}{\frac{1}{2} * \mathcal{N}_d * \varepsilon_y} = \frac{2 * M_y}{\mathcal{N}_d * \phi_y} \quad (\text{A-19})$$

Again, the yield moment and yield curvature were determined through a moment-curvature analysis of the unjacketed column.

Three frame elements were used to model the remainder of the column. The center portion of the column typically remains uncracked under lateral loads and was therefore

modeled with gross section properties. The top and bottom of the column are where most of the cracking and deformation occur; therefore, the column at these ends was modeled with cracked section properties. The length of the cracked section was approximated by first assuming that the yield moment ( $M_y$ ) occurs at the top and bottom of each of the columns. The cracking moment of the column ( $M_{cr}$ ) was then determined through a moment-curvature analysis.

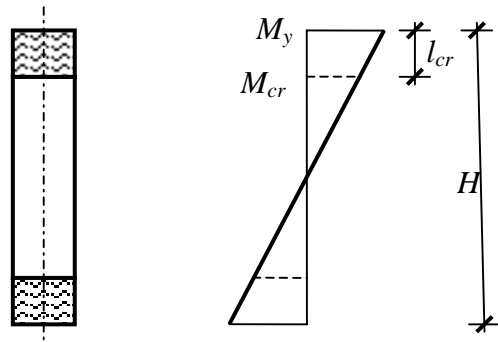


**Figure A-4: Extent of Cracking in Column**

The length over which the column is cracked depends on  $M_{cr}$  and  $M_y$ , as shown in Figure A-5, and, for a symmetrically loaded column, is given by

$$l_{cr} = \frac{H}{2} \left( 1 - \frac{M_{cr}}{M_y} \right) \quad (\text{A-20})$$

On the basis of a cracking stress of  $7.5\sqrt{f'_c}$ , 20 to 35 percent of the column height was found to be a good estimate of the average length of the cracked section for the columns. However, on the basis of a cracking stress of  $10\sqrt{f'_c}$ , 10 to 15 percent of the column height was found to be a good estimate. The cracking stress is probably in between the two values, and therefore, the cracked length was taken as 20 percent of the column height. The cracked stiffness,  $EI_{cr}$ , was taken as the secant stiffness at first yield, given by

$$EI_{cr} = \frac{M_y}{\phi_y} \quad (\text{A-21})$$

The yield moment,  $M_y$ , and the yield curvature,  $\phi_y$ , were determined from a moment-curvature analysis of the column section.

## References

- Nuncio-Cantera J.A., and Priestley, M.J.N., "Moment Overstrength of Circular and Square Bridge Columns," Research Report SSRP-91/04, Department of Applied Mechanics and Engineering Sciences, University of California, San Diego, La Jolla, CA, September 1991.
- Park, R., and Paulay, T., "Reinforced Concrete Structures," John Wiley & Sons, Inc., New York, 1975, 769 pp.
- Priestley, M.J.N., Seible, F., Xiao, Y., and Verma, R., "Steel Jacket Retrofitting of Reinforced Concrete Bridge Columns for Enhance Shear Strength – Part 1: Theoretical Considerations and Test Design", ACI Structural Journal, Vol. 91, No. 4, July/August 1994a, pp. 394-405.
- Priestley, M.J.N., Seible, F., Xiao, Y., and Verma, R., "Steel Jacket Retrofitting of Reinforced Concrete Bridge Columns for Enhance Shear Strength – Part 2: Test results and Comparison with Theory", ACI Structural Journal, Vol. 91, No. 5, September/October 1994b, pp. 537-551.
- Raynor, D.R., Lehman, D.E., and Stanton, J.F., Bond-Slip Response of Reinforcing Bars Grouted in Ducts, ACI Structural Journal, September/October 2002, Vol. 99, No.5, pp. 568-576.

## **APPENDIX B: Moment and Bar Stress Demand Calculation Procedure for As-Existing Outriggers**

One of the most critical elements in the structure is the joint between the outrigger beam and column. The demands on the joint are determined largely by the forces in the beam and column reinforcement. It is therefore necessary to develop a methodology for determining those bar forces from the output of the finite element (FE) analyses. The FE analysis was linear, at least as far as the outrigger beam and column elements are concerned, so it was first necessary to estimate from the displacement output the inelastic rotation and curvature at the locations of the real plastic hinges. The sequence of steps used was thus as follows:

- Obtain the plastic hinge rotations from the global displacement field, by assuming the location of the hinges in the plastic mechanism and assuming that the displacements are the same for the elastic and plastic response.
- Obtain the curvatures from rotations by dividing by the plastic hinge length.
- Obtain the bar stresses from the curvature through the use of a moment-curvature analysis of the cross-section.

The details of the first two steps are given in Sections B.1 and B.2 for different plastic hinge patterns. The moment-curvature analysis is a standard procedure and is described in Section 4.2.1.

## B.1 Case 1: Strong Column, Weak Beam System

### B.1.1 Development of Rotations from Displacements

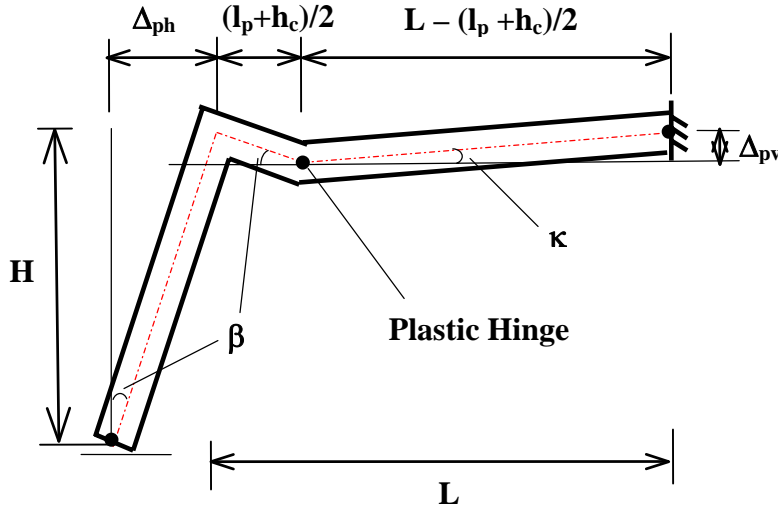


**Figure B-1: Yielding of Outrigger Beam**

Figure B-1 shows the mechanism used to determine the plastic hinge rotation when the beam is weaker than the column, and the critical plastic hinge forms in the beam. One plastic hinge is assumed to form at the base of the column. The beam contains two plastic hinges, as close as possible to the beam-column joint and to the deck, respectively. The distance from the centerline of the column to the center of the beam plastic hinge is therefore

$$distance = \left( \frac{l_{p1} + h_c}{2} \right) \quad (\text{B-1})$$

The plastic rotation at the beam hinge nearest the column is:

$$\theta_p = \beta + \kappa \quad (\text{B-2})$$

where:

$\theta_p$  = plastic rotation at plastic hinge

$\beta$  and  $\kappa$  = rotation angles of column and beam as shown in Figure B-1

$h_c$  = column width

$l_{p1}$  = curvature component of the plastic hinge length (explained below)

The angle  $\kappa$  arises because the two plastic hinges in the beam displace vertically relative to each other. That displacement consists of one component due to the rotation of the column multiplied by the horizontal distance from the column centerline to the hinge location, and another due to the relative vertical displacements of the outrigger column and the mainline column. The latter arises because, at each hinge, the column centerline elongates (Kim et al. 2004) by a distance  $\Delta_{axial}$ , given by

$$\Delta_{axial} = \theta_p \left( \frac{h_c}{2} - c \right) \quad \text{(B-3)}$$

where

$c$  = the neutral axis distance

$\Delta_{axial}$  = axial elongation of column due to rotation of one hinge

Because the outrigger columns contain one hinge, but the mainline columns contain two, the main line columns elongate twice as much as the outrigger columns and rise relative to them. The angles  $\kappa$  and  $\beta$  are thus:

$$\kappa \approx \frac{\Delta_{pv}}{\left( L - 2 * \frac{l_{p1}}{2} - \frac{h_c}{2} \right)} \approx \frac{\beta * \left( \frac{l_{p1} + h_c}{2} \right) + \beta * \left( \frac{h_c}{2} - c \right)}{\left( L - l_{p1} - \frac{h_c}{2} \right)} = \frac{\beta * \left( \frac{l_{p1}}{2} + h_c - c \right)}{\left( L - l_{p1} - \frac{h_c}{2} \right)} \quad \text{(B-4)}$$

and

$$\beta \approx \frac{\Delta_{ph}}{H} \quad \text{(B-5)}$$

where:

$\Delta_{pv}$  = differential vertical deflection between plastic hinge and beam to deck connection

$\Delta_{ph}$  = horizontal displacement demand on the outrigger due to plastic hinge rotation

$H$  = height of column to centerline of beam

$L$  = length between deck and center-line of outrigger column

$h_c$  = depth of the column

$c$  = column neutral axis depth

Note that  $\kappa$  is likely to be significantly smaller than  $\beta$  unless the beam span/depth ratio is low. The plastic hinge rotation now becomes:

$$\theta_p = \beta \left( 1 + \frac{\left( \frac{l_{p1}}{2} + h_c - c \right)}{L - l_{p1} - \frac{h_c}{2}} \right) = \beta \left( \frac{L - \frac{l_{p1}}{2} + \frac{h_c}{2} - c}{L - l_{p1} - \frac{h_c}{2}} \right) \quad (\text{B-6})$$

If second order quantities such as  $\left( \frac{h_c}{L} \right)^2$  are ignored and the value for  $\beta$  is substituted from Equation B-5, this simplifies to

$$\theta_p \approx \frac{\Delta_{ph}}{H} \left( 1 + \frac{h_c - c}{L} \right) \quad (\text{B-7})$$

### B.1.2 Development of Curvature from Rotations

By definition, the plastic curvature demand is the plastic rotation divided by the plastic hinge length:

$$\phi_p = \frac{\theta_p}{l_p} \quad (\text{B-8})$$

The plastic rotation can be obtained from Equation B-7. The plastic hinge length is given by Paulay and Priestley (1992) as:

$$l_p = l_{p1} + l_{p2} = 0.08L_{cant} + 0.15d_b f_y \quad (\text{B-9})$$

where:

$l_p$  = plastic hinge length

$l_{p1}$  and  $l_{p2}$  = plastic hinge length components

$L_{cant}$  = length of a cantilever column,

= distance from inflection point to fixed end in any other column

$d_b$  = bar diameter of longitudinal reinforcement

$f_y$  = yield strength of longitudinal reinforcement (ksi)

The first term in Equation B-9,  $l_{p1}$ , represents the distance between the locations where the moment is equal to  $M_y$  and  $M_n$ . The second term,  $l_{p2}$ , is the component of plastic hinge length attributable to strain penetration into the joint. The distinction is necessary because the strain penetration component does not influence the location of the plastic hinge in the member. If the plastic hinge is to be located with one side coincident with the column face, the center of the beam hinge must be  $l_{p1}/2$  from it.

Because a plastic hinge exists at each end of the beam, the distance between hinge centers is  $2L_{cant}$  and can be defined in terms of the clear length between the deck and the column face as:

$$2L_{cant} = L_{clear} - 2 * \frac{1}{2} l_{p1} = L_{clear} - 0.08L_{cant} \quad (\text{B-10})$$

from which  $L_{cant}$  is found to be:

$$L_{cant} = \frac{L_{clear}}{2.08} \quad (\text{B-11})$$

and  $l_{p1}$  is:

$$l_{p1} = 0.08L_{cant} = 0.0385L_{clear} \quad (\text{B-12})$$

The second term,  $l_{p2}$ , represents the strain penetration into the adjacent concrete. It depends on the yield strength and the bond strength of the bar. Equation B-9 is based on the bond strength of bars with modern lug patterns. However, the reinforcement in common use when the structure was built has fewer, lower-profile lugs and therefore should be expected to develop lower bond strength. No data were available to define that bond strength, so a value of  $9d_b$  was used for  $l_{p2}$ , assuming by default that the ratio of bond strength to yield strength was the same for bars from both eras.

## B.2 Curvature Demand – Strong Column System

Figure B-2 shows the mechanism used to determine the plastic hinge rotation when the column, rather than the beam, yields. The geometry, and therefore the equations, differs slightly from those described in Section B.1.

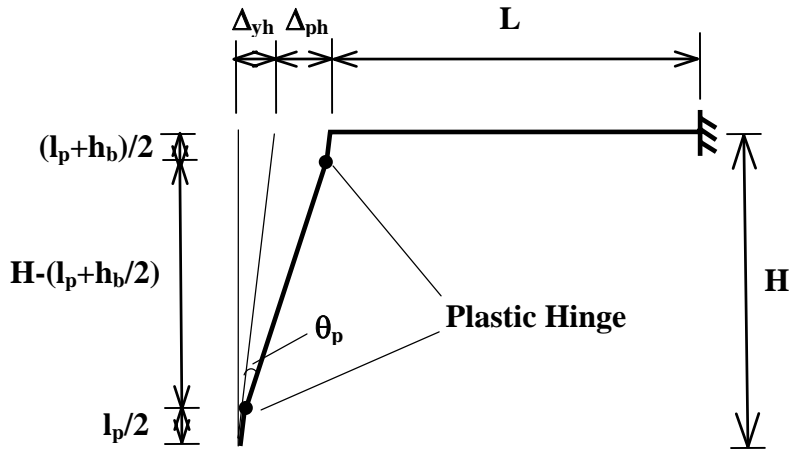


**Figure B-2: Yielding of Outrigger Column**

The plastic mechanism consists of hinges at the top and bottom of the outrigger column and the top and bottom of the main line columns. No plastic hinges form in the beam. The effect on the plastic rotations of column elongation due to cracking is therefore negligible because the main line and outrigger columns experience approximately the same rotation and elongate by approximately the same amount, if they are close to the same size. Therefore, there is no differential vertical deflection between the different joints, and no rotation component arising from it.

The plastic hinge rotation is then

$$\theta_p \approx \frac{\Delta_{ph}}{H - \left( 2 * \frac{l_{p1}}{2} + \frac{h_b}{2} \right)} = \frac{\Delta_{ph}}{H - \left( l_{p1} + \frac{h_b}{2} \right)} \quad (\text{B-13})$$

where:

$h_b$  = depth of the beam

### **B.2.1 Development of Curvature from Rotations**

The plastic hinge length differs from the one used for the beam because of the presence of the steel jacket around the columns. Priestley et al. (1994a and 1994b) recommended calculating the plastic hinge length of jacketed columns as:

$$l_p = g + 2\chi d_b \quad (\text{B-14})$$

where:

$g$  = length of the gap between the end of the jacket and the footing or joint face

$\chi$  = 6 or 9 for Grade 40 or Grade 60 steel, respectively.

The second term in Equation B-14 represents the strain penetration effects and is similar to the one used in Equation B-9. However, the strain penetration effects are included twice because the jacketed column is assumed to not crack and to be relatively rigid, in which case the elongation of the bars through strain penetration must be accounted for on both sides of the plastic hinge. Because the bars in the as-existing structure are believed to have relatively poor bond properties, it is recommended, as before, that  $\chi = 9$  be used even for the nominal grade 40 steel.

Again, the plastic hinge length can be separated into a part due to curvature,  $l_{p1}$ , and a part due to strain penetration,  $l_{p2}$ . Here, strain penetration occurs up into the joint and down into the column, so the  $l_{p1}$  component, which is used to locate the plastic hinge within the column, comprises the curvature part and one strain penetration part, to give:

$$l_{p1} = g + \chi d_b \quad (\text{B-15})$$

while the  $l_{p2}$  component consists of one strain penetration component alone:

$$l_{p2} = \chi d_b \quad (\text{B-16})$$

In most cases the gap is on the order of 2 in. The strain penetration component for No. 11 bars is approximately 12 in., so  $l_{p1}$  and  $l_{p2}$  will be nearly equal. The plastic curvature is defined using the entire plastic hinge length as:

$$\phi_p = \frac{\theta_p}{l_p} = \frac{\Delta_{ph}}{\left( H - \left( l_{p1} + \frac{h_b}{2} \right) \right) l_p} \quad (\text{B-17})$$

and the total curvature is the sum of the yield and plastic components:

$$\phi_{tot} = \phi_y + \phi_p \quad (\text{B-18})$$

where:

$\phi_{tot}$  = total curvature

$\phi_y$  = yield curvature

### B.3 Moments and Bar Stresses

Once the curvature demand has been calculated, the moment and bar stress demand can be determined. For each outrigger bent, a moment-curvature analysis was performed on the member that yielded first. The plastic hinge moment was determined from the associated curvature, for which the plastic component was defined by Equation B-8 or B-17. The moment in the non-yielding element was then determined through equilibrium of the joint. The bar stresses were obtained from the moment-curvature analysis for the yielding element, or from elastic theory in the non-yielding element. Both the moment and bar stresses were used for determining demands on the outrigger components.

### References

Kim J., Stanton J., and MacRae G. A., "Effect of Beam Growth on Reinforced Concrete Frames," ASCE Journal of Structural Engineering, Vol. 130, No. 9, September 2004. 

Paulay, T., and Priestley, M.J.N., "Seismic Design of Reinforced Concrete and Masonry Buildings," John Wiley and Sons, Inc., New York, 1992, 744 pp.

Priestley, M.J.N., Seible, F., Xiao, Y., and Verma, R., "Steel Jacket Retrofitting of Reinforced Concrete Bridge Columns for Enhance Shear Strength – Part 1: Theoretical Considerations and Test Design", ACI Structural Journal, Vol. 91, No. 4, July/August 1994a, pp. 394-405.

Priestley, M.J.N., Seible, F., Xiao, Y., and Verma, R., “Steel Jacket Retrofitting of Reinforced Concrete Bridge Columns for Enhance Shear Strength – Part 2: Test results and Comparison with Theory”, ACI Structural Journal, Vol. 91, No. 5, September/October 1994b, pp. 537-551.

